MODELING AND EXPERIMENTAL STUDY OF POLYURETHANE FOAMING REACTIONS

A Dissertation

presented to

the Faculty of the Graduate School

at the University of Missouri-Columbia

In Partial Fulfillment

of the Requirements for the Degree

Doctor of Philosophy

---

by

Yusheng Zhao

Dr. Galen Suppes, Dissertation Supervisor

December 2015

The undersigned, appointed by the dean of the Graduate School, have examined the dissertation entitled

MODELING AND EXPERIMENTAL STUDY OF POLYURETHANE FOAMING REACTIONS

presented by Yusheng Zhao,

a candidate for the degree of Doctor of Philosophy,

and hereby certify that, in their opinion, it is worthy of acceptance.

Professor Galen Suppes

Professor Fu-hung Hsieh

Professor Sheila Baker

Professor John Gahl

ACKNOWLEDGEMENTS

Acknowledgements, first and foremost go out to the members of my committee: Drs. Galen Suppes, Fu-hung Hsieh, Sheila Baker and John Gahl. I would like to express my special gratitude to my advisor, Dr. Galen Suppes for granting me the opportunity to work on this project, and for his support, encouragement, and guidance in developing these experiments.

This work could not have been completed without the help of my co-researchers, and I would like to show my deepest appreciation to Rima Ghoreishi, Harith Al-Moameri, and all the members in polyurethane foam research group for their support and dedication.

I would like to thank the United Soybean Board for financial support of the experimental studies used to validate the modeling work and thank FSI. Company providing foam formulas and technology support. I also thank University of Missouri Bioinformatics Consortium (UMBC) for providing the HPC resources to run the computations and technical support for running jobs on the supercomputer.

I would also like to thank my parents, Gengzhen Zhao and Huifang Wu for their unconditional love and support in my decision to pursue higher education.

Yusheng Zhao

TABLE OF CONTENTS

LIST OF TABLES

LIST OF FIGURES

LIST OF ABBREVIATIONS

c	Concentration
r	Reaction Rate
k	Reaction Rate Constant
k_0	Reaction Rate Constant under the Reference Condition
A	Pre-exponential Factor
E_a	Activation Energy
R	Ideal Gas Constant
T	Temperature
cat	Catalyst
Pcat	Product of Tin Catalyst and Polymer
cat5	Pentamethyldiethylenetriamine (PMDETA)
cat8	Dimethylcyclohexylamine (DMCHA)
K	Equilibrium Constant
H	Heat of Reaction
MF	Methyl Formate
OF	Objective Function
MDI	Methylene Diphenyl Diisocyanate
TDI	Toluene Diisocyanates
HDI	Hexamethylene-1,6-diisocyanate
PMDI	Polymeric MDI
NMR	Nuclear Magnetic Resonance
P	Vapor Pressure
ΔH_{vap}	Enthalpy of Vaporization
P_i	Partial Vapor Pressure of Component i
x_i	Mole Fraction of Component i
OSHA	Occupational Safety and Health Administration
ppm	Parts-per-million
PMDS	Polydimethylsiloxane
PEO-PPO	Polyethylene Oxide-co-Propylene Oxide
C	Concentration of Surfactant
σ	Surface Tension
cmc	Critical Micelle Concentration
r	Bubble Radius
θ	Contact Angle
F	Force
ρ	Density
g	Standard Gravity
h (Eq. 4-2)	Rising Height of Liquid
O.D.	Outside Diameter
I.D.	Inside Diameter
L	Length

MW	Molecular Weight
Fn	Functionality
W	Energy Introduced by Mixing
Nc	Number of Nucleation Sites
p_b	Pressure in the Bubble
p_a	Pressure of the Liquid at the Bubble Surface
τ_{rr}	Radius Component of Viscous Stress Tensor in Liquid
p_∞	Ambient Pressure
μ	Newtonian Viscosity
h (Eq. 4-8)	Film Thickness
t	Time
$\dot{A}$	Angstrom
V_{Re}	Velocity of Film Thinning
V_t	Overall Velocity of Film Thinning
λ	Characteristic Length of the Thickness Non-homogeneities
ϵ_t	Total Amplitude of the Thickness Non-homogeneities
D_i	Probability Values
V	Volume
h_0	Initial Film Thickness
ave	Average
h_c	Critical Film Thickness
ccc	Closed Cell Content
V_r	Bubble Rising Velocity
d	Bubble Diameter
X_p	Ratio of Primary Alcohol
X_s	Ratio of Secondary Alcohol
X_{HS}	Ration of Hindered-secondary Alcohol
DFT	Density Functional Theory
PCM	Polarizable Continuum Model
IEF-PCM	Integral-Equation-Formalism Polarizable Continuum Model
TS	Transition State
H_{total}	Total Enthalpy
ε_{ZPE}	Zero Point Vibrational Energy
$\Delta_r H^0$	Reaction Enthalpy
DEG	Diethylene Glycol
UMBC	University of Missouri Bioinformatics Consortium

ABSTRACT

Polyurethanes are very important polymers and are used in a wide range of applications. A theoretical model was developed to simulate polyurethane foaming reactions. In the model, multiple ordinary differential equations were solved by MATLAB program and the model was able to predict temperature, foam height and concentration profiles. This model can provide a better understanding of fundamental polyurethane chemistry and the foaming process.

Further modeling and experimental studies were performed to improve accuracy and to expand capability of the simulation program. Impact of side reactions, impact of catalyst and surfactant concentrations and impact of catalysis poisoning were taken into consideration and included in the model. The revised model was able to predict bubble radius, inside bubble pressure, vapor pressure of pure isocyanate as well as more reasonable temperatures, foam height, and concentration profiles. Reaction kinetics and thermodynamics parameters used in the simulation program were verified by experimental and/or computational methods respectively.

The use of simulation offers a way to control the complexity and transform materials design, just as process simulators have transformed engineering design. This perspective presents a case that simulation is ready to change the way we research, develop, and design polyurethane formulations.

1. INTRODUCTION

Chapters 2-5 of this dissertation are presented as independent works related to simulation of polyurethane foaming reactions. These works are extensions of previous studies on modeling reaction kinetics of polyurethane foaming process. This dissertation work turned into four published papers and one paper under review.

A MATLAB program was developed to simulate reaction rates, component concentrations and the temperature profiles for polyurethane foaming reactions. The program was able to predict performance of a recipe which contains one isocyanate and up to three polyols. In Chapter 2, the program was revised to include the impact of catalyst types and amount of catalyst loadings. Tin based catalysts and amine based catalysts were applied into gel and foam recipes separately to evaluate the impact of each catalyst on both gel and blow reactions. The revised model successfully predicts performances of diverse foam recipes and can be effective for "sensitivity studies" useful in designing form formulations. The simulations have been validated for estimating catalyst loadings, identifying the tradeoff between higher catalyst loadings versus preheating of reagents, and providing insight into fundamental mechanisms/reactions.

In Chapter 3, the program was revised to include more side reactions of isocyanate and the ASTM titration was applied to track isocyanate concentration during reactions. The isocyanate concentration profiles were consistent with previously published kinetics parameters for reactions of isocyanates with alcohols as well as reactions with urethane moieties. This work is on the use of modeling of concentration profiles in rigid

foams to quantify the concentration of isocyanate moieties in rigid foams from the onset of reaction until several days after the setting of the foam. The data indicate how the isocyanate index and epoxy co-reagents can be used to reduce isocyanate emissions. Partial pressures of isocyanate monomers are calculated based on temperature and isocyanate concentration profiles, these data can be used to understand and reduce emissions in work zones.

Surfactants play an important role in forming, stabilizing, and setting urethane foams, thus developing a simulation with the impact of surfactants can help better predict performances of foam formulations. Chapter 4 evaluated the relationship between surface tension and surfactant amount experimentally by using the capillary rise method and developed a model to simulate the impact of surfactants on polyurethane foam polymerization based on the mechanism that surfactants have a critical role in the initial stages of gel formation and through the point where viscosity is high enough to create resistance to support the foams. Bubble sizes were calculated based on the number of nucleation sites, gas generation rate, surface tension and bubble inner pressure. Since important properties of polyurethane foam, such as compressive strength, closed cell content, and thermal conductivity can be related to the bubble sizes, this model can be used to predict foam performance and to develop new foam formulations.

In Chapter 5, computational calculations were performed on urethane-forming reactions using Gaussian 09 software (ie molecular modeling) toward the goal of providing thermodynamic parameters. Total electronic and thermal enthalpies and zero-

point vibrational energies of reactants and products were computed by the software and then reaction enthalpies were calculated based on these results. The location of functional groups has the most significant impact on reaction enthalpies while molecular size, chain length and solvent effect have relatively less impact on reaction enthalpies. By comparison to new experimental studies and values reported in the literature, better-informed recommendations on which values of reaction enthalpies to use for urethane foam process simulation were provided. The utility of computational chemistry results succeeded in being an enabling technology to improve foam process simulation. In turn, simulation of urethane-forming reactions is useful to bridge the gap between fundamental computational chemistry calculations and practical applications.

This series of work provides a reliable simulation program to track important profiles (temperature and concentration) during reactions and to predict final product properties (density, bubble radius and isocyanate vapor pressure) of foams with various recipes. This simulation program also provides a detail insight into fundamental polyurethane chemistry and can be used as a tool to develop new formulations.

2. MODELING IMPACT OF CATALYST ON POLYURETHANE FOAMING REACTIONS

2.1 Introduction

Polyurethane (PU) is a polymer composed of a chain of organic units joined by carbamate (urethane) links and are formed by reaction an isocyanate with a polyol. Both the isocyanates and polyols used to make polyurethanes contain on average two or more functional groups per molecule. The products are thermoset foams or elastomers that are often directly formed into final devices. The nature of this application is that hundreds of different manufacturers have unique foam recipes. The reaction engineering demands for this application tend to be much greater than needed to design the large-scale thermoplastic polymerization reactors.

Current practices in this market are for foam recipes to be developed by chemists with years of experience. The goal of this work is to change the paradigm of this industry to a paradigm where software is used to simulate the urethane-forming reactions, including foaming processes.

The chemistry of isocyanate is complex since it entails a variety of reactions such as with alcohols or amines, in addition to self-additions and trans-condensations. There are essentially hundreds of possible different reaction rate constants[1, 2] for the reaction of the same moieties as attached to molecules of ever-increasing molecular weight, in an environment of increasing viscosity, and in an environment of slightly changing molecular as chemical moieties react and convert.

Catalysts have a most important role in making urethane foams[3-5]. Two kinds of

catalysts are widely used in polyurethane foam industry: one is amine based catalyst and the other is metal based catalyst. Tin catalysts were introduced as a metal based catalyst to compare with traditional amine based catalysts. Inorganic and organo-tin compounds have found industrial use as catalysts in a very wide range of applications, from heterogeneous oxidation catalysts based on tin(IV) oxide (as employed, for example, in commercial gas sensor devices) to homogeneous catalysts for industrial organic and polymeric reactions.

Manufacture of polyurethane (PU) foam is by far the most important catalytic use in terms of tin tonnage. Tin(II) 2-ethylhexanoate (also commonly referred to as 'stannous octoate') is an important tin chemical used in PU production, although several organotin compounds, including dibutyltin diacetate and dibutyltin dilaurate, have also been evaluated over the years.

Although traditionally mainly used in flexible foam production, recent demand for rigid insulation foams in 'green' buildings has greatly increased urethane usage in this sector. It is believed that this application will be one of the high growth areas for tin catalysts.

The impact of catalysts on polyurethane foaming reaction has been of great interest. Research results[6-12] show that the match between the gelatinizing rate and the foaming rate could be adjusted by specifying catalyst and changing catalyst amounts, thus the structure and properties of the polyurethane foam could be controlled. With a good selection of the catalyst, the desired profile in reaction, foaming, flow-ability, and foaming properties can be obtained. Depending on concentration of catalysts in

foaming recipe, the activity will be different. This activity relates to the catalysis of the gel and blow reaction, which has a great impact on the properties and functions of the foam[13-16].

Chang[1] and Baker[17] measured rate constants for a model isocyanate-alcohol reaction catalyzed by tertiary amines and provided relative rate constants respect to different catalyzed conditions. Their relative reactivity data depending on catalyst concentration indicates that the reaction rate is in direct proportion to the amount of catalyst used. Empirically it seems that the addition of catalyst reduces activation energy, however based on the results of Van Maris et al[10], some special amine catalysts (such as Cyclic amines, F22 and Dibutyltindilaurate) may have a higher activation energy than the homogeneous reaction.

The state of the art in developing new foam formulations is based on the modification of established foam formulations by chemists who apply expertise in a qualitative sense. It would be highly desirable to elevate this process to a science including the simulation of the chemical reactions, physical processes, and ultimate the foam's physical properties. The demands for this application go beyond what has been previously achieved in this area; the application demands full consistency of performance of catalysts and monomers in diverse formulations. The primary method to obtain consistency is identifying the proper and complete (from impact perspective) set of fundamental reactions and mechanisms.

Zhao et al[18, 19] have initiated the first of several phases of modeling that includes the capability of using polyol mixtures, impact of common side reactions, impact of

catalyst loading and the methodology of using primary, secondary, hinder-secondary hydroxyl contents to characterize polyols. The introduction of metal-based catalysts is necessary to enrich the choices in foam recipe designing. Different types and amounts of tin based catalysts were used in this study to evaluate the catalysis effect of them and were compared with traditional amine based catalysts. Because of their different structures and different activation mechanisms, tin based catalysts behave different from amine based catalysts. The goal is to have a better understanding on the difference between amine based catalysts and tin based catalysts. The goal is to use these two kinds of catalysts appropriately based on requirements on foam properties and to improve the versatility of simulation for predicting temperature profile, component concentration profiles and reaction rate profiles during urethane foam-forming processes.

2.2 Mechanism of Catalysis

Figure 2-1 presents different mechanisms of amine based catalysts and metal based catalysts in polyurethane foaming reactions[9].

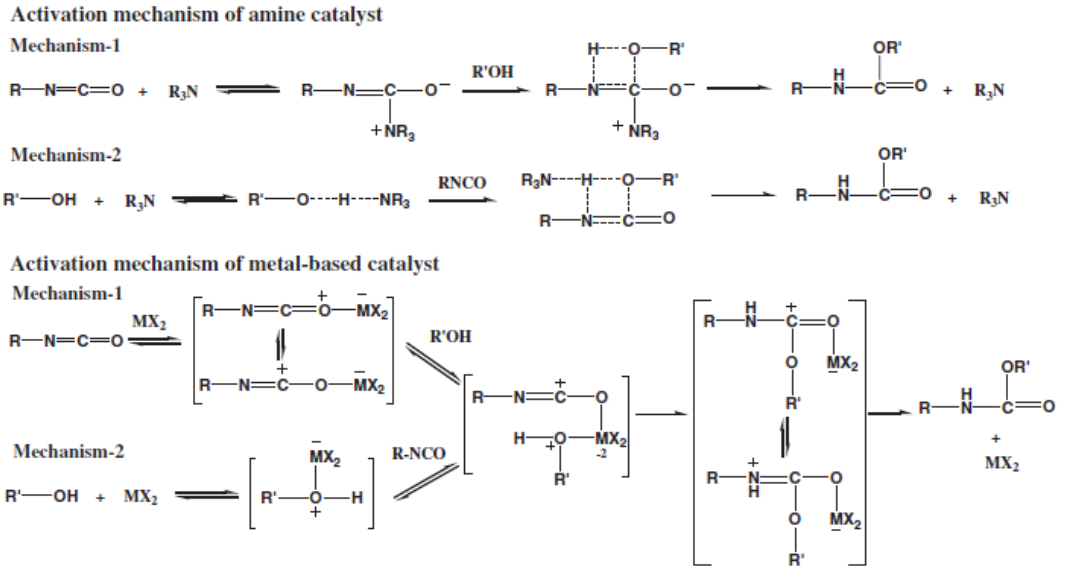

Figure 2-1 Mechanisms of amine based catalysts and metal based catalysts in PU foaming reaction

In general, the tertiary amine coordinate to the positive electron charged carbon of the NCO group or hydrogen of the OH group and forms a transition state to activate urethane formation reaction. It is claimed that a tertiary amine can be tuned by maximizing its ability to form a hydrogen bond with alcohol, thereby activating the O–H bond so it can attach to the isocyanate more easily.

On the other hand, a metal-based catalyst, which acts as a Lewis acid, primarily coordinates to the oxygen atom of the NCO group and activates the electrophilic nature of the carbon.

2.3 Modeling

Zhao et al[18, 19] have initiated the first of several phases of modeling that will be necessary to this work. Zhao et al's modeling work have included simulation of up to three polyols, a methyl formate physical blowing agent, water reaction blowing agent, and impact of catalyst loading. This work extends those initial studies to include modeling of homogeneous catalysts for foam forming reaction.

Figure 2-2 presents the MATLAB algorithm to simulate temperature and concentration profiles. FoamSim is the script file that first calls upon the function Recipe that contains the formulation. The Database function sets the kinetic and thermodynamic parameters. MATLAB's ODE45 function is then used to solve the ordinary differential equations set up in the ReacSim function. This code includes use of water reactions to form foams; the approach for using physical blowing agents is outside the scope of this paper.

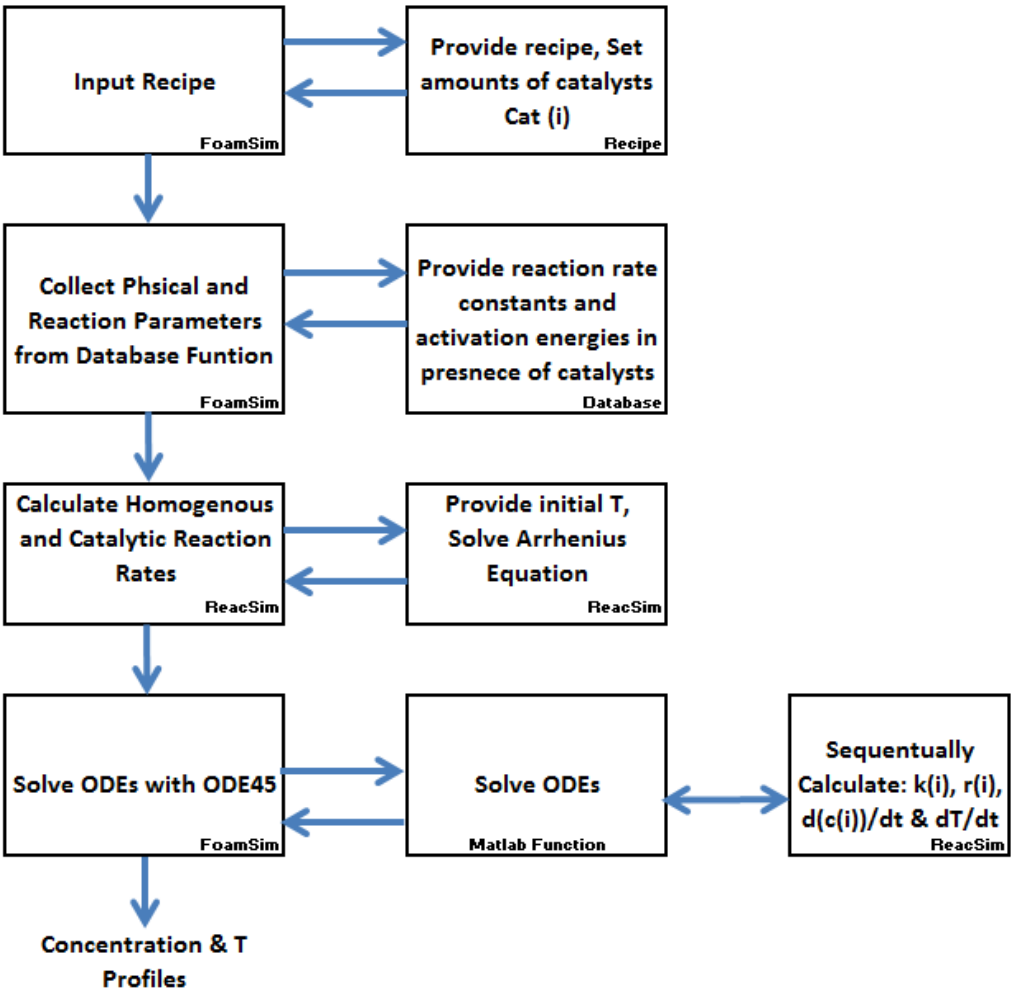

Figure 2-2 Algorithm for addition of catalysis to simulation

A key difference between modeling reactions of polymer-forming monomers and simple molecules is that for monomers the kinetics is based around the concentrations of the reactive moieties (e.g. c_{iso}, c_{OH}) rather than molecules. The initial gel reaction rate and blow reaction rate equations used in the modeling are expressed as:

$$r_{gel} = (k + k_{cat8} * c_{cat8} + k_{cat5} * c_{cat5}) * c_{iso} * c_{OH} \quad \text{Equation 2-1}$$

$$r_{blow} = (k' + k'_{cat8} * c_{cat8} + k'_{cat5} * c_{cat5}) * c_{iso} * c_{water} \quad \text{Equation 2-2}$$

$$k = A * e^{-E_a/(RT)} \quad \text{Equation 2-3}$$

where k and k' respectively represent the gel reaction rate and blow reaction rate under uncatalyzed conditions, $k_{cat\,A}$ is the gel reaction rate in presence of catalyst A,

$k_{cat\ B}$ is the gel reaction rate in presence of catalyst B, $k'_{cat\ A}$ is the blow reaction rate under the effect of catalyst A and $k'_{cat\ B}$ is the blow reaction rate under the effect of catalyst B. Arrhenius Equation (Equation 2-3) was used to include the impact of reaction temperature on reaction rates. The goal is to accurately simulate temperature profiles under multiple catalyst loading conditions.

Preliminary experimental data identified that the reaction rate is not in direct proportion to the amount of tin based catalyst. The hypothesis is that catalyst poisoning happens between tin based catalyst and another compound in the system that bonds chemically to its active surface sites. This leads to a decreasing in the total number of catalytic sites and the poisoned sites can no longer accelerate the reaction with which the catalyst was supposed to catalyze. The poisoning reaction was viewed like any other chemical reaction in this process:

$$\mathrm{Cat} + \mathrm{P} \leftrightarrow \mathrm{Pcat} \qquad \textbf{Equation 2-4}$$

$$\text{Catalyst} + \text{Poison} \leftrightarrow \text{Composite Compound}$$

Based on this reverse reaction an equilibrium equation can be listed as:

$$K = \frac{k_p}{k_{pr}} = \frac{Pcat}{Cat*P} = \frac{x}{(Cat_0 - x)*(P_0 - x)} \qquad \textbf{Equation 2-5}$$

where K is the equilibrium constant, Cat is the amount of tin based catalyst, P is the amount of polymer which can react with tin, and Pcat is the amount of the product of tin and polymer. By solving the value of "x" in Equation 2-5, the effective amount of catalyst ($\mathrm{Cat}_0 - \mathrm{x}$) can be calculated.

In addition to using the MATLAB program to simulate urethane-forming reactions, the same code must be used to identify the best-fit kinetic parameters. Figure 2-3 shows the algorithm for fitting of kinetic parameters. Initial guess of reaction rate constants

and activation energies were input to obtain preliminary simulation result. This result was compared with experimental data to revise the kinetic parameters.

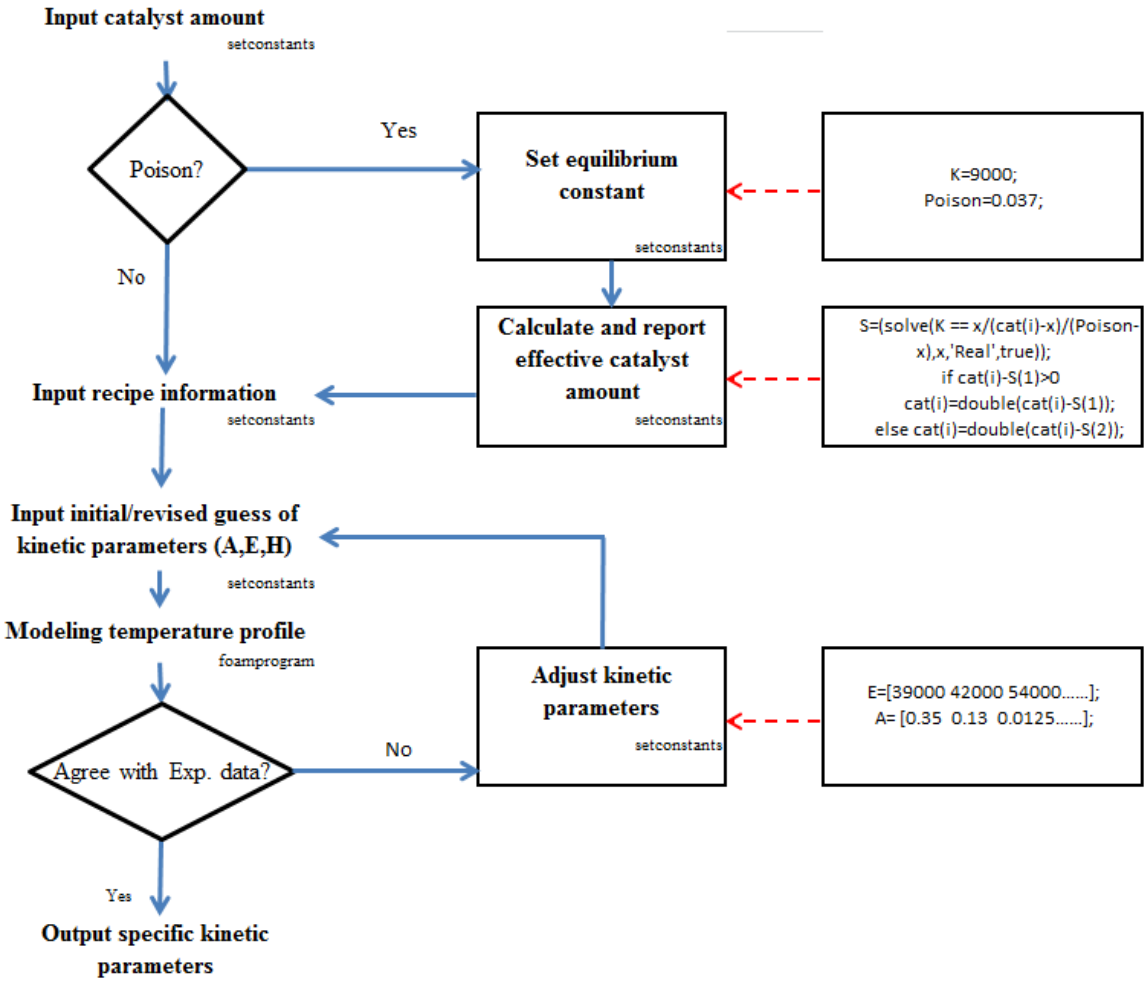

Figure 2-3 Algorithm for fitting of kinetic parameters

Table 2-1 lists heuristics used in the development of the model. These heuristics were used to help limiting degrees of freedom of the kinetic parameters to a manageable and reasonable level. The validity, within experimental error, of these heuristics is routinely evaluated. As the simulation process evolves with associated increasing demands for accuracies, these heurists would also evolve. These represent a base case set of heuristics.

Table 2-1 Heuristics used to limit kinetic parameters degrees of freedom to a manageable level

Polyols:
• Polyols consist of different ratios of primary, secondary and hinded-secondary hydroxyl • Same type of hydroxyl in different polyols have the same reaction rate constants (k_0) • Catalytic reaction rate constants (k_0) are unique to the catalyst
Catalysts:
• Catalysts will not react with any components in the system • The structure and reactivity of catalysts will not change during the reaction process • Catalysts will reduce activation energy (ΔE) relative to non-catalytic reaction • Catalysts have no impact on heat of reaction (ΔH) • There is no interaction between the catalysis impact from two or more catalysts
Others:
• Other additives (surfactant and fire retardant) have no catalysis impact on reactions • Foam has a lower heat transfer coefficient than gel

2.4 Materials and Methods

2.4.1 Materials

RUBINATE M (Standard Polymeric MDI) was the isocyanate used in this study and the petroleum-based polyols were Poly G76-635, Voranol 360 and Jeffol R315x

from Huntsman Company and Dow Chemical Co. The specifications are shown in Table 2-2 [20, 21]. N,N-dimethylcyclohexylamine (DMCHA) and N,N,N′,N″,N″-Pentamethyldiethylenetriamine (PMDETA) were used as catalysts. Several tin catalysts (Fomrez®UL-1,6,22,29,38) from Galata Chemicals LLC were used as catalysts in this study. Table 2-3 lists several catalysts and their properties. Figure 2-4 shows structures of these amine based catalysts. Momentive L6900 was used as the surfactant, TCPP was used as the fire retardant, distilled water and methyl formate were used as the blowing agents.

Table 2-2 Material properties

Component	**Isocyanate**	**Polyol**	**Polyurethane**	**Water**	**Carbon Dioxide**	**Amine**
Heat Capacity (J/g-K)	1.799	1.57 ~1.89	1.4~1.5	4.19	0.846~0.939 (300K~400K)	1.55~ 1.64
Heat Capacity (J/equiv-K)	242.86	264. 86	362.5	75.42	39.6	128

Product	**Fn**	**Sp. @25℃**	**Gravity**	**% NCO**	**Eq. Wt.**	**Viscosity cps@25℃**
RUBINATE M	2.70	1.23		31.2	135	190

Product	Poly G76-635	Voranol 360	Jeffol R315x
OH number	635	360	315
Equivalent Weight(g/mol OH)	88.3	155.8	178

Table 2-3 Amine/Tin based catalysts and their properties

Amine Based	Product Name	Formula	MW. (g/mol)
DMCHA	Dimethylcyclohexylamine	$C_8H_{17}N$ /$C_6H_5N(CH_3)_2$	127.23
PMDETA	Pentamethyldiethylenetriami	$C_9H_{23}N_3$	173.3

	ne	/$((CH_3)_2NCH_2CH_2)_2NCH_3$	
TMEDA	Tetramethylethylenediamine	$C_6H_{16}N_2$ /$(CH_3)_2NCH_2CH_2N(CH_3)_2$	116.2
DMP	1,4-Dimethyl-piperazine	$C_6H_{14}N_2$ $CH_3N(CH_2CH_2)_2NCH_3$	114.19
DBTDL	Dibutyltin Dilaurate	$C_{32}H_{64}O_4Sn$ /$(C_4H_9)_2Sn(OOCC_{11}H_{23})_2$	631.56
Tin Based			Wt. % Tin
Fomrez®UL-1	dibutyltin mercaptide		17.6
Fomrez®UL-6	dibutyltin mercaptide		18.0
Fomrez®UL-22	dibutyltin mercaptide		19.7
Fomrez®UL-29	dioctyltin bis(2-ethylhexylthioglycolate)		16.3
Fomrez®UL-38	dioctyltin carboxylate		16.7

DMCHA

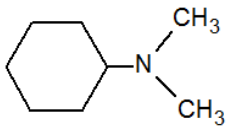

PMDETA

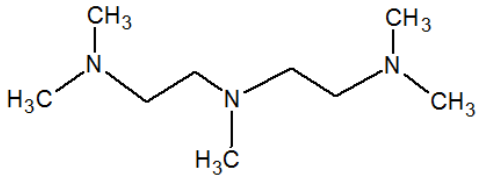

TMEDA

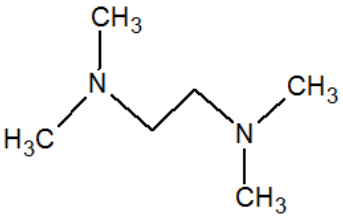

DMP

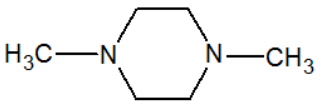

DBTDL

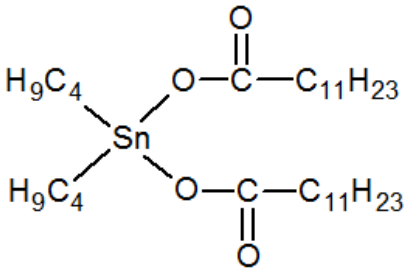

Figure 2-4 Example catalysts structures

2.4.2 Experimental Design

Blowing agents (water and MF) are taken out from the recipe for the gel reaction. Gel reactions with different catalysts and different catalyst amount were performed during this study.

Based on the Temperature-Time profiles, reaction rate pre-exponential factor, activation energy and heat of reaction can be estimated. The reaction rate at the beginning was determined by pre-exponential factor and the highest temperature during reaction process was dependent on heat of reaction. By plotting ln(k) as a function of 1/T, a straight line was obtained and activation energy can be calculated based on the slope. Reagent mixture was prepared with an electronic balance with an accuracy of ± 10^{-2} g in which the buoyancy effect was neglected, since errors in measuring mass fractions introduced by this work were much smaller than 0.1%. When weighting the mixture, all components were added at the same amounts throughout the experiments except for catalysts. The same approach was applied in the study on each polyol. Isocyanate indices in all runs were designed to lock in 1.15, however, there was deviation in actual numbers since it was uncontrollable when adding pre-weighted isocyanate.

2.4.3 Gel/Foam Preparation and Data Collection

The following steps were used in the foam experiments:

1. Polyols, water, catalysts, fire retardant and surfactant (B-side components) were added into a plastic cup successively.
2. The B-side components were mixed for 10-15 seconds.

3. The mixture was allowed to degas for 2 min.
4. Thereafter, pre-weighed isocyanate (A-side material) was added and mixed at the same speed for 7-10s.
5. The reacting mixture was then quickly poured into a box lined with aluminum, and the foam was allowed to rise and sit at ambient conditions (25 ˚C) during curing.

All the B-side chemicals were added in the foam reaction while blowing agents and blowing catalyst were not added in the gel reaction. Since the volume of gel mixture is much smaller than that of foam, the fluid level in wood box is too low to gather accurate data while performing gel reaction. Instead of using wood box for both reactions, step 5 was not performed in gel reactions and temperature was directly measured in plastic cups which could give a more accurate profile.

A high speed mixer blade (2000 rpm) attached to a floor-model drill press was used to mix the chemicals. LabVIEW software was used to monitor the temperature of the gel or foam reactions for the first 10 minutes with a type-k thermocouple attached through a National Instruments SCB-68 box to a National Instruments PCI 6024E data acquisition card.

2.5 Results and Discussion

2.5.1 Amine Based Catalyst

Experimental data and modeling results of the impact of amine based catalyst were presented in a previous study[19]. Figure 2-5 shows the temperature profile of V360 gel reaction and the modeling results of temperature and reaction rate changes.

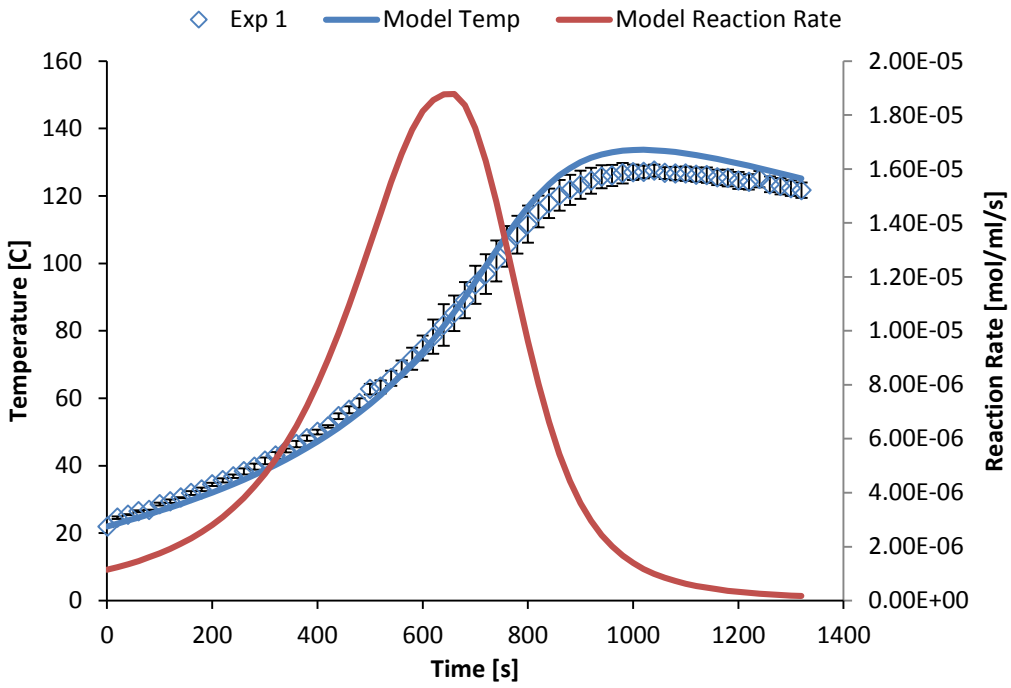

Figure 2-5 Temperature profile of V360 gel reaction and modeling results of temperature and reaction rate

The modeling successfully simulated the temperature change during this reaction process. The fastest reaction rate occurs at about 650s at which the temperature profile had the largest increasing gradient.

Figure 2-6 presents modeling temperature profiles under different catalyst amount loading conditions and Figure 2-7 presents the relationship between catalyst loading and reaction rate constant at the beginning of the reaction.

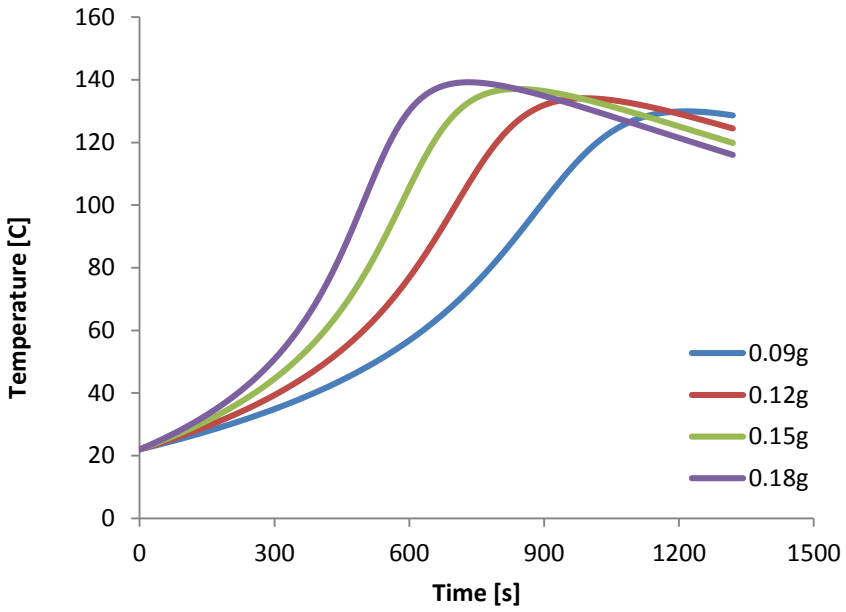

Figure 2-6 Modeling of temperature profiles under different catalyst loadings

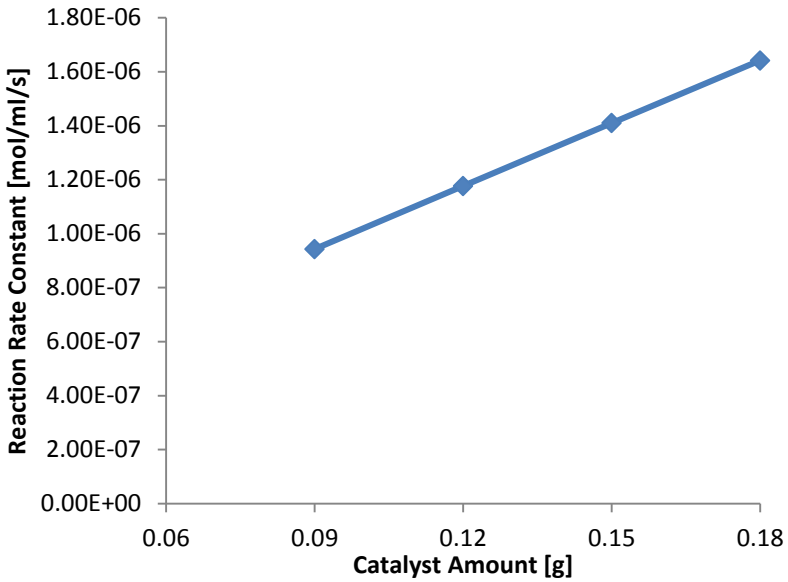

Figure 2-7 Relationship between reaction rate constants and catalyst loadings of amine based catalyst

Based on the results above, reaction rate constant is in direct proportional to the amount of catalyst loading. Larger reaction rate constant gives an earlier temperature rise and a higher peak temperature.

2.5.2 Tin Based Catalyst

Figure 2-8 presents experimental temperature profiles and modeling results of V360 gel reaction under tin catalyzed condition (Fomrez®UL-22). Different amounts of catalyst loading were used to evaluate the impact of tin catalyst and the relationship between reaction rate constant and catalyst loading amount.

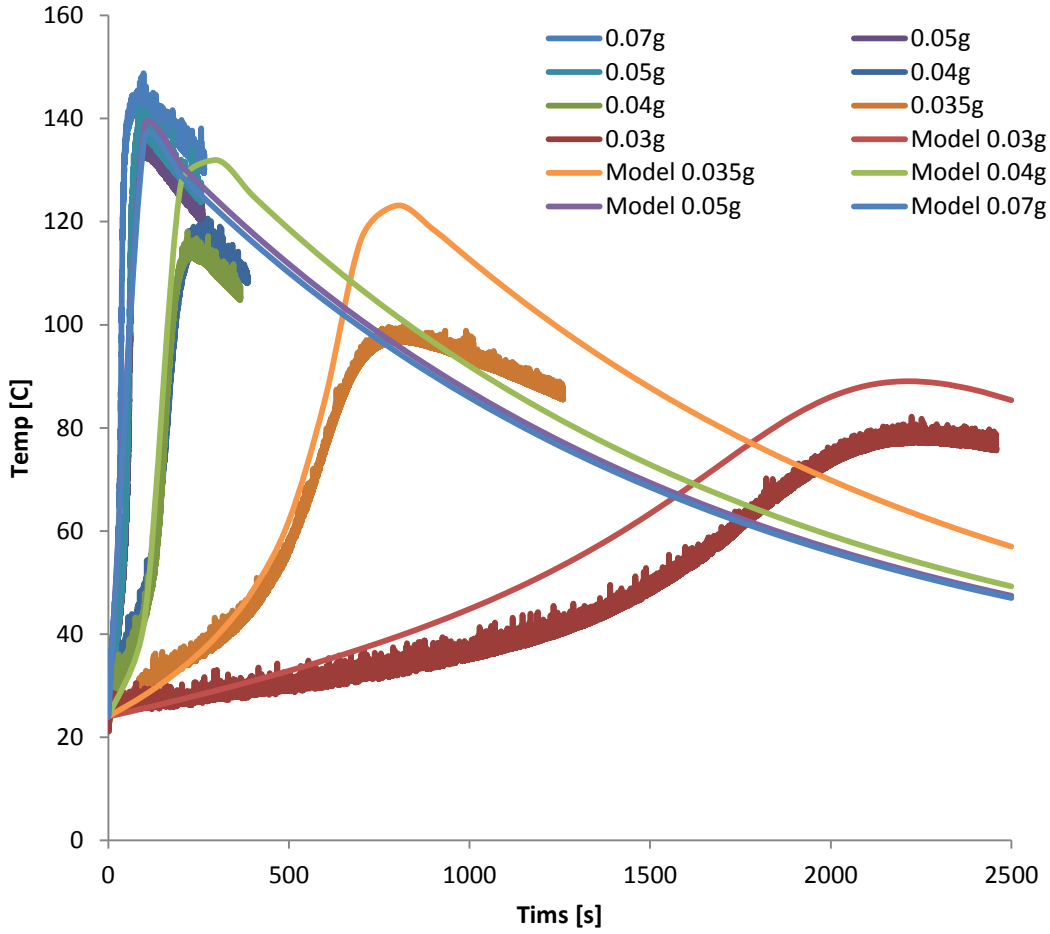

Figure 2-8 Temperature profile of V360 gel reaction and modeling results under tin catalyzed condition (Fomrez®UL-22)

Unlike the amine catalyst data of Figure 2-6, the experimental data in Figure 2-8 shows a non-direct proportional relationship between reaction rate and amount of catalyst loading. Low concentration tin catalysts have little catalysis effect and the increment in high concentration area doesn't make a significant difference since the

reaction is already over catalyzed. Therefore, a catalyst poisoning mechanism was introduced into this model. Equation 2-5 was used to calculate the effective catalyst amount based on different initial catalyst loadings. Table 2-4 presents the actual effective catalyst content respect to different initial catalyst loadings. An objective function (OF) was introduced to minimize the difference of equilibrium constants between the left side and the right side in Equation 2-5. Figure 2-9 shows the relationship between catalyst loading and reaction rate constant at the beginning of the reaction under tin catalyzed condition (Fomrez®UL-22).

Table 2-4 Effective catalyst amount respect to different initial catalyst loadings due to catalyst poisoning

Initial Cat Loading (g)	OF	Pcat (g)	Effective cat loading In System (g)
0.03	4.26612E-05	0.029558643	0.000441357
0.035	0.000890475	0.033818797	0.001181203
0.04	0.013654958	0.035999999	0.004000001
0.05	-0.005106865	0.036693601	0.013306399
0.06	0.00733688	0.036823464	0.023176536
0.07	-0.00217988	0.036876301	0.033123699

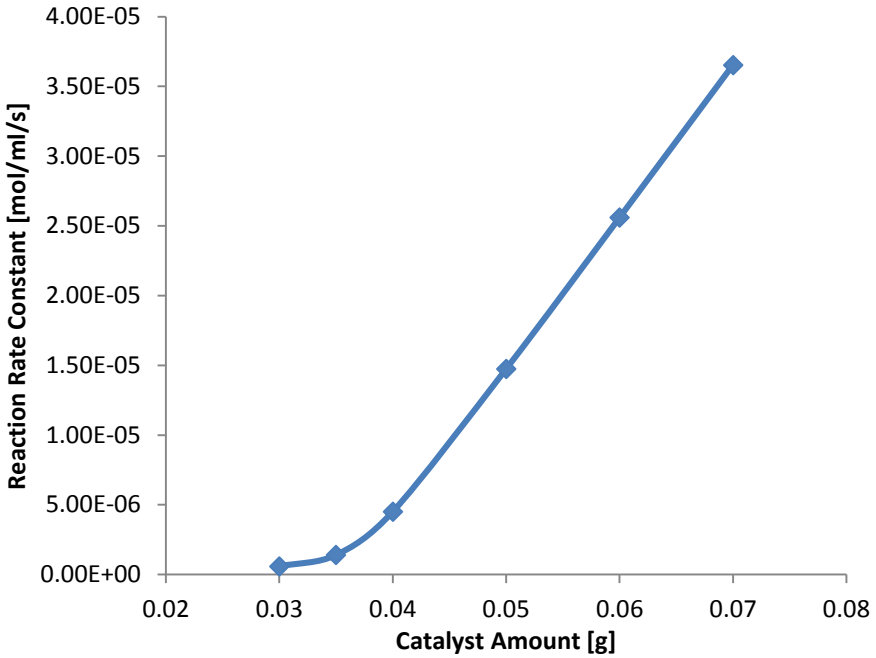

Figure 2-9 Relationship between reaction rate constants and catalyst loadings of tin based catalyst (Fomrez®UL-22)

Different from amine based catalyst, Figure 2-9 shows that the catalysis effect of tin based catalyst in low concentration is much weaker than that in high concentration. Due to the catalyst poisoning the poisoned sites can no longer accelerate the reaction with which the catalyst was supposed to catalyze, so that appropriate amount of tin based catalyst should be used to ensure the system being catalyzed but not over catalyzed.

Several kinds of tin based catalysts from Galata Chemicals LLC were tested in this study. Modeling results of temperature profile were presented in Figure 2-10 and the constants used in Equation 2-5 (K & P_0) were reported in Table 2-5 respectively. k_0 was reported in ml/(mol*s*g catalyst) and E was reported in J/mol.

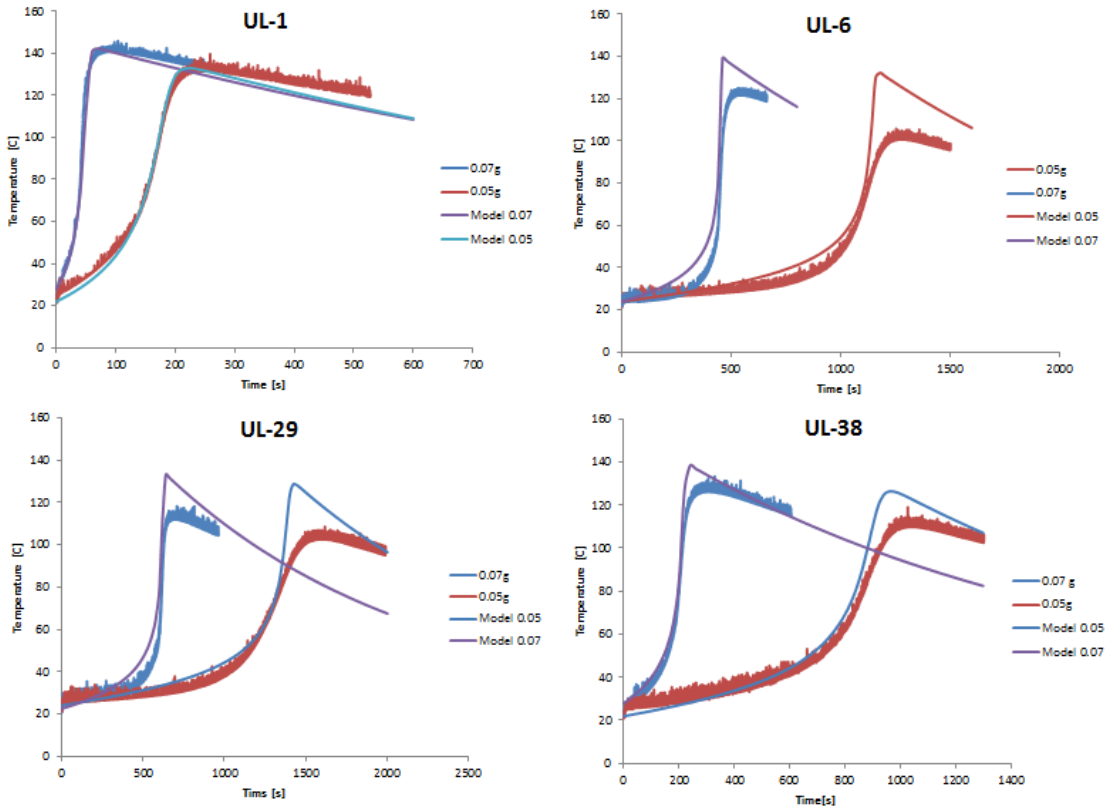

Figure 2-10 Modeling results of V360 gel reaction with different tin based catalysts

Table 2-5 Catalyst poisoning equilibrium constants and kinetic parameters respect to different tin based catalysts

	K	P0 (g)	Primary		Secondary		Hindered-Secondary	
			k_0	E	k_0	E	k_0	E
Fomrez®UL-1	9000	0.037	-	-	8000	40000	1300	50000
Fomrez®UL-6	9000	0.037	-	-	300	58000	65	82000
Fomrez®UL-22	9000	0.037	-	-	10000	46000	3000	52000
Fomrez®UL-29	9000	0.037	-	-	270	56000	60	78000
Fomrez®UL-38	9000	0.037	-	-	600	50000	150	65000

Kinetic parameters of secondary and hindered-secondary hydroxyl were evaluated based on experimental data and the results from previous study which the ratio of

secondary over hindered-secondary in V360 was fixed. The model fit assumes that all tin based catalysts having the same equilibrium constants (for poisoning) and different kinetic parameters.

Peak temperatures of modeling results are consistently higher than that of experimental data. This is believed to be due to the incomplete consumption of isocyanate. Isocyanate, which has a larger density than polyols, was observed to be in the bottom of several of the samples in an unreacted state after reaction.

When times for greater than 90% conversion take longer than about 200 seconds, isocyanate tended to settled to the bottom of the vessel. As observed by the model lines, the model parameters fit well for the onsets of reactions and are believed to be accurate. Kinetic parameters of primary hydroxyl were no reported because the reaction of primary hydroxyl with isocyanate was too fast to accurately measure by temperature profile using the existing experimental system. Ratios of relative reaction rates[22] can be used to estimate primary hydroxyl parameters and the change of catalyst amount had no obvious impact on primary hydroxyl according to both simulated and experimental results.

2.6 Conclusion

Temperature profiles of urethane gel and foam formulations were simulated using single-polyol and single-catalyst system parameters and the simultaneous solution of several ordinary differential equations that describe reactions and physical properties. This work goes beyond what has been previously attained, including: accurate simulation of mixtures of polyols based on performance of single polyols, simulation

of both water reaction and physical processes for gas formation, and accurate simulation of the impact of catalysts including the impact of catalyst concentration.

These studies validate the elementary reaction mechanism where, for a limited range of catalyst, the reaction rate is proportional to the catalyst concentration and where the non-catalystic and catalytic reactions are assumed to occur in parallel. This validated mechanism and the modeling method provided good agreement with experimental data.

Based on pure component kinetic parameters this model can be used to predict the performance of foams which have multiple combinations of isocyanate, polyols, catalysts, chemical blowing agents (such as water), and physical blowing agents (such as methyl formate) in recipes when parameters on pure component (e.g. single polyol) performance are behavior. This advantage can expedite the ability to develop new foam formulations by simulation – especially for incorporation of new bio-based polyols into formulations.

This work extended previous work to study on the impact of tin based catalysts on polyurethane foaming reaction that goes beyond what have previously been achieved, including: simulating impacts of catalysts including the impact of catalyst concentrations on reaction rates, simulating performances of tin based catalysts, and simulating impact of catalysis poison. These studies validate the elementary reaction mechanism where, for a limited range of tin catalyst, catalyst poisoning happens in the system so that the poisoned sites are not able to catalyze the reaction as they are supposed to do. After accounting for the poisoning of the catalyst, reaction rates were

proportional to the amount of catalyst loading. This poisoning modeling provided good agreement with experimental data.

A next and vital step to both simulate urethane foam formation and the foam's physical properties is to model and simulate the viscosity profiles. Preliminary data indicate that catalysts can have different selectivities for cross-linking reactions versus random reactions of monomers (as characterized by temperature); this will need to be considered as the simulation capabilities are extended.

3. SIMULATION OF ISOCYANATE CONCENTRATION PROFILES AND EMISSION IN POLYURETHANE FOAMING REACTION

3.1 Introduction

Isocyanate moieties are highly reactive with active hydrogens moieties. When this high reactivity is put on a small molecule and/or a slightly volatile molecule it can lead to adverse health effects. In a March 2014 report (140313) [23] the California Environmental Protection Agency put the spotlight on residual isocyanate content of spray foams. This could be a milestone toward eventual implementation of regulations on use of urethane spray foam insulations.

Specific perceptions that provided motivation for this report are: a) “diisocyanates are the leading attributable cause of asthma in the workplace” and b) “review found that 5-15% of polyurethane industry workers exhibit adverse health effects related to isocyanates exposure”. The report specifically mentions the following isocyanates:

- MDI
    - Generic methylene diphenyl diisocyanate (MDI) mixed isomers, Chemical Abstract Service Registry Number (CAS #): 26447-40-5
    - 4,4’-methylenediphenyl diisocyanate, CAS #: 101-68-8
- TDI
    - Toluene Diisocyanates, mixed (TDI), CAS #: 26471-62-5
    - 2,4-Toluene diisocyanate, CAS #: 584-84-9
    - 2,6-Toluene diisocyanate, CAS #: 91-08-7

- Hexamethylene-1,6-diisocyanate (HDI), CAS #: 822-06-0
- Polymeric MDI (PMDI) is not mentioned in the report

Exposure of workers to diisocyanates in the polyurethane foam manufacturing industry is well documented. However, very little quantitative data have been published on exposure to diisocyanates from the use of paints and coatings. Also, spray foam application details can vary considerably from site-to-site; and so, a fundamental approach based on quantifying emissions from the source would be useful. Therefore, trying to track the concentration of diisocyanates in a working zone and estimate re-entry time for workers are quite significant.

Curtis et al. [24] evaluated emission of 2, 4-TDI, 2, 6-TDI, and isophorone diisocyanate from a commercially available two-stage concrete coating and sealant. Diisocyanate concentrations were determined by derivatization and analysis with UV detection. However, the data differ significantly with the only other published emission data from an epoxy sealant product [25].

Simulation has found acceptance in many environmental applications because of its cost-effective implementation in applications where the size/expanse of pollution dissipation makes it very costly to collect and analyze samples. Simulation can also be very useful for applications where it is difficult to obtain representative samples. For urethane spray foams the low concentrations of isocyanates in gas phases can present sampling problems as well as the low concentrations and “trapped” nature of isocyanates in resin phases.

This paper uses simulation of the urethane foaming process to better understand

isocyanate profiles in rigid foams. The simulations are based on fitting of kinetic and physical property parameters as previously published in four published papers [19, 26-28] and multiple papers in stages of review.

Characterizing polyurethane reactions is more complex than most polymerization systems due to the monomers having multiple reaction moieties, the large number of parallel reactions that can occur, the hundreds of different oligomer and polymer products formed as reactions going to completion, and the hundreds of different formulations in use.

In addition to polymerization and blowing reactions, urethane formulations continue to react after setting due to the highly reactive nature of the isocyanate group. The urethane-forming reaction is based around moieties of isocyanate and alcohol reacting to form urethane moieties. Isocyanate reactions with water, amines, and urethane moieties are the most common side reactions that occur.

As summarized by Equation 3-1, urethane moieties react with isocyanates to form allophanate. Equation 3-1 is a more prominent reaction that can occur.

$$R_2OCONHR_1 + R_3NCO \longrightarrow R_3NHCON(R_1)COOR_2 \qquad \textbf{Equation 3-1}$$

Urethane Isocyanate Allophanate

Duff and Maciel [29] demonstrated that side reactions can play an important part in polymer crosslinking. They demonstrated that isocyanate groups continue to react after all the alcohol is consumed and that the reactions impact the polymer properties. Singh and Boivin [30] found when the dimer of 2,4-tolylene diisocyanate was reacted with alcohols at about 90°C, the corresponding diurethanes were formed, giving only traces of allophanates. Higher temperatures in the range of 125°C to 160°C and catalysts such

as triethylamine and N-methyl illorpholiile appeared to be necessary for the formation of allophanates. Querat [31] found that allophanate formation can be catalyzed by dibutyltindilaurate, but dissociation occurs at high temperature.

The rates of dissociation of allophanates are also affected by the nature of the nucleophilic agent (alcohol, amine). Heintz et al. [32] observed 5.2% - 7.9% conversion by side reactions at temperatures between 122°C and 145°C. They used ^{1}H NMR spectroscopy at 108°C to detect allophanate nitrogen present as 1.8% of the sample's nitrogen content. Lapprand et al. [33] identified that allophanates comprised 10% of the total product after 1hr of reaction at 170°C and an isocyanate index of 1. Vivaldo-Lima et al. [34] used a model to study the polymerization process where the rate of allophanate generation was proportional to the urethane-forming reaction.

If water is present, it can react with isocyanates to form urea, and the isocyanate can then further react with the urea according to Equation 3-2

$$R_1NCO + R_2NHCONHR_3 \underset{K_{eq}=\frac{k_1}{k_{-1}}}{\Longleftrightarrow} R_2NHCON(R_3)\,COOR_1 \qquad \textbf{Equation 3-2}$$

Isocyanate Urea Biuret

Delebecq, E., et al. found that this reaction tended to be equilibrium limited [35]. For systems with low water contents, urea formation is negligible. Dusek found [36] side reactions occur when isocyanate is in excess with selective catalysts. Initially, the formation of biuret was faster than allophanate. It [35] has also shown that isocyanate groups undergo homocyclization in addition to forming allophanates which is characterized as dimerization (Equation 3-3) and trimerization (Equation 3-4). These reactions happen at lower temperatures with the monomers favored at higher temperatures.

$$R_1NCO + R_2NCO \Leftrightarrow Uretdione \quad \text{Equation 3-3}$$

$$R_1NCO + R_2NCO + R_3NCO \Leftrightarrow Isocyanurate \quad \text{Equation 3-4}$$

As with the biuret-forming reaction, these reactions are equilibrium limited. When competing with reactions that are not equilibrium-limited, the product mixture will eventually be dominated by those products that are not equilibrium limited.

Recent work has shown that epoxy moieties can also participate in reaction networks of urethane formulations [37, 38]. Epoxy reactions are of particular interest for bio-based B-side components of urethane systems because they can be formed reliably and at lower cost from bio-oils like soybean oil. Little data are available on the rates and mechanisms of these reactions. Based on previous work [39, 40], the epoxy could react with isocyanate through two paths including reactions with the monomer (Equation 3-5) and oligomers (Equation 3-6).

Low isocyanate concentration:

$$R_1NCO + R_2COCHR_3 \rightarrow Oxazolidone \quad \text{Equation 3-5}$$

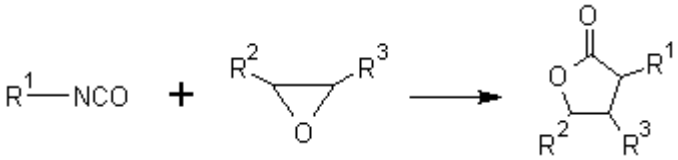

High isocyanate concentration:

$$Isocyanurate + R_2COCHR_3 \xrightarrow[Cl^-]{} Oxazolidone \quad \text{Equation 3-6}$$

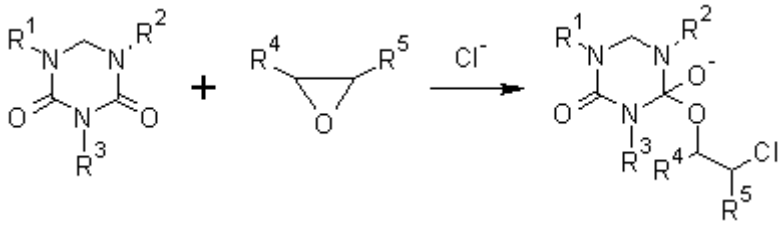

Epoxy moieties also react with alcohols and water using nucleophilic substitution

(e.g SN1) as illustrated by Equation 3-7 and Equation 3-8.

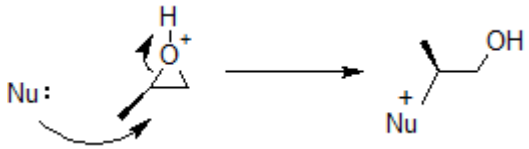

Equation 3-7

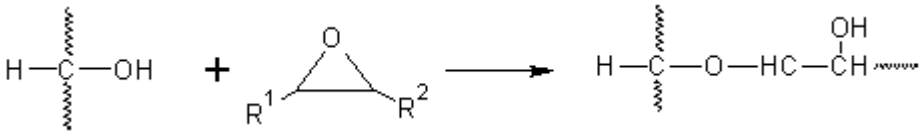

Equation 3-8

While the isocyanate-alcohol reaction takes place at reasonable rates at ambient temperature [41], the reactions of epoxy with alcohols require temperatures in excess of 100 °C for most commercial processes.

Table 3-1 summarizes reactions 1-8 including whether or not the product is equilibrium limited. The challenge of studying these reactions resides in the fact that there are multiple parallel reactions that can occur. When the reaction is free of water, biuret formation becomes negligible. The dimer and trimer forming reactions are of less interest since actual urethane form formulations will tend not to have a high excess of isocyanates, and so, the emphasis of this work is on the allophanate-forming reaction and the reactions with epoxy. The isocyanate-alcohol reaction will dominate the other reactions in urethane systems until the alcohols are substantially consumed (for isocyanate index greater than 1). The allophanate-forming reaction can be followed after the alcohol runs out.

Table 3-1 Summary of impact of potential reaction products

Products	Equation	Conclusion	Importance	Source
Allophanate	Eq.1	Major byproduct if excess isocyanate is present.	Yes	[29, 30]
Biuret	Eq.2	Only presents in systems where water is used in the formulation. It is equilibrium limited.	No	[30, 35, 36]
Uretdione Isocyanurate	Eq.3	Dimer and timer of isocyanate that are equilibrium limited. Reactions happen at lower temperatures with the monomers favored at higher temperatures	No	[30, 35]
Oxazolidone	Eq.5, Eq.6	Another main reason causing isocyanate consumed when epoxy exists.	Yes	[37, 38]
Alcohol Product From Epoxy	Eq.7, Eq.8	Could be neglect due to high reality reactivity of isocyanate-alcohol reaction and isocyanate-epoxy reaction	No	[41]

Thus, the focus of this work is on reactions 1, 5, 6, 7, and 8. While these reactions have previously been studied, this work not only studied on likely fates of unreacted isocyanate and developed experimental plan to measure reaction rates of excess isocyanate in solvents, but also optimized the model to include these side reactions and provided isocyanate concentration profiles to evaluate isocyanate emissions.

The works done by Zhao and Ghoreishi [19, 26-28] placed a high emphasis on model development with robust experimental methods, primarily temperature profiles, to assist in model development based around isocyanate-alcohol reactions. Better understandings and more accurate data on the alcohol-isocyanate reactions provide an improved foundation for studying these other reactions. Use of temperature profiles is particularly insightful at time ranges of 5 to 500 seconds where the response time of the thermocouple is fast relative to the changes in temperature and where heat losses are

relatively low as compared to heats of reaction. The previous modeling work were based on temperatures profiles; the objective of this work is to follow isocyanate concentration profiles to check the accuracy of modeling work to date and to provide insight into some of these other reactions. Use of concentration profiles (via sampling and titration) is particularly useful at times scales greater than 5 minutes and specifically for reactions that are sufficiently slow to allow quenching and titration without the related time delays impacting the analyses. The results of this work are neither presented nor intended as definitive; however, useful insight is available from the simulations to allow for more-informed decisions.

3.2 Modeling

In this study, additional equations were added into Zhao's model [19, 26-28]. Assuming reactions Equation 3-1 and Equation 3-6 are elementary, then the reaction rates can be expressed as:

$$r_1 = [NCO] \times [Urethane] \times A_1 \times e^{-\frac{Ea_1}{RT}} \quad \text{Equation 3-9}$$

$$r_6 = [NCO] \times [Epoxy] \times A_6 \times e^{-\frac{Ea_6}{RT}} \quad \text{Equation 3-10}$$

These rate expressions are based on Flory's assumption that the inherent reaction rate per functional group is independent of chain length and are based on the concentration of reactive moieties rather than concentration of compounds [42]. The modeling of these reactions is based on the solution of Ordinary Differential Equations using MATLAB's ODE45 function. Values of pre-exponential factor and activation energy were fitted based on experimental temperature profiles.

3.3 Materials and Methods

3.3.1 Materials

RUBINATE M (Standard Polymeric MDI) was the isocyanate used in this study and the petroleum-based polyols were Poly G76-635, Voranol 360 and Jeffol R315x from Huntsman Company and Dow Chemical Co. N,N-dimethylcyclohexylamine (DMCHA) and N,N,N′,N″,N″-Pentamethyldiethylenetriamine (PMDETA) were used as catalysts. Momentive L6900 was used as surfactant and TCPP was used as fire retardant.

3.3.2 Experimental Design

Gel reaction solution samples were collected and evaluated using the ASTM D2572-97(2010) standard to measure isocyanate concentrations in 1-1 g liquid samples. 1-pentanol and 2-pentanol were chosen as reagents to prevent gel formation and allow sampling at times up to 48 hours where typical urethane formulations would become solid and could not be titrated. Toluene was added as a diluent to limit the temperature increase of the reactions to temperatures more consistent with urethane systems (pentanols have lower heat capacities than typical urethane formulation polyols).

Gel reactions were performed as summarized by Zhao et al [28]. 1 gram samples were picked up from the reaction mixture and mixed with 30 ml of dibutylamine-toluene to quench the reaction by both dilution and temperature reduction. The mixture was titrated within 15 minutes after the quench. During extended-time studies, the reactions proceed about 15 min in a beaker at near-adiabatic conditions which commonly resulted in a peak temperature of about 130 °C at 3 minutes into the reaction.

After the initial 15 minutes of reaction, the alcohol had substantially reacted and heat losses exceeded any heat of reaction. Then, 1-2 grams samples were added into test tubes which were placed in an oven at the specific temperature for extended studies. The samples were then titrated at 1hr, 12hr, 24hr and 48hr to detect isocyanate content.

During the initial 3 minutes of reaction, temperature profiles were followed for the epoxy reactions. Relatively low heat transfer coefficients and relatively high heats of reaction allowed these temperature profiles to be used to characterize the reaction kinetics. Previous modeling work has provided rate constants and heat transfer coefficients which are able to characterize the isocyanate-alcohol reactions. These results provide a starting point for characterizing the reaction. Two approaches distinguish the reactions of this study from the already-characterized isocyanate-alcohol reactions. For time periods greater than 15 minutes and an isocyanate index of 2.0, the alcohol has reacted less than detectible limits and changes in isocyanate concentrations can be attributed to the reactions of Table 3-1. At time less than 15 minutes, reaction temperature profiles are compared to control experiments, the significant increase in temperature can be attributed to epoxy-related reactions.

3.3.3 Standard Test Method for Isocyanate Groups in Urethane Materials or Prepolymers

ASTM D2572-97(2010) is the standard test method for isocyanate groups in urethane materials or prepolymers. The urethane prepolymer is allowed to react with an excess of di-n-butylamine in toluene. After the reaction is complete, the excess of di-n-butylamine is determined by back titration with standard hydrochloric acid.

The following procedures were used in the isocyanate titration:

1. Weigh to 0.1 g a specimen containing approximately 1.1 milliequivalents of NCO (for example, 1.0 g of prepolymer containing approximately 5% NCO) in a 250-mL Erlenmeyer flask.
2. Add 25 mL of dry toluene (If the polymer is insoluble, add 10mL of dry, analytical grade acetone to the toluene.), place a stopper in the flask, and swirl by hand or on a mechanical agitator to dissolve the prepolymer. Solution may be aided by warming on a hot plate.
3. Using a pipet, add 25.00 mL of 0.1 N di-n-butylamine solution and continue swirling for 15 min with stopper in place.
4. Add 100 mL of isopropyl alcohol and 4 to 6 drops of bromphenol blue indicator solution. Titrate with 0.1 N hydro-chloric acid to a yellow end point.
5. Run a blank titration including all reagents above but omitting the specimen.

Calculate the NCO content as follows (Equation 3-11):

$$\text{NCO, \%} = \frac{[(B-V)*N*0.0420]}{W} * 100 \qquad \textbf{Equation 3-11}$$

where:

B = volume of HCl for titration of the blank, ml,

V = volume of HCl for titration of the specimen, ml,

N = normality of HCl,

0.0420 = milliequivalent weight of the NCO group, and

W = grams of specimen weight, g.

3.4 Results and Discussion

3.4.1 Isocyanate-urethane Reaction

Isocyanate titration was performed during gel reaction samples that had not gelled; similar sampling and analysis is not possible with foam-forming samples which are tacky. In the first step, single polyol and single catalyst were chosen to react with isocyanate to study the fundamentals of side reactions. The isocyanate index was set at 1.5 to allow enough excess isocyanate for reaction with urethane. Table 3-2 provides the recipe used for isocyanate profiling studies.

Table 3-2 Recipe used for isocyanate profiling studies (poly G76-635)

B-side Materials	Weight/g	Moles of functional groups
Poly G76-635	25.00	0.2831
Dimethylcyclohexylamine(Cat8)	0.12	
Momentive L6900	0.6	
TCPP	2	
A-side Material		
RUBINATE M	57.33	0.4247
Isocyanate Index	1.5	

Figure 3-1 shows the “titration results” of isocyanate concentration to decrease rapidly at 400 seconds when the system temperature reached about 100°C. The isocyanate concentration tended to zero at later time stage. Even extensive effort to crush and mix the solid polymer would not provide a better result at the higher conversions. It was concluded that the titration samples after 400 seconds did not completely dissolve in the toluene solvent which caused the titration results to be unreliable.

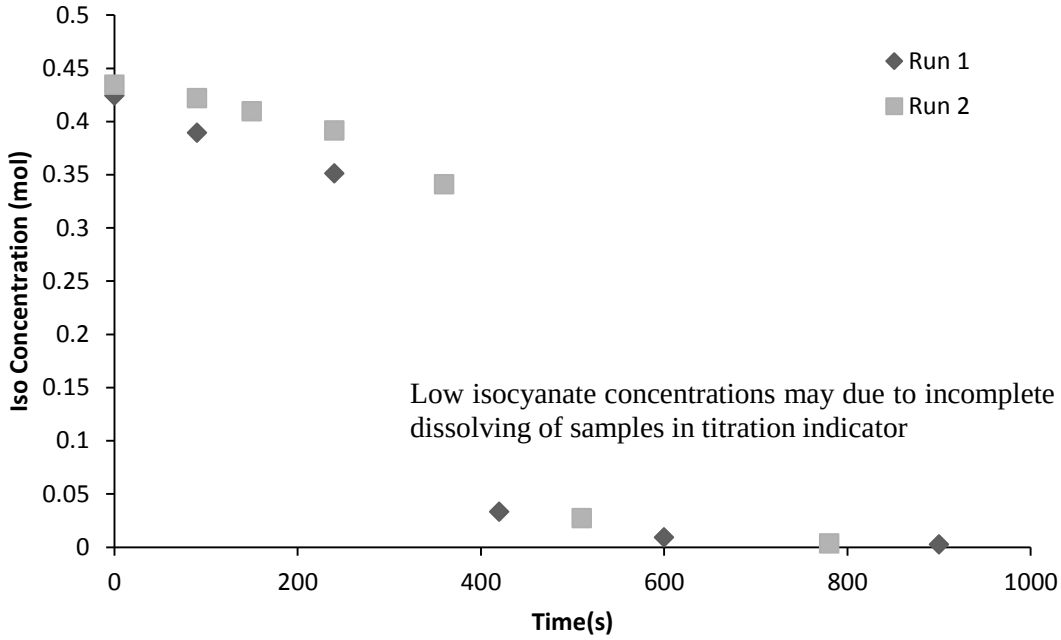

Figure 3-1 Isocyanate concentration profile for reaction of poly G76-635 with PMDI during gel reaction process

An alternative one-functional alcohol (1-pentanol) was then selected to react with isocyanate to avoid issues related to formation of solid phases where unreacted isocyanate was not accessible for titration. Extra toluene (20% in volume) was added into the reactants to avoid overheating which would cause the pentanol boil. Table 3-3 lists the recipes with 1-pentanol or 1-pentanol/epoxy for isocyanate titration.

Table 3-3 Recipes of gel reaction for evaluating iso-urethane and iso-epoxy kinetics parameters

B-side Materials	**Weight/g**		**Moles of functional groups**	
	1-pentanol recipe	Epoxy recipe	1-pentanol recipe	Epoxy recipe
1-pentanol	11.50	11.500	0.130	0.130
Epoxy oil	0.000	3.000		0.013
Cat8	0.120	0.120		
Momentive L6900	0.600	0.600		
TCPP	2.000	2.000		
A-side Material				
RUBINATE M	35.300	35.300	0.260	0.0260
Toluene (solvent)	10.440	10.440		
Isocyanate Index(NCO/OH)	-		2.000	2.000

To focus on the reaction between excess isocyanate and urethane, the isocyanate index was set to be 1.9-2.0. Reacting samples were kept warm in an oven (50°C) to reduce heat transfer to surroundings which could extend time for isocyanate to react with urethane. The study emphasized profiles after 15 minutes where all the alcohol had reacted to completion (in about 3 minutes) and the isocyanate concentration could be followed over a course of hours and days in a mixture isolated from moisture in the air.

In theory, if the reaction between isocyanate and urethane does not happen, there should be about 0.125 moles isocyanate left in the system. Figure 3-2 shows isocyanate titration results in 48 hours period.

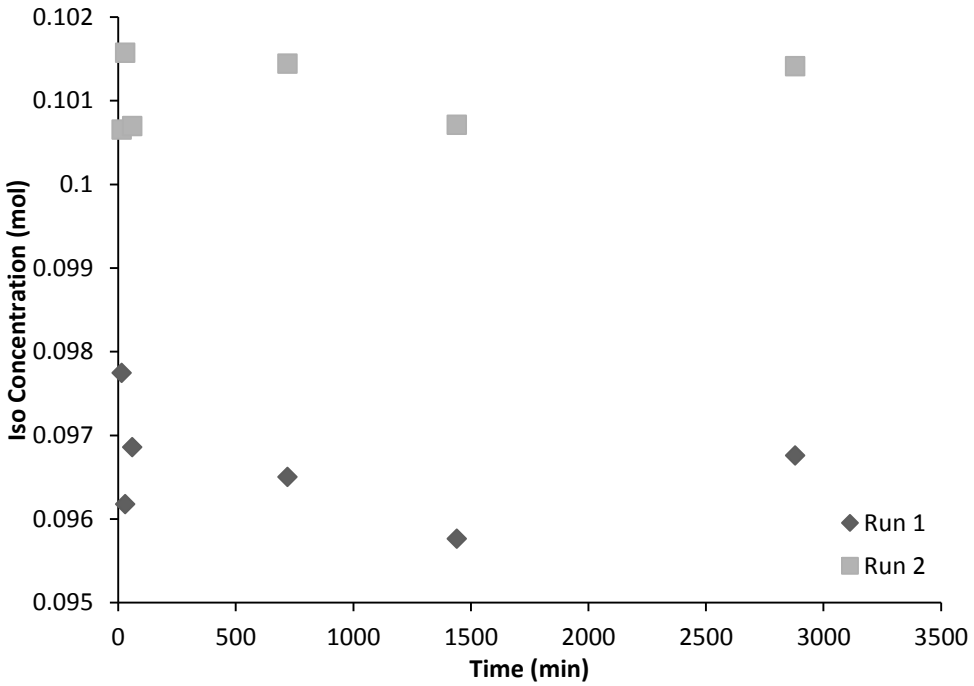

Figure 3-2 Long-term isocyanate concentration profile for reaction of 1-pentanol with PMDI during gel reaction process

The concentration of isocyanate tended to a constant value about 0.1 moles after 15 minutes. The deviations in the figure were within experimental error since the

concentration differences were quite small (<0.5%) compare to the initial concentration of isocyanate. It indicated that there was negligible isocyanate reaction during this 48 hour period.

The excess isocyanate apparently reacted with urethane within 15 minutes of the urethane-forming reaction since the isocyanate concentration was lower than what would be consumed with stoichiometric alcohol reaction. Based on these results it was concluded that isocyanate titration must be performed in the time range between 0 to 15 minutes without catalysts and oven heating to characterize the isocyanate-urethane reaction.

Figure 3-3 shows isocyanate titration results within 15 minutes. As illustrated by Figure 3-2 and Figure 3-3, the polyurethane foaming reaction can be characterized into two regimes. The first regime is where rates are dominated by the reaction between isocyanate and alcohol moieties. An initial rapid reduction in isocyanate concentration is observed during the first 5 minutes due to this regime (Figure 3-3). Commercial urethane reaction processes are typically designed around having adequate reactivity during the first two minutes of reaction to set the polymer—this is achieved through the use of catalysts. The final value of isocyanate concentration approaches a relatively constant value at about half of the initial isocyanate concentration which is consistent with the isocyanate index of 2.0. The second regime applies to systems with excess isocyanate and is dominated by the reaction between isocyanate and urethane moieties (Figure 3-2).

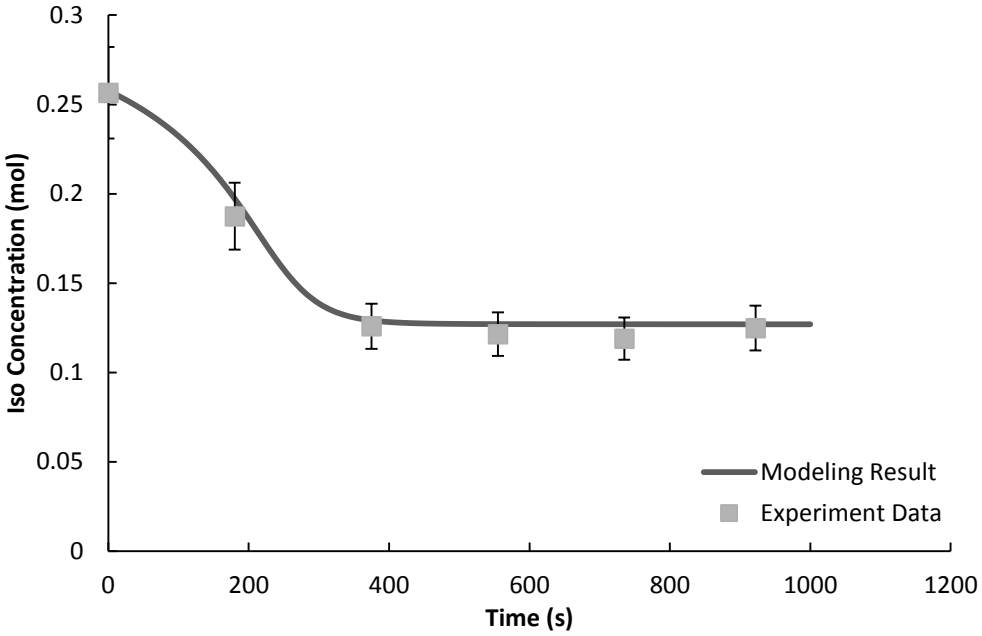

Figure 3-3 Short-term isocyanate concentration profile for reaction of 1-pentanol with PMDI during gel reaction process

The gel reaction kinetic parameters from previously published work [19, 26] were used to predict isocyanate concentration modeling result without any modifications (model line of Figure 3-3). The modeling results match the experimental titration data well. This further validates the model and parameters which to this point were based only on temperature profiles.

Extended time studies of the 1-pentanol system are summarized by Figure 3-4 and Figure 3-5 at 80 ˚C and 110 ˚C where the time scale is in minutes. Model curves are superimposed with the kinetic parameters reported in Table 3-4. The modeling results were based on a rate expression that is first order in both isocyanate and urethane moiety concentrations. The tertiary amine catalyst has significant influence on this reaction.

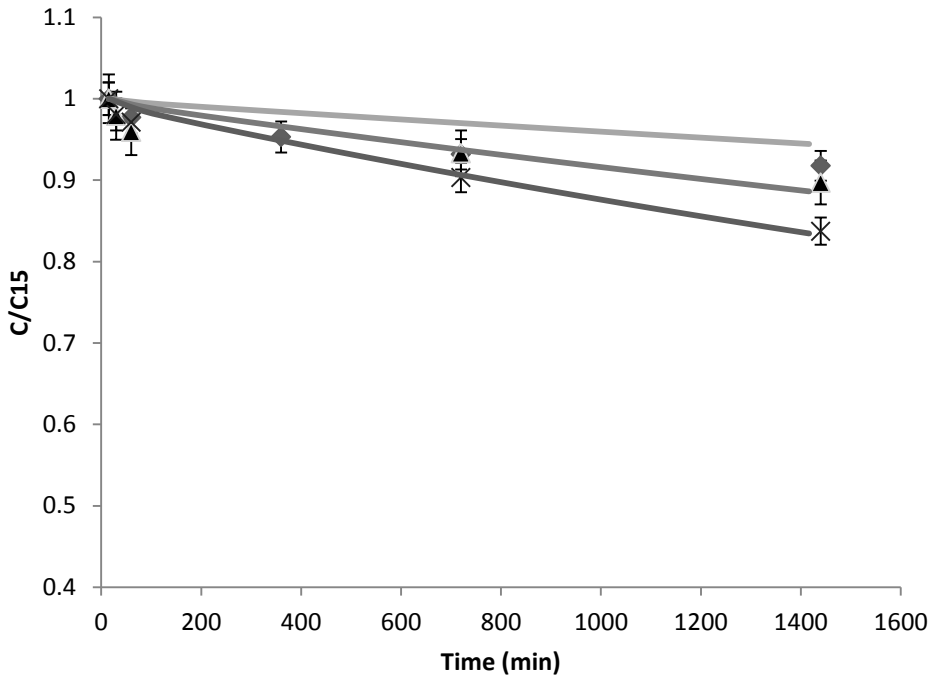

Figure 3-4 Extended time isocyanate reaction profile with fitted model for reaction of 1-pentanol with PMDI at 80°C with different catalysts. C15 is the concentration of isocyanate functional groups at 15 min of reaction. Symbols "▲", "x" and "♦" represent experiment data with Cat5, Cat8 and blank control.

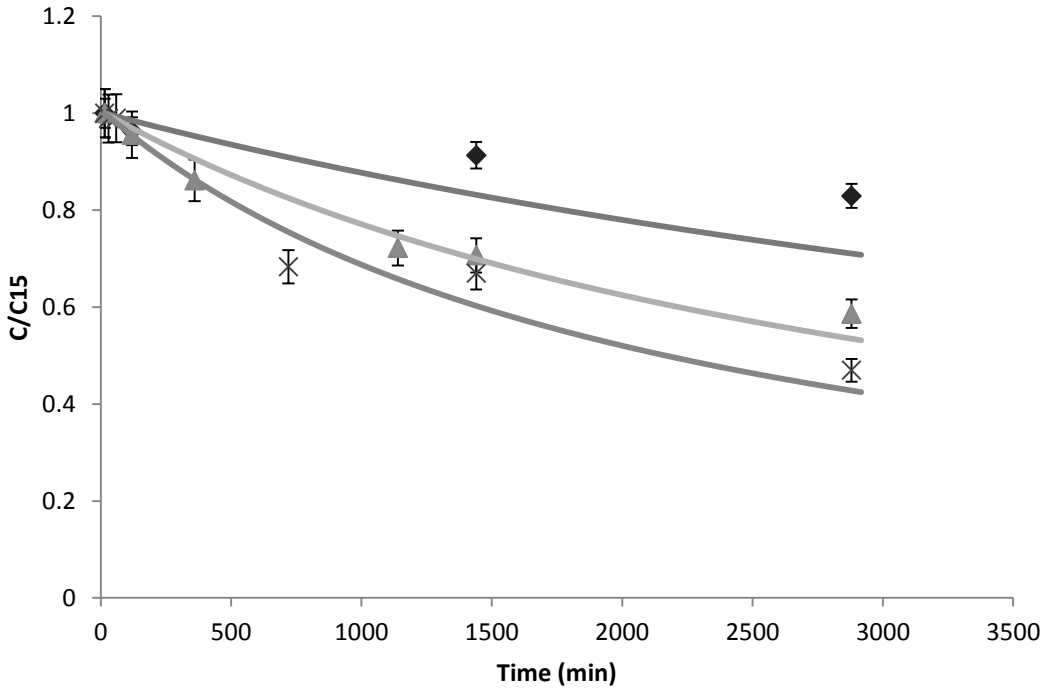

Figure 3-5 Extended time isocyanate reaction profile with fitted model for reaction of 1-pentanol with PMDI at 110°C with different catalysts. Symbols "▲", "x" and "♦" represent experiment data with Cat5, Cat8 and blank control.

Table 3-4 Kinetic parameters of isocyanate-urethane reaction

	Catalyst loading (g)	k_0 ml/(mol*s*g catalyst)	**E**(J/mol)
Blank	0	0.000015	47250
Cat5	0.12	0.01	45000
Cat8	0.12	0.02	45000

Figure 3-6 summarizes reaction profiles for reactions of polyol G76-635 with PMDI at different isocyanate indices. The model, based on parameters of Table 3-4, is able to accurately account for changes in isocyanate index at values between 1.1 and 2.0.

As with the simple alcohols, the reaction parameters as previously determined from temperature profiles effectively describe the isocyanate reaction profile for poly G76-635, except at conversions greater than about 50%. At these higher conversions, the polymer begins to set with very high viscosities transitioning to solid polymers. As with the results of Figure 3-1, some of the data after 400 seconds in Figure 3-6 are influenced by inefficient attempts at titrating isocyanate moieties trapped in solid matrices. The model is believed to be more accurate than the titration results after 400 seconds.

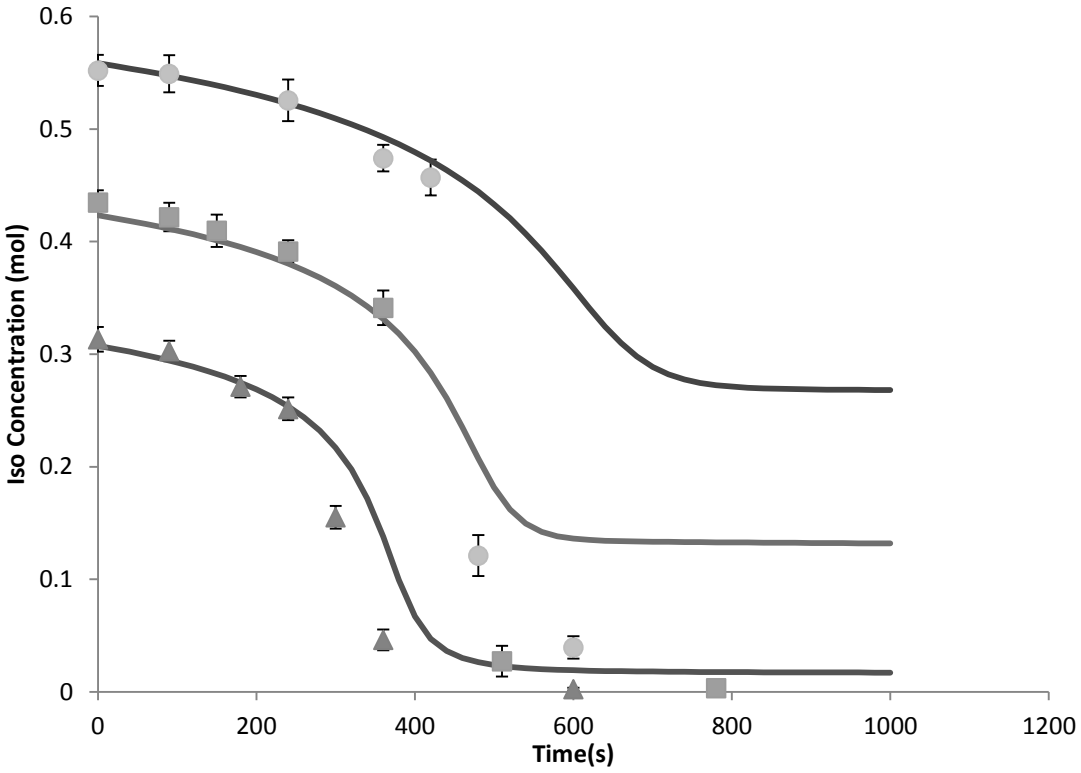

Figure 3-6 Isocyanate reaction profile with fitted model for reaction of poly G76-635 with PMDI at three isocyanate indices. Symbols "▲", "■" and "●" represent experiment data with isocyanate index=1.1, 1.5 and 2.0.

3.4.2 Isocyanate-epoxy Reaction

Figure 3-7 shows the experiment and modeling fitting result of the urethane formulation in the presence of epoxidized soybean oil and Cat8 catalyst.

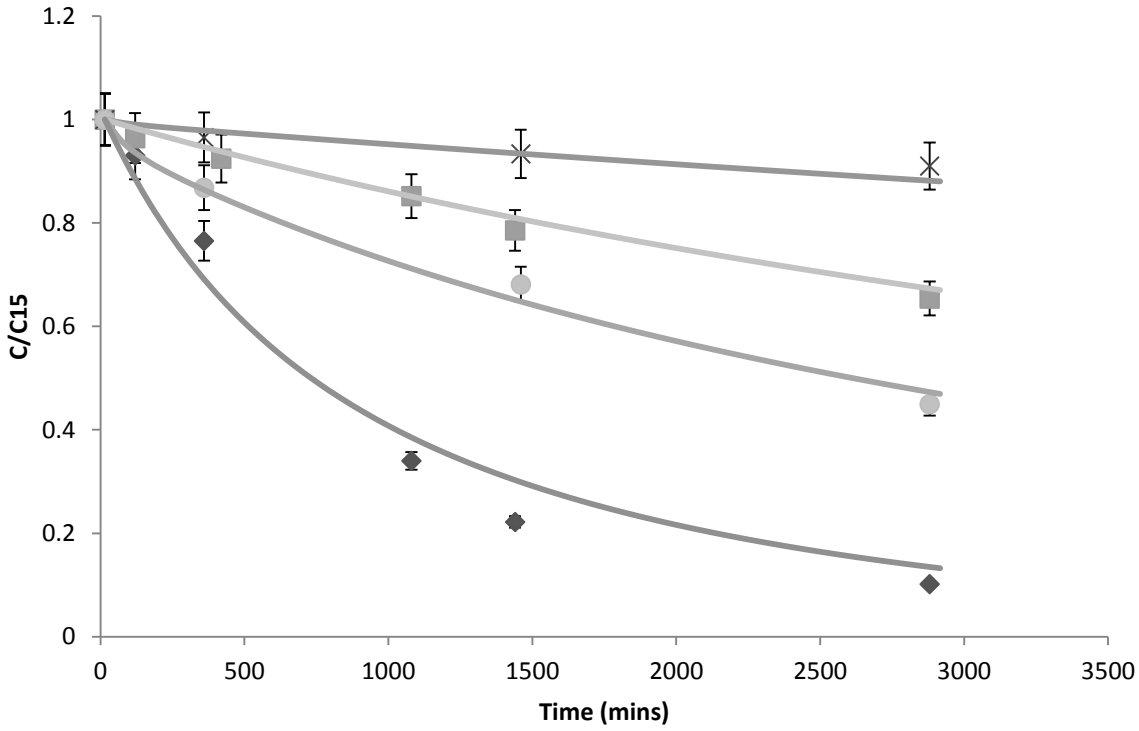

Figure 3-7 Isocyanate concentration profiles with fitted models for reaction of 1-petanol and Epoxy oil with PMDI at an index of 2.0 under different temperatures. Symbols "×" and "■" represent experiment data of reaction without any catalyst at 80°C and 110°C. "●" and "♦" represent experiment data with Cat8 at 80°C and 110°C.

A comparison of the Figure 3-7 profiles with those of Figure 3-4 and Figure 3-5 illustrates that isocyanate have a greater tendency to react with epoxies than with urethanes. This provides evidence that epoxy monomers in a urethane formulation can lead to increased crosslinking as a result of reactions that occur during the hours and days after the initial setting of the urethane polymer. For gel reactions with epoxy present at 80°C, the viscosity of the mixture was observed to continuously increase during the 48 hours of reactions. At 110°C the system remained as liquid when no catalyst was used but formed a solid elastomer in the presence of Cat 8. No gels were observed for the reaction mixtures at similar conditions in the absence of epoxy moieties (ie. where isocyanates reacted with urethanes).

From a polymer device engineering perspective, an adequate amount of alcohol

moiety must be present to set the polymer, but after the polymer is set the epoxy can impact properties and enhance performance (for certain applications) during a curing period of hours and days.

Table 3-5 summarizes the kinetic parameters of isocyanate-epoxy reaction used by the model to estimate concentration profiles. Within experimental error, the reactivity of the isocyanate moieties with urethane moieties is independent of whether the isocyanate is on PMDI or on a urethane polymer.

Table 3-5 Kinetic parameters of isocyanate-epoxy reaction

	Catalyst loading (g)	k_0 ml/(mol*s*g catalyst)	**E**(J/mol)
Blank	0	0.000001	60000
Cat5	0.12	0.017	55000
Cat8	0.12	0.03	55000

The results indicate that within the time frames of urethane foaming processes the impact of the allophanate-forming reaction is negligible. As a result, the generation of heat and increased degree of polymerization that are possible with this reaction can be ignored in the foaming simulation during the timeframe when the polymer is set. During curing time, increased crosslinking could impact properties and performance if excess isocyanate is used in the formulation.

The results from these studies enable the investigation of the following sections on vapor pressures of isocyanate monomers in urethane formulations.

3.4.3 Isocyanate Emission

The vapor pressure of pure isocyanates can be estimated by the Clausius-Clapeyron (Equation 3-12) and the Antoine (Equation 3-13) Equations.

$$ln\frac{P_2}{P_1} = \frac{\Delta H_{vap}}{R}\left(\frac{1}{T_1} - \frac{1}{T_2}\right)$$ Equation 3-12

Table 3-6 lists reported vapor pressure information of different isocyanates. TDI and HDI have much higher vapor pressure at the same temperature, indicating that they will be more problematic during application.

Table 3-6 Vapor pressure of pure isocyanates

	4,4'-MDI	2,4-TDI	HDI
Vapor pressure (mmHg)	0.000005 (20°C)	0.01 (25°C)	0.05 (25°C)
Enthalpy of vaporization (J/mol)	90000	60000	49000

$$\log P = A - \frac{B}{C+T}$$ Equation 3-13

Table 3-7 lists Antoine Equation Constants of TDI and MDI in different temperature ranges [43, 44]. The data of HDI is not available. MDI-2 results have higher values in vapor pressure than MDI-1, and therefore will be used in the simulation as a worse condition.

Table 3-7 Antoine Equation Constants of isocyanates

	TDI (P-bar, T-K)	MDI-1 (P-bar, T-K)	MDI-2 (P-mmHg, T-C)
A	4.59647	2.41991	6.32463
B	2064.243	969.926	1923.1995
C	-75.176	-253.28	165.068
T	293-443	442-530	196.12-446.87

Based on isocyanate concentration profiles and vapor pressure data over temperature, the partial vapor pressure of isocyanate in gas phase can be estimated by Raoult's law (Equation 3-14).

$$P_i = P_i^* * x_i$$ Equation 3-14

where P_i is the partial vapor pressure of the component in the gaseous mixture (above the solution), P_i^* is the vapor pressure of the pure component, and x_i is the mole

fraction of the component in the mixture (in the solution). The OSHA Permissible Exposure Limit (PEL) of isocyanate in general industry is 0.02 ppm, about 2E-8 atm. Figure 3-8 presents partial vapor pressure of isocyanate and temperature profiles over time during a control foaming reaction using MDI. The results from Antoine Equation have higher values than that from Clausius-Clapeyron Equation, and therefore can be used to compare with published regulations as the worst case condition. It is important to recognize that the vapor pressure profiles of Figure 3-8 are only made possible with concentration and temperature profiles that are only possible based on both the simulation and newly acquired kinetic parameters as reported in the previous section.

The highest emission occurred when the peak reaction temperature was reached and the value was about 0.00025 atm. As the temperature cooled the partial vapor pressure of isocyanate decreased and proceeded below the limitation after 4000 seconds.

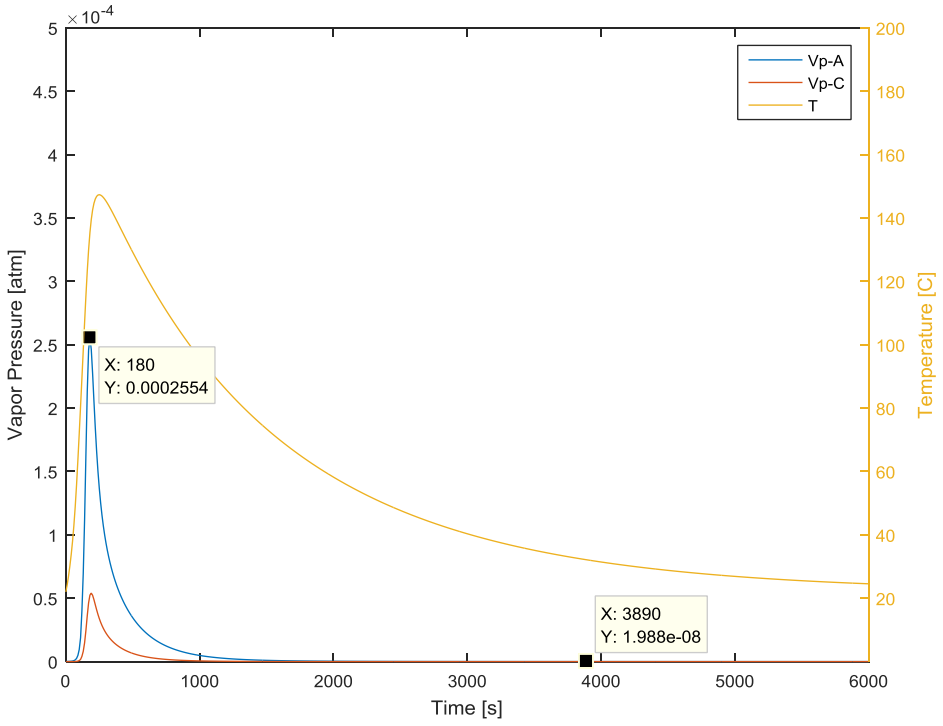

Figure 3-8 Partial vapor pressure of isocyanate and temperature profiles over time during a control foaming reaction using MDI. The blue line is calculated based on Antoine Equation and the red line is based on Clausius-Clapeyron Equation.

Figure 3-9 compares partial vapor pressure results of MDI, TDI and HDI with the OSHA Limit indicated by the dashed line. The highest emissions of TDI and HDI also occurred around the peak temperature and the values were much higher than that of MDI. And the vapor pressures were still beyond the limitation even after 6000 seconds. Therefore, TDI and HDI were not recommended in spray foam applications.

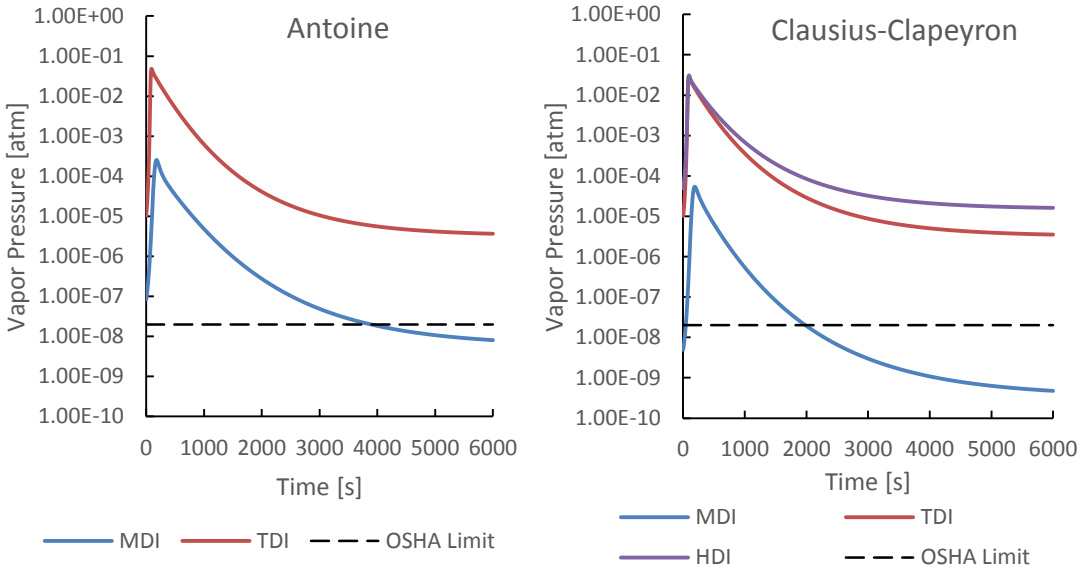

Figure 3-9 Comparison of partial vapor pressure between MDI, TDI and HDI over OSHA limit. The left graph is based on Antoine Equation and the right graph is based on Clausius-Clapeyron Equation.

PMDI (oligomerized MDI) is not able to be simulated since vapor pressure data is not available. However, with certainty the vapor pressure of PMDI would be even less than MDI. It must be emphasized that the MDI results are worst-case scenario. The qualitative results of PMDI and MDI vapor pressures, and exposure, being the least are accurate based circumstantial evidence related to the lower risk of becoming sensitized to PMDI and MDI versus TDI. The qualitative results indicating a peak in exposure due

to the combination of temperature and monomer concentration is soundly founded in the science behind this modeling.

Figure 3-10 presents partial vapor pressure of isocyanate for foams with different isocyanate indices. The results indicate that a higher isocyanate index leads to more isocyanate emission and that takes longer time to reach the OSHA safety limit. However, low indices can result in incomplete reacted alcohols and poor foam qualities. Therefore, a proper isocyanate index is very important in designing a foam recipe.

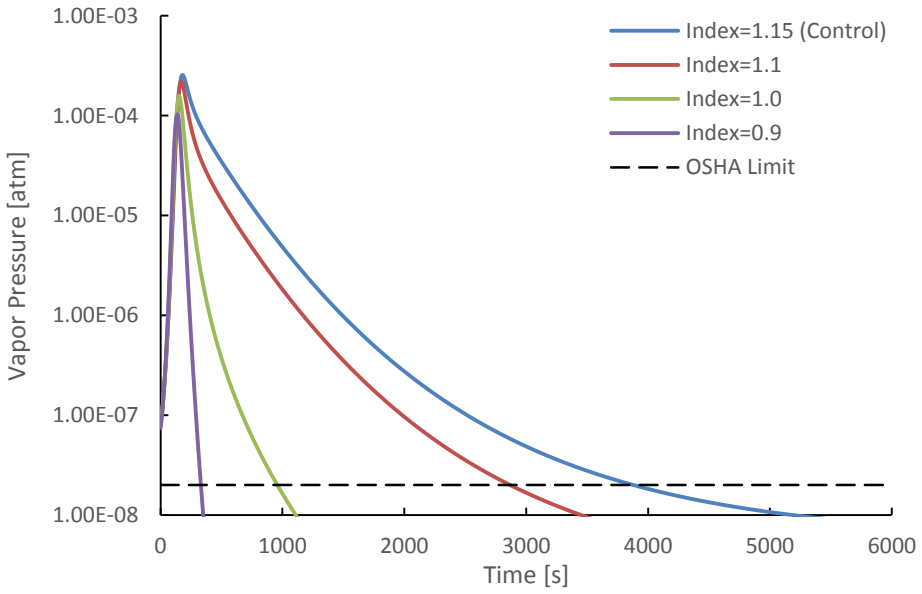

Figure 3-10 Partial vapor pressure of isocyanate for foams with different isocyanate indices

A factor not taken into account in these simulations is that with the setting of the urethane polymer (gel point, tack-free time), mass transfer rates in the resin phase rapidly decrease by orders of magnitude. The gel point time of the formulations of Figure 3-9 and Figure 3-10 are 70s for HDI/TDI and 110s for MDI. At times subsequent to the gel point, there may be a thermodynamic driving force for isocyanate monomer vapor pressure, but these monomers are unable to reach the resin surface and escape into the air surrounding the foam before they are chemically bound to the non-volatile

urethane polymer. Once the monomers are bound to the polymer, any remaining isocyanate moieties of the solid resin will react to extinction.

3.5 Conclusion

Reactions of isocyanates in urethane formulations subsequent to complete reaction of alcohols were studied, and the kinetic parameters for these reactions were incorporated into simulation software. The revised simulation allowed isocyanate concentration profiles and isocyanate monomer partial pressures to be estimated from start of the foaming process until hours subsequent thereof.

This work has several interesting findings going beyond what have been previously achieved, including:

- Modeling results of isocyanate concentration profiles in urethane-forming reaction systems matched the experimental data well and indicated that the previously reported reaction kinetics parameters were reasonable.
- Allophanate-forming and other side reactions have a negligible impact on heat generation and degree of polymerization during the first three minutes of reaction for typical urethane production; however, their formation can impact the polymer structure in the hours after the initial urethane-forming processes and are likely critical in curing and obtaining peak performance from urethanes.
- Reaction with active hydrogen on urethane may be as important as moisture in air for extinction of isocyanate moiety, especially since moisture from air will not readily penetrate the cured resin phase.

- Reaction of isocyanate with epoxy moieties was observed to have a minor impact in the early timeframe and have significant impacts on crosslinking and gel formation during longer timeframes (0.5-12 hours after setting of polymer). It indicates that epoxy co-reagents can be used to reduce isocyanate emissions.
- Peak emissions of isocyanate monomers (by evaporation) occur at times of 50-200 seconds after which emissions drop rapidly.
- For MDI, vapor pressure emissions (not including what has already evaporated) fall below OSHA limits after 4000 seconds based on a model with no resin phase mass transfer limits. With mass transfer limits, it is likely that the emissions fall below OSHA limits after 400 seconds.
- Of the monomers MDI, TDI and HDI, MDI has advantages related to lower vapor pressures as pertinent during application. The highest emission of MDI is estimated to be only 0.00025 atm while that of TDI/HDI could reach 0.03-0.05 atm. PMDI will have lower emissions than MDI.
- Among the most important parameters that can be selected to ensure low gas phase isocyanate concentration are: a) choice of isocyanate (preference of PMDI/MDI), b) a proper isocyanate index (about 1.10, the lower the better but not less than 1.0), c) use of other additives (e.g. epoxy co-reagents), and d) formulation to reduce peak reaction temperature.

4. MODELING IMPACT OF SURFACTANTS ON POLYURETHANE FOAM POLYMERIZATION

4.1 Introduction

The polyurethane foaming process involves two competing reactions (gel reaction and blow reaction). The gel reaction involves the reaction of an isocyanate group with an alcohol group to give a urethane linkage. In the blow reaction, an isocyanate group reacts with water to yield a thermally unstable carbamic acid which decomposes to give an amine functionality, carbon dioxide, and heat [2, 45-47]. The carbon dioxide gas will provide volume for bubble expansion and occupy over 95% of the final volume of the foam product [48]. Figure 4-1 shows the four stages of the foaming process of flexible foams:

(1) Bubble generation and growth,

(2) Packing of the bubble network and cell window stabilization,

(3) Polymer stiffening and cell opening,

(4) Final curing [49].

In rigid foams, most of the cells or bubbles are not broken; they resemble inflated balloons or soccer balls, piled together in a compact configuration. Both the closed cells and the solid resin walls contribute to the final strength of the rigid foam.

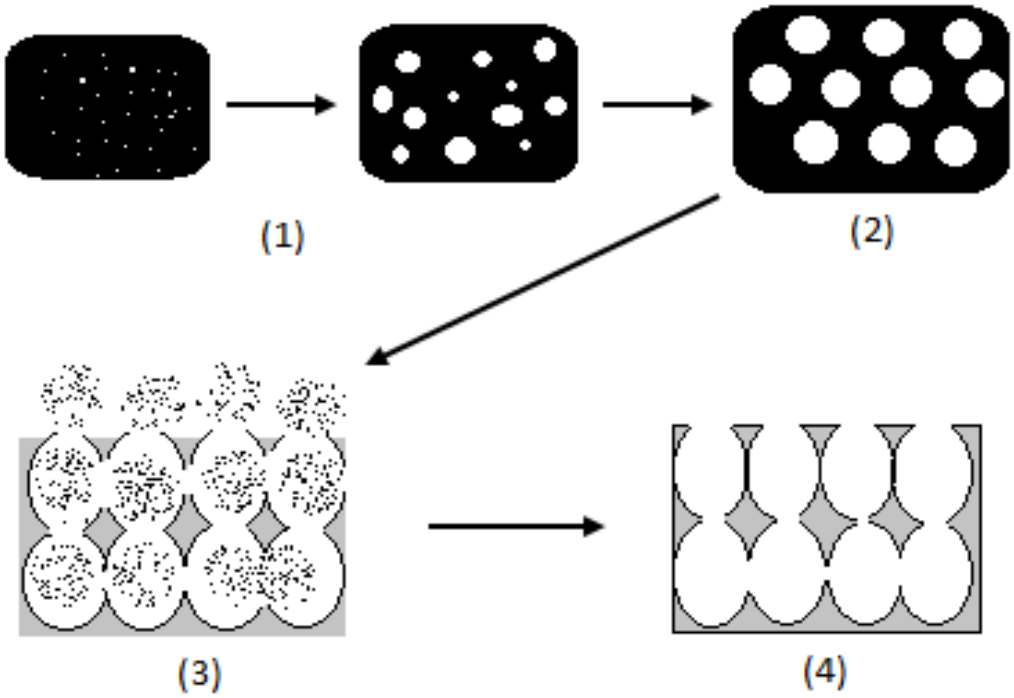

Figure 4-1 Macroscopic view of different stages during foaming of flexible foams

Silicone surfactants, which consists of a polydimethylsiloxane (PDMS) backbone and polyethylene oxide-co-propylene oxide (PEO-PPO) random copolymer grafts, are used as surfactants in polyurethane foaming systems [50]. Figure 4-2 shows the structure of a typical silicone surfactant used in polyurethane foaming systems. It was shown that these surfactants do not alter the reaction kinetics in the polyurethane foaming process [51]. A foaming system in absence of these surfactants will often experience catastrophic coalescence and foam collapse.

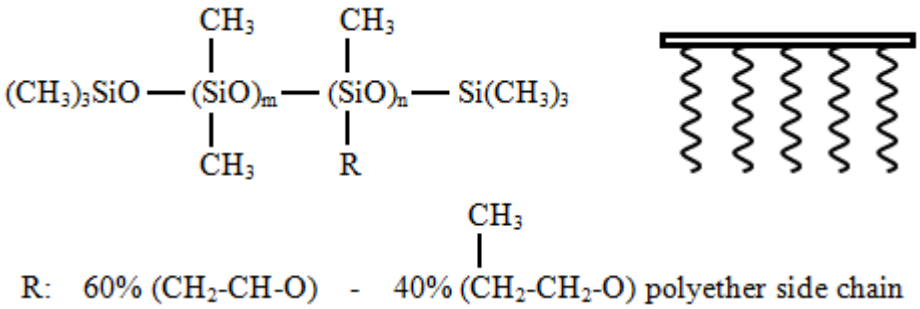

Figure 4-2 Structure of a typical silicone surfactant used in polyurethane foaming systems

These surfactants concentrate at the air-resin interface and assist with both bubble generation and bubble/cell stabilization in the polyurethane foam-forming process. The mechanical properties of the cured polyurethane foam, such as air permeability and foam cell size, are affected significantly by the structure of the silicone surfactant used in the formulation [48]. Surfactants with higher silicone content will provide lower surface tension and thus help increase the number of air bubbles introduced during mixing. Entrain gases (e.g. nitrogen) in the liquid serve as the starting point for foam cell growth. As a result, the cured polyurethane foam made with higher silicone content surfactant has a smaller bubble size. It is also shown that silicone surfactant can reduce the cell "window" drainage rate due to the surface tension gradient along the cell window.

The major role of silicone surfactants in rigid formulations are cell size control (providing a fine-celled structure with a narrow cell size distribution) and emulsification. A significant amount of gravitational and surface energy is adsorbed during foam formation. In polyurethane foams this energy is provided by high shear mixing and the release of chemical energy during the formation of the polyurethane.

The earliest interfacial process is the initial formation of bubbles in the liquid. Kanner and coworkers demonstrated that there is no spontaneous nucleation of the bubbles in polyurethane foams; the bubbles have to be stirred in [52]. These initial bubbles are small, their diameters being on the micrometer scale. Once bubbles have formed, they must remain stable during their growth phase. As CO_2 gas is formed in the blowing reaction, it expands these tiny bubbles. They can also expand when

auxiliary blowing agents such as pentane volatilize. The expansion of the bubbles increases the overall surface area; the total surface energy absorbed can be lessened by reducing the energy per unit area of the liquid (or equivalently, the surface tension). In polyurethane foams, the surface tension of the liquid is reduced by the addition of silicone surfactants. Figure 4-3 shows the surface tension isotherm which is the dependence of σ on lnC [53], where σ is the surface tension of the solution, and C is is the concentration of surfactant. The surface tension of the solution decreases with increase of the concentration of surfactant molecules in the system. The concentration at which the micelles formation starts is called critical micelle concentration (cmc). For C lower than the cmc, surfactants are distributed between the bulk of the solution and the surface. After C reaches cmc, all added 'excess' surfactants form micelles so that the bulk concentration of the individual surfactant molecules is constant and equal to the cmc. The surface concentration also reaches the saturation level.

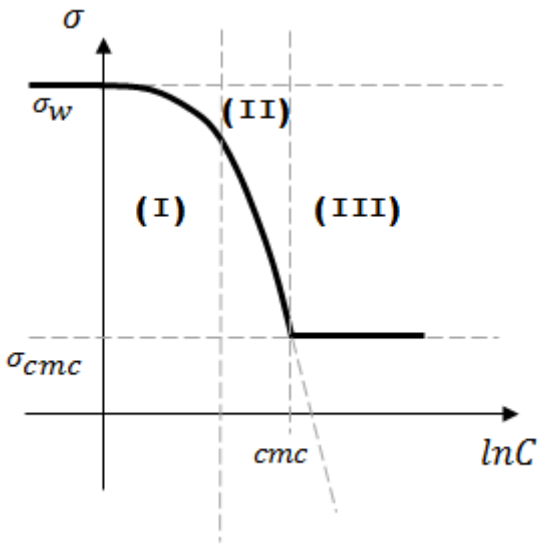

Figure 4-3 Schematic representation of typical surface tension isotherm of water/surfactant solution

As the surface tension decreases, more air bubbles per unit volume of solution were

generated in the system. The energy required to generate the bubble surface with radius r is $4\pi r^2\sigma$. Surfactants with higher silicone/polyether ratios will give a lower surface tension value and thus reduce bubble generation energy. As a result, a higher bubble count was obtained after mixing for systems with a lower surface tension. For a molded foam, at a fixed energy input, reduction of the surface tension of the liquid results in the formation of more and necessarily smaller bubbles as the available surface area is increased. For a free-rise foam, a reduction in surface tension can result in an increase in foam volume and/or a decrease in bubble size. It has been shown that addition of a silicone surfactant to a polyether polyol allows five to seven times more gas to be mixed with the polyol than when the surfactant is absent. This increase in foam volume is consistent with the reduction of liquid surface tension by the surfactant. The stability of a foam is inversely proportional to the rate at which surface and gravitational energy is released. Any process that reduces the surface area of a foam releases energy. These processes include bubble coalescence and the diffusion of gas from smaller to larger bubbles. Gravitational energy is released during the drainage of liquid down the foam.

For a surfactant to aid in the growth and stabilization of polyurethane foam, it must reduce the surface tension of the foaming liquid, which is predominantly a polyether polyol. The surface tension of these polyols ranges from 33 to 40 mN/m. This value is so low that it cannot be further reduced by the adsorption of hydrocarbon-based surfactants. Essentially, they are not surface active in this medium. However, silicone surfactants can reduce the polyol surface tension to a much lower value of 21-25 mN/m [54]. A requirement for these surfactants, allowing them to stabilize the foam, is to

reduce the surface tension of the liquid polyether polyols by 8-12 mN/m. The adsorption of these surfactants at the polyol-air interface appears to yield a molecular configuration of the surfactant where the siloxane portion is folded over itself. This adsorption also increases the surface viscoelasticity, which aids in stabilizing the foam. These surfactants also appear to be active at the water-polyol and urea-polyol interfaces. This activity increases the miscibility of water in polyol and prevents a catastrophic collapse of the foam after the onset of urea phase separation.

4.2 Methodology

Capillary rise method is used to measure surface tension of sample solutions. Capillarity is the combined effect of cohesive and adhesive forces that causes water and other liquids to rise in thin tubes or other constricted spaces. Inside a thin glass tube, the adhesive force, the attraction between the water and the glass wall, draws water up the sides of the glass tube to form a meniscus. The cohesive force, the attraction of the water molecules to each other, then tries to minimize the distance between the water molecules by pulling the bottom of the meniscus up against the force of gravity. A simple relationship determines how far the water is pulled up the tube. The force upwards due to the surface tension is given by the following relationship:

$$F_{up} = \sigma\,(2\pi r)\cos\theta \qquad \text{Equation 4-1}$$

In this relationship, σ is the liquid-air surface tension at 20 ℃, 2πr is the circumference of the tube, and θ is the contact angle of water on glass, a measure of the attraction of the liquid to the walls. The opposing force down is given by the force of gravity on the water that is pulled above the reservoir level.

$$F_{down} = \rho g\ (h\pi r^2)$$ **Equation 4-2**

Here, ρ = 1000 kg/m^3 is the density of water, g = 9.8 m/s^2 is the acceleration due to gravity, and ($h\pi r^2$) is the volume of the water in the column above the reservoir.

One method to measure the surface tension of a liquid is to measure the height the liquid raises in a capillary tube. By setting the two forces above equal, surface tension can be calculated. For pure water and clean glass, the contact angle is nearly zero. In a typical lab, this may not be the case, but θ is small and we assume that cos θ is close to 1.

$$\sigma = \frac{\rho g r}{2} \frac{h}{\cos\theta} \approx \frac{\rho g r}{2} h$$ **Equation 4-3**

Water/surfactant and polyol/surfactant solutions with different surfactant loadings were prepared and surface tension of these solutions were measured using capillary rise method. A figure of surface tension versus ln(C_{surf}) was plotted to evaluate the relationship between surface tension and surfactant concentration. Capillary tubes (O.D.=1.00mm, I.D.=0.50mm, L=7.5cm) were used in the experiment.

Foam samples with different amounts of surfactant were prepared to evaluate the relationship between surface tension and cell size. Foam samples with different mixing time (5, 10, 15, 25 seconds) were also prepared and evaluated. The foam recipe was listed in Table 4-1.

Table 4-1 Foaming formulation of rigid polyurethane foam

B-side Materials	Weight/g
Polyol (MW:360, Fn:4.5)	35
Dimethylcyclohexylamine(Cat8 gelling catalyst)	0.12
Pentamethyldiethylenetriamine(Cat5 blowing catalyst)	0.32
Surfactant	0.1, 0.2, 0.4, 0.6
Fire Retardant	2

Distilled Water (Blowing Agent)	1.6
A-side Material	
Standard Polymeric MDI (MW:364.5, Fn:2.7)	59.8

4.3 Modeling

Surfactants are known to be important in urethane formulations. Figure 4-4 shows four roles of surfactant in urethane foaming process:

- Emulsification – improving compatibility of raw materials
- Nucleation of bubbles
- Prevention of coalescence (slow-down of diffusion)
- Stabilization

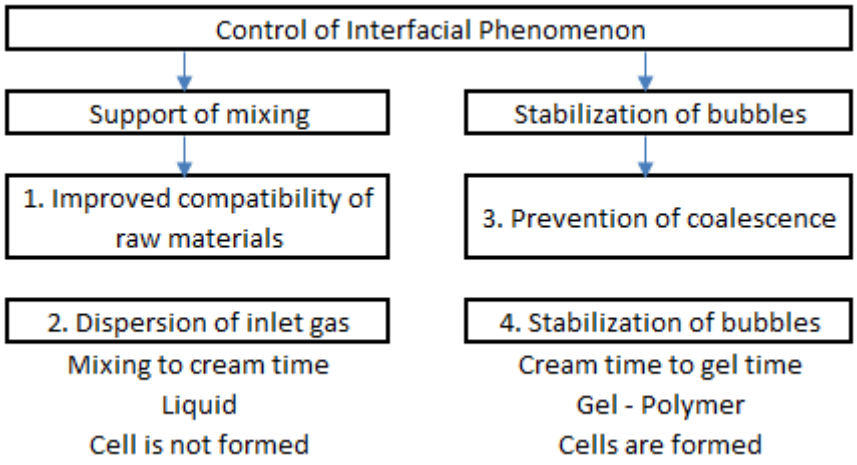

Figure 4-4 Four roles of surfactant in urethane foaming process

This modeling focuses on three key aspects:

- Surfactants impacting the number of nucleation sites and bubble radius for cell growth.
- Surfactants impacting the stability of bubbles and tendency for bubbles to coalesce.

- Surfactants impacting the escape of bubbles through rising to the surface of the forming foam.

4.3.1 Bubble Growth

Based on the previous research results mentioned above, several assumptions were made in the modeling calculations: (1) Bubbles are introduced by the process of mixing the foam components and are sufficient to account for all of the cells in the final foam. (2) Nucleation of bubbles is essentially absent and is thermodynamically unfavorable under the conditions of foam formation. New bubbles are not seen during the formation of a foam. It is simpler for carbon dioxide gas to diffuse from solution to existing bubbles than to nucleate new bubbles. (3) When bubble introduction by mixing is deliberately held to a minimum, the rate of carbon dioxide evolution is decreased considerably and the foam produced is grossly coarse celled.

According to the results of Kanner's study on average bubble size distribution [52], the initial bubble radius was found to be $3.4*10^{-3}$ cm and a cell count of $1.4*10^{8}$ in the solution with a surface tension of 25 mN/m after 10 seconds mixing at 1200 rpm. The energy adsorbed by these generated bubbles were:

$$W = Nc * 4 * \pi * r^2 * \sigma = 1.4 * 10^8 * 4 * \pi * (3.4 * 10^{-3})^2 * 0.025 = 0.05\ J$$

where W is the energy introduced by mixing which is in direct proportional to mixing time at a constant stirring speed, Nc is the number of nucleation sites, r is the bubble radius and σ is the surface tension of solutions. Assume that the same stirring condition was applied and therefore the same energy was introduced. Then the number of nucleation sites will be dependent on the surface tension of solutions.

$$\mathrm{Nc} = \frac{W}{4*\pi*r^2*\sigma} \qquad \text{Equation 4-4}$$

During the bubble growth process, a force balance can be written at the bubble surface [55]:

$$p_b - p_a + \tau_{rr} = \frac{2\sigma}{r} \qquad \text{Equation 4-5}$$

in which p_b is the pressure in the bubble, p_a is the pressure of the liquid at the bubble surface, and τ_{rr} is the radius component of viscous stress tensor in the liquid. The radius component of the stress tensor within the bubble was neglected since we take the gas viscosity to be zero. And in a Newtonian liquid:

$$p_\infty - p_a = -4\mu * \frac{1}{r} * \frac{dr}{dt} \qquad \text{Equation 4-6}$$

where p_∞ is the ambient pressure and μ is the Newtonian viscosity. Substitution of Equation 4-6 into Equation 4-5 results in an expression:

$$p_b - p_\infty - \frac{2\sigma}{r} = 4\mu * \frac{1}{r} * \frac{dr}{dt} \qquad \text{Equation 4-7}$$

Based on the ideal gas law, inner bubble pressure can also be obtained. Equation 4-7 was calculated in the MATLAB program in addition to the temperature and foam height profiles [19, 26, 28]. Figure 4-5 shows the algorithm for calculating bubble radius during foaming process.

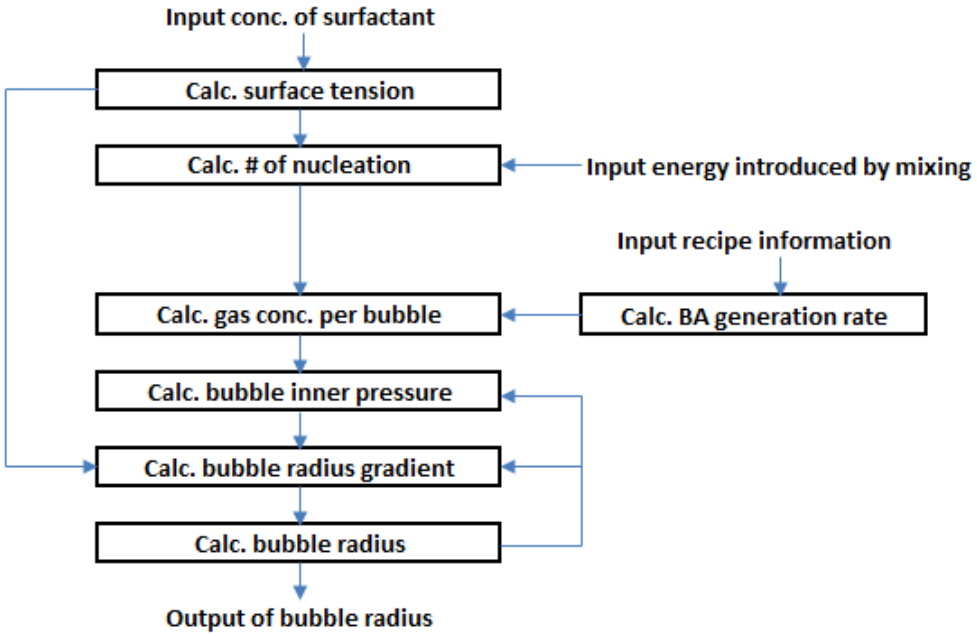

Figure 4-5 Algorithm for calculating bubble radius during foaming process

4.3.2 Film Thinning

The rate of thinning of films affects the stability and lifetimes of dispersions such as foams and emulsions. Reynolds, in his century-old investigation of the theory of lubrication, derived the following expression for the velocity of thinning of a plane-parallel, tangentially immobile fluid film [56],

$$V_{Re} = -\frac{dh}{dt} = \frac{2h^3}{3\mu r^2}\Delta P \qquad \text{Equation 4-8}$$

where h is the film thickness, t is the time, μ is the dynamic viscosity, r is the radius of the film, and ΔP is the pressure drop causing the drainage. The driving force per unit area (ΔP) consists of the capillary pressure, buoyancy (if present), and the disjoining pressure that owes its origin to the London van der Waals interactions and becomes significant only for very thin films (h<1000$\dot{A}$). While numerous investigations regarding foam and emulsion films have employed Reynold's equation, recent experimental studies have all concluded that Equation 4-8 is essentially incorrect for

describing the drainage from thin films, especially for films with radii greater that 10^{-2} cm. Therefore, Ruckenstein and Sharma [57] developed a revised overall film thinning equation:

$$V_t = V_{Re}[1 + 7.35\left(\frac{r}{\lambda}\right)\left(\frac{\epsilon_t}{h}\right)] \quad \text{Equation 4-9}$$

where λ is the characteristic length (wavelength) of the thickness non-homogeneities, which was indirectly inferred to be about $5*10^{-3}$ cm, $\epsilon_t \approx 2\epsilon = (797r^{0.25} - 209)\dot{A}$ is the total amplitude (on both faces of the film) of the thickness non-homogeneities and is given as a function of the film radius by correlation.

Initial average film thickness can be calculated by Equation 4-10 based on resin phase volume, initial bubble radius and number of nucleation. The actual film thickness are assumed to follow normal distribution, the corresponding probability values (D_i) are listed in Table 4-2.

$$h_{0,ave} = \frac{V_l}{4\pi r^2 * N_c} \quad \text{Equation 4-10}$$

Table 4-2 Distribution of actual film thickness

$*h_{0i}$	0.4	0.6	0.8	1.0	1.2	1.4	1.6
D_i	0.0062	0.0606	0.2417	0.3830	0.2417	0.0606	0.0062

Redoev et al. [58] measured directly the velocity of thinning at the critical thickness, i.e., thickness at which the primary film ruptures due to the dispersion force-mediated growth of surface corrugations. Their data for the critical thickness are well represented by the following correlation (10^{-2} < r < 10^{-1} cm),

$$\log h_c = 0.1145 \log r + 2.6598 \quad \text{Equation 4-11}$$

where h_c is the critical thickness in angstroms and r is in centimeters. When a thinning film reaches the critical film thickness it will be regarded as an open cell and therefore

closed cell content can be calculated based on final film thickness. Figure 4-6 presents the algorithm for calculating film thickness and closed cell content.

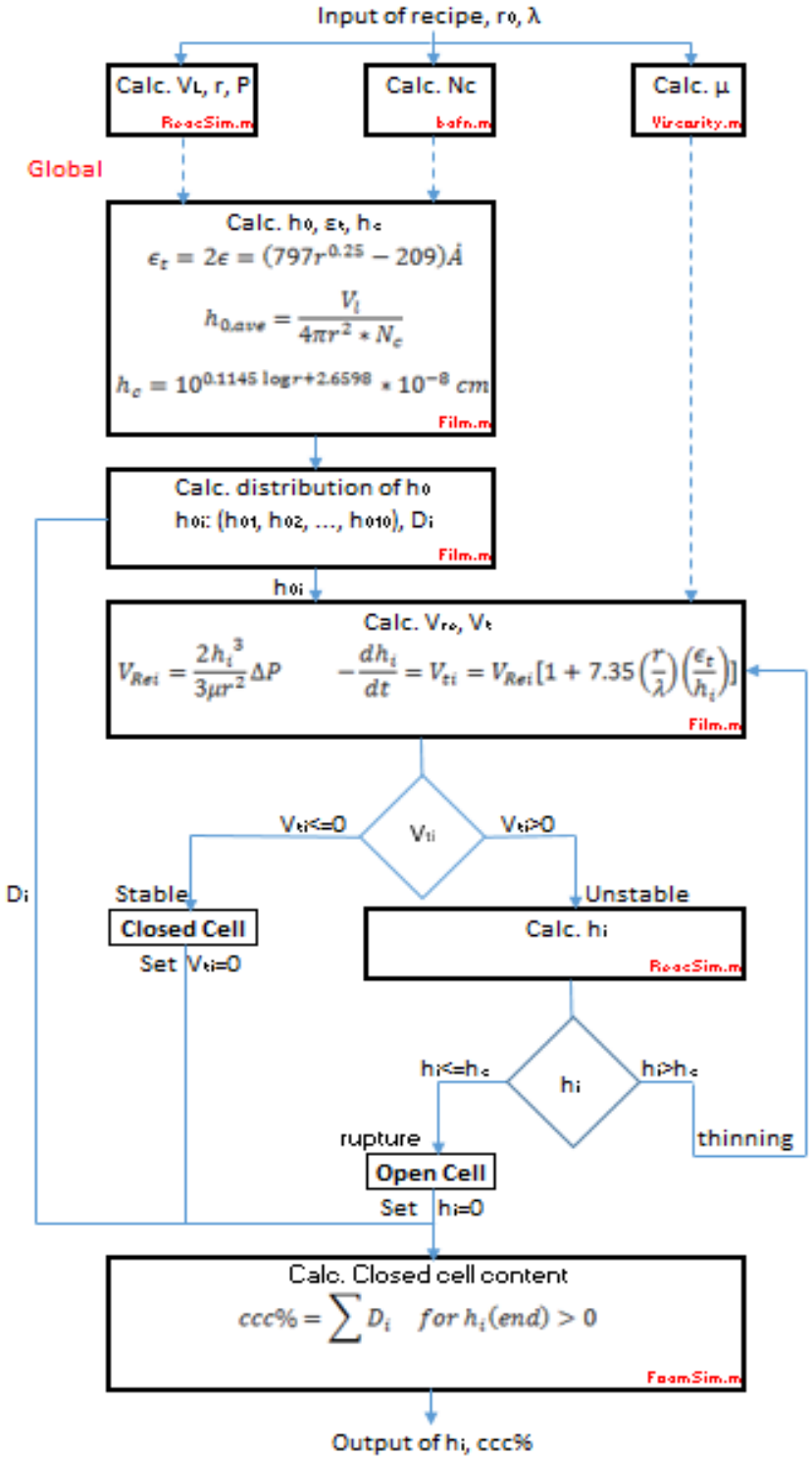

Figure 4-6 Algorithm for calculating film thickness and closed cell content

4.3.3 Bubble Rising

Within a certain center distance, the deformation and coalescence process are similar, the rising velocity of lower bubble is greater than the upper bubble, coalescence time of two bubbles with same diameters increases as the center distance increases.

To two bubbles with different diameters within a certain center distance, when the bigger bubble located beneath at the initial time, the bigger bubble move upward all the way while the smaller bubble moves upward first and then moves downward before two bubbles coalescence. However, when the smaller bubble located beneath at the initial time, after velocities of two bubbles become stable, the velocity of the bigger bubble is greater than the smaller bubble, so bubble coalesce cannot happen.

The rise of a bubble in liquid is a function of several parameters viz. bubble characteristic (size and shape), properties of gas-liquid systems (density, viscosity, surface tension, concentration of solute, density difference between gas and liquid), liquid motion (direction), and operating conditions (temperature, pressure, gravity) [59].

In surface tension force dominant range:

$$V_r = \sqrt{\frac{2\sigma}{\rho_L d} + \frac{(\rho_L - \rho_G) g d}{2}} \qquad \text{Equation 4-12}$$

In viscosity dominant range:

$$V_r = \frac{1}{18} \frac{g d^2 (\rho_L - \rho_G)}{\mu_L} \qquad \text{Equation 4-13}$$

where g is the acceleration due gravity, d is the diameter of bubble, μ_L is the dynamic viscosity of liquid, ρ_L is the density of liquid and ρ_G is the density of gas.

4.4 Results and Discussion

4.4.1 Experimental Data

Surface tension was plotted as a function of ln(C_{surf}) in Figure 4-7. Surface tension of solution decreased as surfactant amount increasing. Within the range of surfactant amounts studied, surface tension was a linear function of ln(C_{surf}) and therefore the surface tension can be calculated based on the concentration of surfactant in solutions as:

$$\sigma = -1.4378 * \ln C_{surf} + 21.046 \qquad \text{Equation 4-14}$$

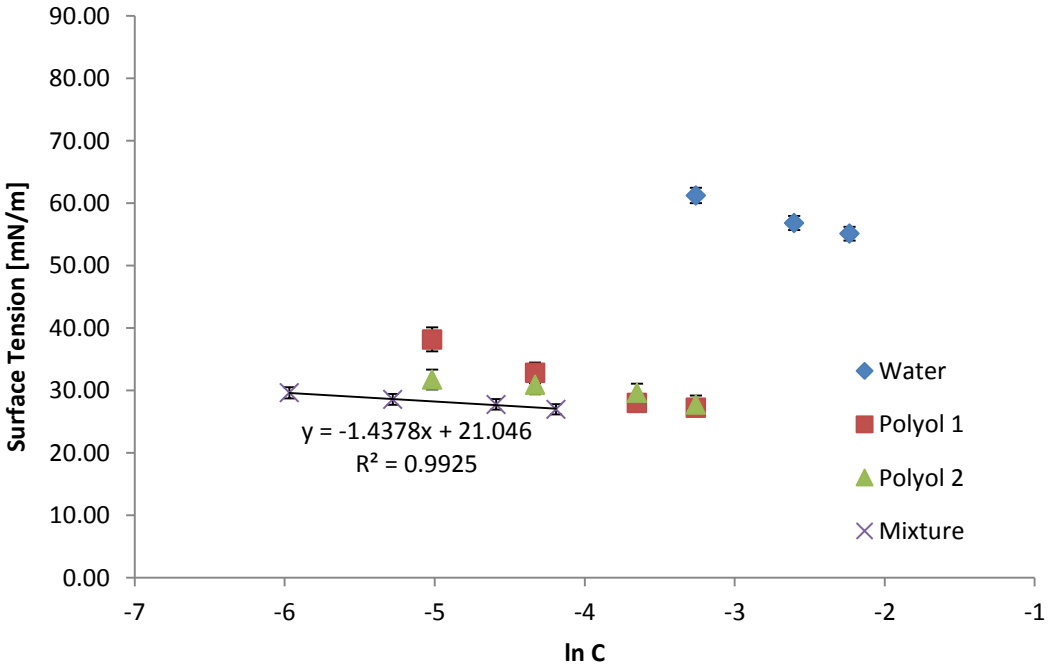

Figure 4-7 Surface tension versus ln(Csurf) in different solutions

Figure 4-8 presents temperature profiles of the foams with different surfactant loadings. The results indicated surfactant had no impact on reaction kinetics and thermodynamics which agreed with the assumption made in modeling calculation.

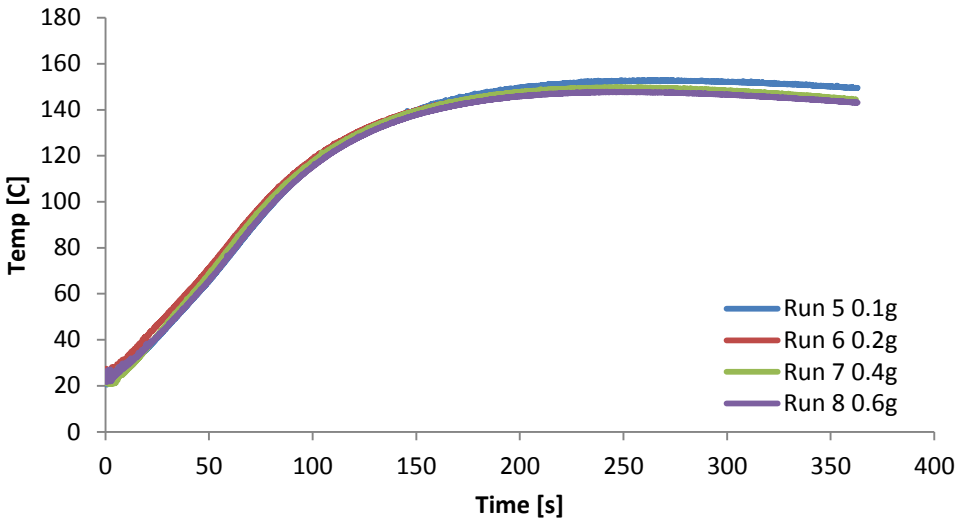

Figure 4-8 Temperature profiles of foams with different concentration loadings

Figure 4-9 shows the longitudinal sections of the foams with different surfactant loadings. Obviously foam #5 had the lowest surfactant loading thus leading to the least nucleation sites (number of bubbles). As the volume changes were the same, the bubbles in foam #5 had the largest radius. Differences between foams #6-#8 cannot be told easily by naked eyes and therefore microscope observations were performed (Figure 4-10). The bubble size of foam #5 was too big to take a microscope observation and therefore was not presented.

Figure 4-9 Longitudinal sections of foams with different surfactant loadings

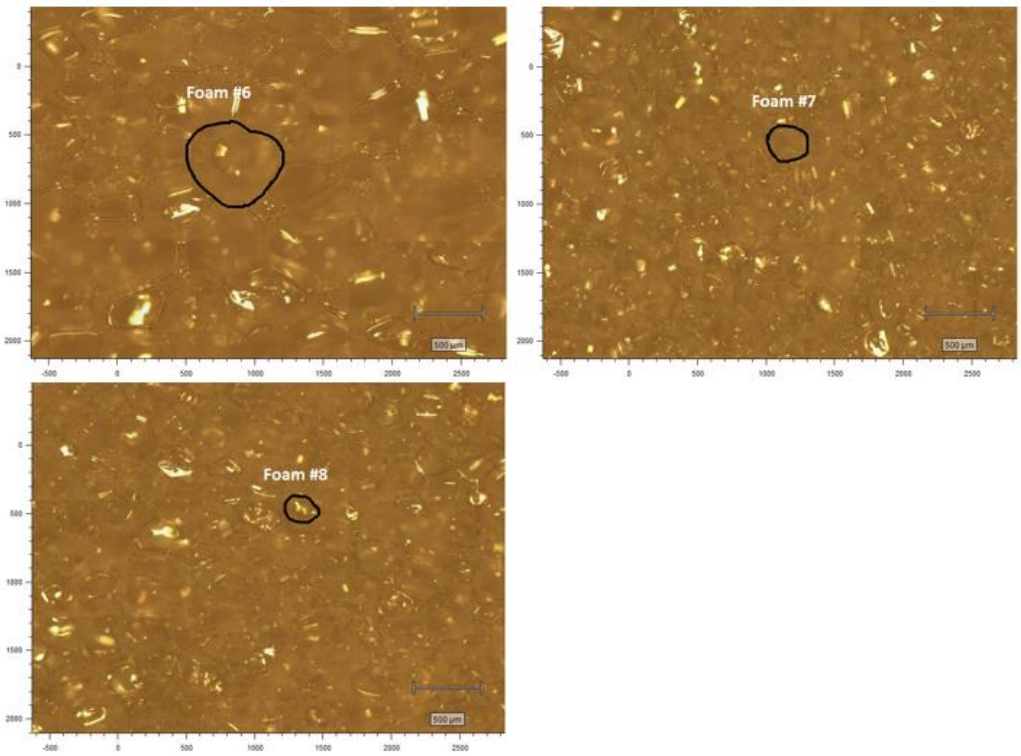

Figure 4-10 Microscope observations of foams with different surfactant loadings

Figure 4-11 shows microscope observations of foams (#1-#4) which have different mixing time (5, 10, 15, 25 seconds) and the same control formulation (0.6 g surfactant). Longer mixing time introduced more nucleation cells and led to smaller bubble radius as the volume changes were the same.

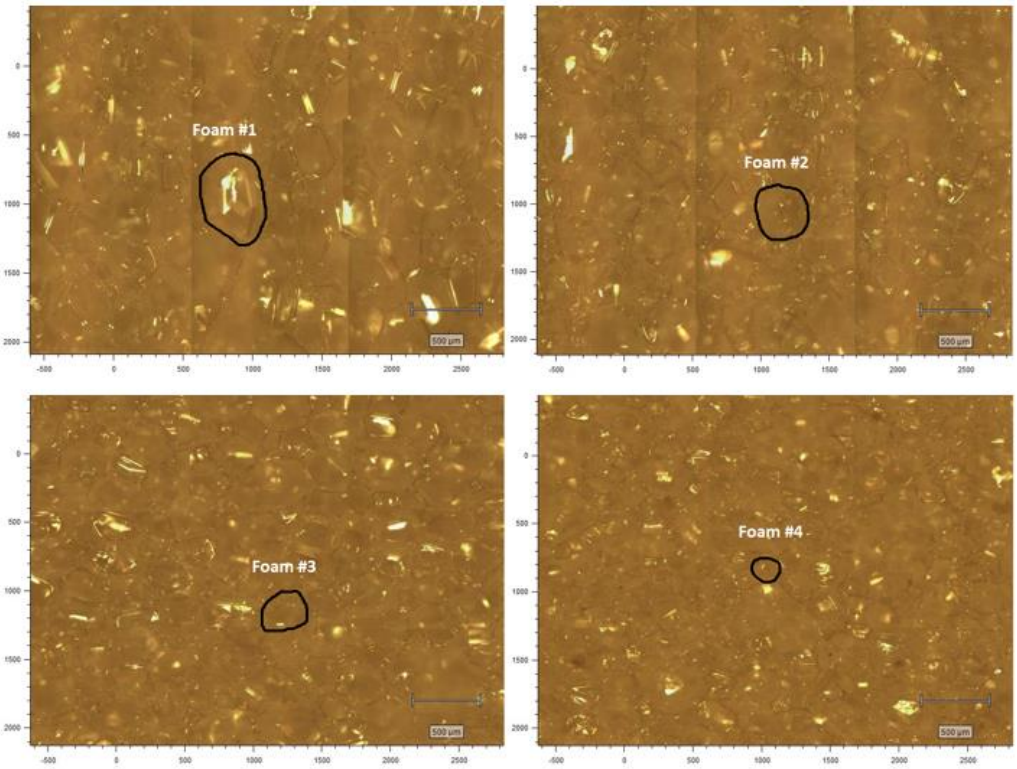

Figure 4-11 Microscope observations of foams with different mixing time

4.4.2 Preliminary Modeling Results

Simulation results from MATLAB program were presented in Figure 4-12. The results included temperature, foam height, bubble radius, bubble inner pressure and film thickness profiles. At the beginning carbon dioxide was generated rapidly by blow reaction and the gas volume change expanded the existing bubbles. At later time stage when viscosity was large enough to provide the strength bubbles stopped to growth and foam stopped to rise. After setting bubble radius stayed as a constant, and then bubble inner pressure slightly decreased as temperature cooled down. Temperature and foam height results agreed with experimental data and therefore bubble radius and pressure results were believed to be reasonable.

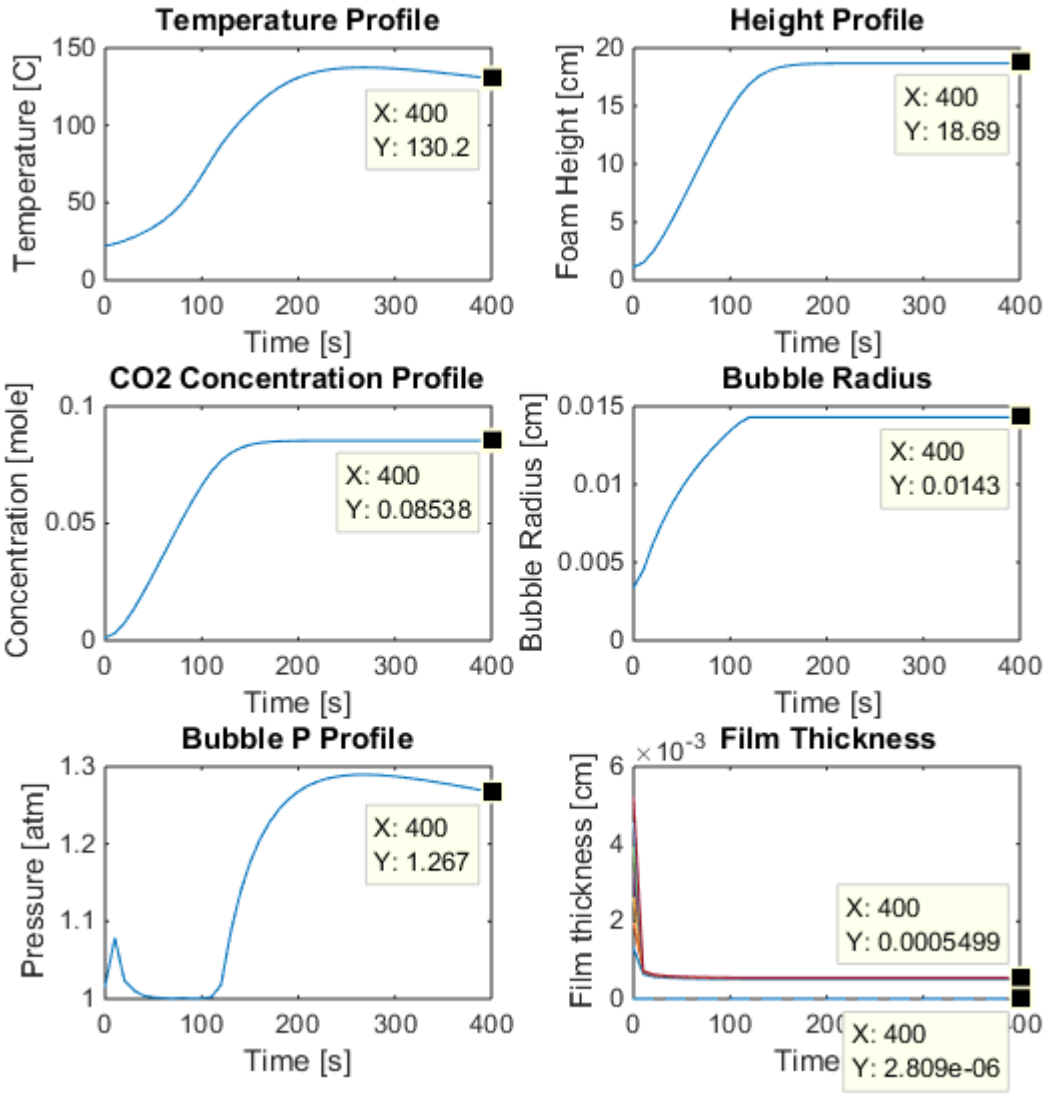

Figure 4-12 Simulation results from MATLAB program

Mixing time and surfactant amount were changed respectively to get simulated bubble radius of foams #1-#8. Twenty bubbles were chosen from Figure 4-10 and Figure 4-11 to calculate average experimental radius. Figure 4-13 shows comparison of experimental and modeling bubble radius as mixing time increasing. Figure 4-14 shows comparison of experimental and modeling bubble radius as surfactant amount increasing.

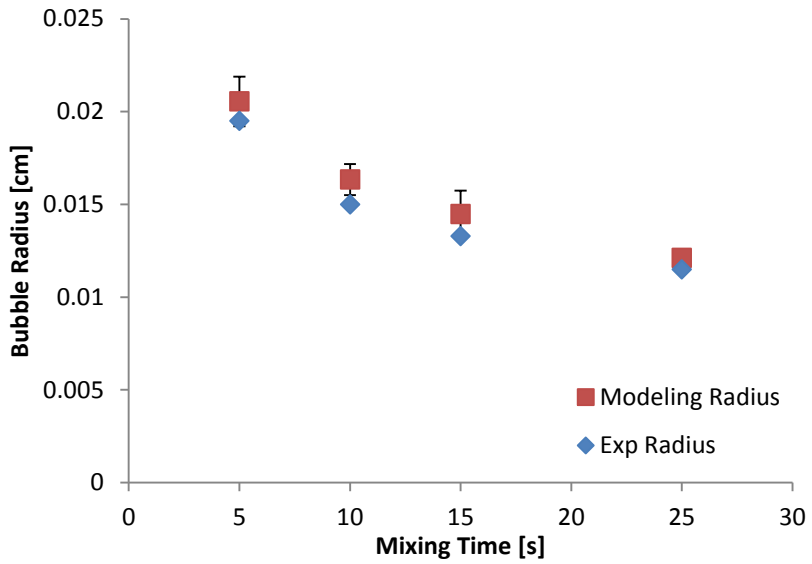

Figure 4-13 Comparison of experimental and modeling bubble radius as mixing time increasing

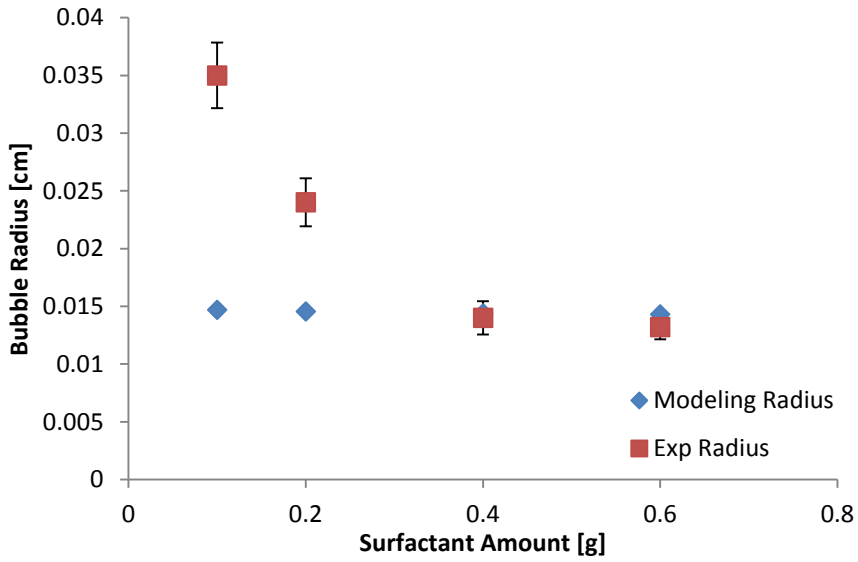

Figure 4-14 Comparison of experimental and modeling bubble radius as surfactant amount increasing

The simulation successfully predicted final bubble radius as long as appropriate surfactant amount was used. Simulation of bubble growth is not sufficient to model the complicated foaming process and therefore modes of failure need to be taken into consideration. Film thinning is considered as one possible source for bubble coalescence and rupture. However, based on the simulation results from Figure 4-12, the final film thickness is about $55000\dot{A}$, which is much thicker than the critical

thickness 281$\dot{A}$. This indicates the critical thickness is too thin to be generally reached within the bubble radius range in this study. Experimental film thickness was measured based on Figure 4-10 and Figure 4-11. The actual film thickness was about 50000$\dot{A}$, which means the simulation calculation was accurate. Therefore, this mode of failure was proved not happening in rigid foams.

Another possible reason causing foam failure may due to bubble rising during foaming process. Bubbles close to top surface may escape from the resin phase due to buoyancy and bubbles far from top may coalesce with each other because a larger bubble has a faster rising velocity than a small bubble which leads them to meet and coalesce. Moreover, if a bubble rises at a critical velocity it may rupture due to shear force. Detailed impact of bubble rising on foam failure will be studied further. Figure 4-15 presents single bubble rising velocity versus time during foaming process and the impact of blowing agent loading was evaluated. Table 4-3 summarizes the modes of foam failure and current status of these studies.

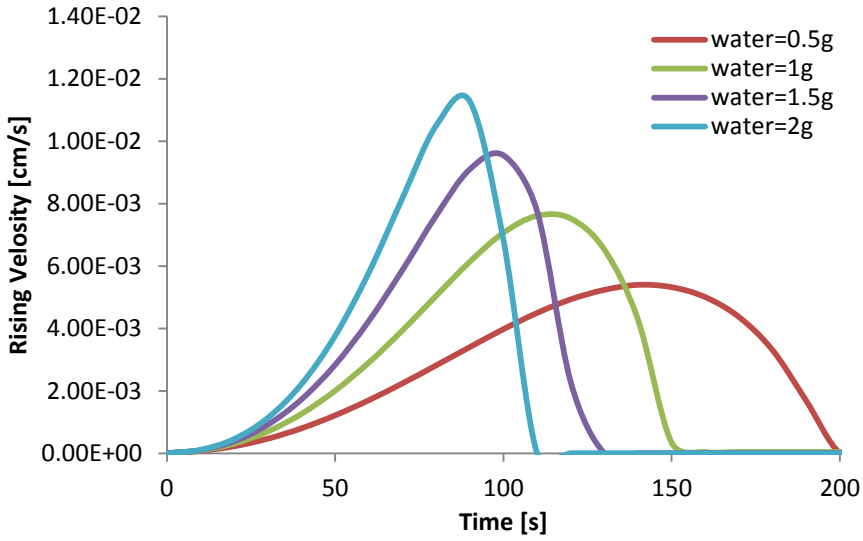

Figure 4-15 Impact of blowing agent loading on single bubble rising velocity

Table 4-3 Modes of foam failure and current status of studies

RELATED TO CELL SIZE (Category 1)	
Course cell structure leading to poor thermal conductivity and low compression strength.	More/better surfactant increases the number of cell nucleation sites resulting in smaller gas cells in the foam.
RELATED TO RATE OF RISE OF BUBBLES IN RESIN (Category 2)	
Bubbles rise in resin "liquid" and eventually escape through rupture of top surface of the foam.	More/better surfactant leads to smaller gas bubbles that rise slower than large gas bubbles. Simulation can be used to better understand how viscosity and bubble size translate to changing rise velocities of bubbles during foaming. Is there a critical bubble buoyancy-driven rise velocity that leads to failure?
Resin cures too slowly resulting in low viscosity that allows bubbles to rise and escape.	
Rise of bubbles leads to concentration of bubbles at top of resin where coalescing occurs in addition to surface rupture and escape.	
RUPTURE OF CELLS DISPERSED IN MATRIX (Category 3)	
Bubble growth causing film thinning	Not applied. Critical thickness is too thin to be generally reached.
*Bubble coalescing due to different rising velocity	Questionable. Bubble sizes and locations need to be specified and discussed.
*Bubble rupture due to shear force	Questionable. Critical bubble rising velocity needs to be identified.
Cascade collapse of rigid foam OR the desired "blow" of a flexible foam.	Complex phenomena. Could be due to pressure buildup in cells, herniating of cells at surface of foam, and cascade herniating-type failures as pressures in upper cells reduce.
RELATED TO FINAL RESIN MORPHOLOGY	
Resin does not adequately cure to form a strong solid/elastic phase.	Not substantially related to surfactant.

4.5 Conclusion

An initial critical analysis of how surfactants impact urethane foam-forming processes has been performed which included a survey of literature, summary of available theory/models, and preliminary simulations. The following conclusions are a result of this analysis.

- Surfactants reduce the surface tension of bubble-resin interfaces resulting in the stabilization of higher concentration of bubbles and bubble nucleation sites in resin mixtures.
- The combination of adequate mixing (associated energy input) and surfactants is necessary to form sufficient bubble nucleation sites at the onset of the urethane-foam-forming process to form the desired fine cell structures in quality urethane foams. Up to the limit of "adequate" mixing and surfactant loadings, longer mixing time and higher surfactant loading leads to more bubble counts and smaller bubble radius.
- Within the appropriate range of surfactant loadings, surface tension is a linear function of $\ln(C_{surf})$ and therefore the surface tension can be calculated based on the concentration of surfactant in solutions.
- Surfactants have minimal impact on reaction kinetics and thermodynamics for systems where solubility of the reagents is not an issue.
- The MATLAB simulation successfully predicts bubble radius, inner pressure and film thickness during foaming process in addition to temperature and foam height profiles as long as surfactant is sufficient.

- The critical film thickness (as predicted by Redoev's model[58]) is too thin to be generally reached within the bubble radius range in this study.

The mechanisms through which surfactants lead to foam failure is not well validated in literature suggesting that the mechanisms are not well understood beyond the basic concept that surfactants can slow down the coalescing and rupturing of bubbles/cells in a foam. The key to better understanding the mechanisms through which surfactants lead to successful foam formation likely lies in the analysis of modes of foam failure and how surfactants reduce the modes of failure.

A conclusion of this analysis is that the impact of surfactants in foam formulations can be grouped into three categories with each having different methods to critically investigate and understand as follows:

Category 1 – Role of surfactants in forming cell nucleation sites where the role of the surfactant is critically couples with the energy input during mixing to form nucleation sites.

Category 2 – The surfactant plays a role in impacting nucleation sites, but after that point the inter-relationship of cell growth, viscosity, and buoyancy lead to a velocity for bubble rise in the system. A rise velocity beyond a critical value could lead to failure.

Category 3 – As pressure builds in foam that is not fully set, weak spots of cells at the top of the foam could urinate leading to either a cascade collapse or the desire "blow" of a flexible foam.

Both Category 2 and Category 3 types of failures involve the complex inter-relationship of how the cell grows during foaming, how pressure in the cell increases during foaming, and how viscosity increases. For these types of failures, no simply theory or model will adequately quantify the failure; simulation is needed.

5. COMPUTATIONAL STUDY ON REACTION ENTHALPIES OF URETHANE-FORMING REACTIONS

5.1 Introduction

Reaction of alcohols with isocyanates to form urethanes is the basis of the polyurethane industry [49] with annual sales in the tens of billions of dollars. The simulation of thermosets formed in these reactions includes generating solutions under the constraints of dozens of differential equations under material balance, energy balance, and constitutive relationships. The many equations and the large number of oligomers with their isomers result in a problem-solving environment where the number of number of model parameters greatly exceed what can be reasonably obtained from fitting parameters to experimental data.

Heuristics such as those provided in Table 5-1 provide a starting point for simulations. These heuristics allowed for the proof-of-concept by comparison of simulation results on temperature and foam height profiles to justify further efforts to increase accuracy and provide increasingly useful results.

Table 5-1 Heuristics for initial efforts in simulating urethane-foaming reactions

Polyols:
• Polyols consist of different ratios of primary (X_p), secondary(X_s) and hindered-secondary hydroxyl (X_{HS}) where the same type of hydroxyl in different polyols have the same reaction rate constants (k_0) [26] • The heat of reaction is assumed to be the same for independent of X_P, X_S, and X_{HS} • Flory's assumption is assumed to hold where the reactivity a hydroxyl group is independent of the size of molecule to which the hydroxyl group is attached • Catalytic reaction rate constants (k_0) are unique to the catalyst [19, 60]
Catalysts:
• Catalysts will not react with any components in the system • The structure and reactivity of catalysts will not change during the reaction process

• Catalysts will reduce activation energy (ΔE) relative to non-catalytic reaction • Catalysts have no impact on heat of reaction (ΔH) • There is no interaction between the catalysis impact from two or more catalysts
Others:
• Use of step growth mechanisms as elementary processes can be used to obtain reaction rate expressions for the reactivity of moieties • All isocyanate groups have the same reactivity • Other additives (surfactant and fire retardant) have no catalysis impact on reactions • Foam has a lower heat transfer coefficient than solid resin • Foam height (density) can be estimated by assuming ideal gas behavior, a modified Raoult's law equilibrium and an overall efficiency in gas cell formation [27]

Use of Xp and Xs - The reaction parameters of polyols are predominantly influenced by the fraction of primary, secondary, and hindered-secondary hydroxyl groups. This characterization reduces the number of parameters needed to characterize a polyol's reactivity and provides useful insight into how a polyol will react in a formulation—these are more meaningful that Arrhenius parameters to most researchers in the area.

In addition, impacts of catalysts are expected to be less dependent on the actual polyol and more dependent on the impact of primary, secondary, and hindered-secondary alcohols. Early work on simulation by Zhao et al has extended this approach of characterizing reactivity base on type of hydroxyl moiety to the characterizing of the impact of catalysts on reactivity [19, 26, 28, 60]. This approach has utility for extrapolating the performance of a catalyst from one polyol to another.

The utility of the simulation approach resides in using physical properties and fitted parameters to pure components (such as the fraction of primary alcohol) to perform simulation on the multitudes of useful combinations of the components in

formulations/recipes. For fitting parameters such as the fraction of primary versus secondary alcohol content, fitting parameters to experimental data can be performed with confidence due to the reactivity of the primary alcohols being more than an order of magnitude greater than the reactivity of the secondary alcohols. These parameters that can be readily determined by fitting to experimental data could be characterized as "first tier" fitted parameters.

A "second tier" of parameters that are not as readily obtained by curve fitting emerge, but are needed to improve the accuracy of simulation, especially when extrapolating results outside the range where accuracy has been verified. Example second tier parameters include:

- Impact of polymer size on moiety reactivity (Flory's assumption is not impact)
- Variations of heat of reaction with primary, secondary, and hindered secondary alcohol groups.
- Generalizations that can be made on the impact of catalysts (e.g. is the reduction in activation energy the same for reactions with secondary alcohols as with primary alcohols)

This chapter is on an approach that uses molecular modeling to determine the sensitivity of parameters to these second tier variations in molecules. When the molecular modeling indicates little variation in parameters, the simulation results are put forward as verification that the first order approximations are adequate. When the molecular modeling indicates that parameters (e.g. heat of reaction) vary by more than about 1%, verification of the variations is pursued so as to improve the accuracy of the

simulation.

Reaction enthalpies and rate constants for isocyanate-alcohol reactions catalyzed by tertiary amines were modelled by Chang [1] and Baker [17]; they reported relative rate constants with respect to different catalyzed conditions. Baser et al developed theoretical models for physical blowing agent blown rigid polyurethane foam formation [46] and water-blown polyurethane foams [45]. All the above models are based on an assumption that the reactivity of two molecules having different chain lengths (or molecular weights) are the same as long as they have the same type of functional groups. They reported the enthalpy of isocyanate-polyol reaction as a constant regardless of location of functional groups, molecular size and chain length.

Other research showed the relationship between reaction enthalpy/rate constant and chain length. Lovering et al [61] performed thermochemical studies on alcohol-isocyanate reactions. They reacted isocyanate with n-butanol, s-butanol and i-butanol respectively and measured the heats of reaction using a differential microcalorimeter of the Tian-Calvet type. It was found that the heat of reaction decreased in the order normal> iso> secondary.

More-detailed studies on the impact of molecule size on reactivity are available with other chemistries. Figure 5-1 shows the plot of esterification rate constant, kA vs. average polymer chain length, N for CH3CH2OH + H(CH2)NCOOH [62], the reaction rate was linearly decreasing as the chain length number increasing from 1 to 3 and it tended to a constant after the chain length number reaching 4 or more. The phase transition and viscoelastic transition of polymer may influence the reaction of polymer

chain [63, 64], but in this study the structure of polymer chain was assumed stable.

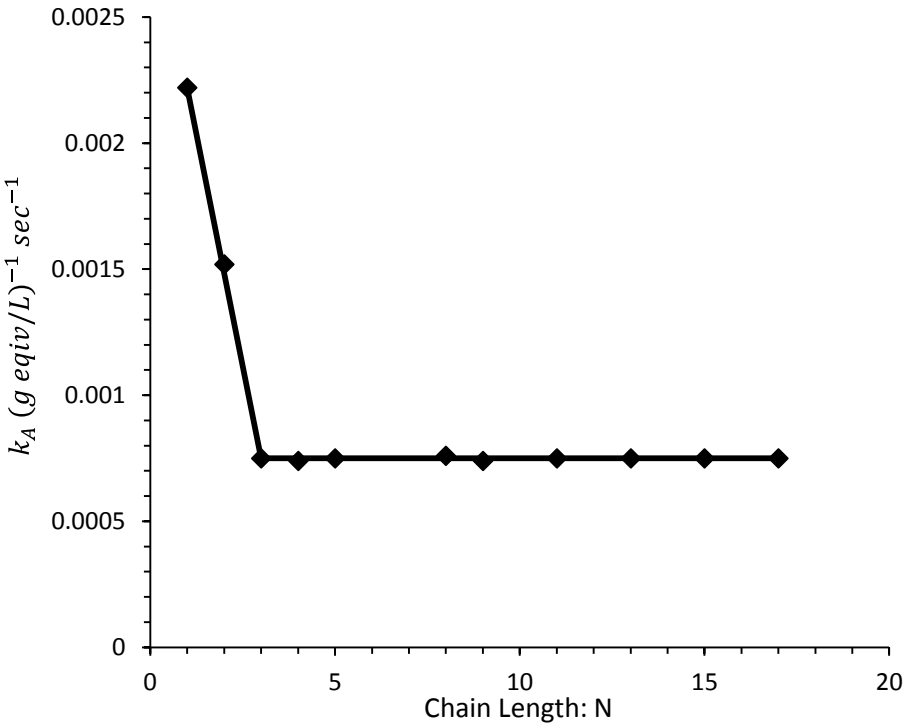

Figure 5-1 Plot of esterification rate constant, kA vs. average chain length, N for CH3CH2OH + H(CH2)NCOOH

Zhao [19, 28, 60] and Rima [26] have initiated an approach to simulate near-adiabatic foam-forming reactions that included catalysis impact and treat polyols as fraction of primary, secondary and hindered-secondary hydroxyl. Large differences in Arrhenius parameters allowed experimental data to be used to identify parameters specific to primary, secondary, and hindered secondary hydroxyl groups. However, the uncertainty of the fitted parameters for enthalpies of reaction relative to data did not justify the use of different values for the heats of reaction. The introduction of computation study on this topic can provide more information on how sensitive the heats of reaction are to alcohol moiety isomers.

Several computational studies have been performed on the general characteristics

of urethane formation reactions [7, 14, 65-67]. Early mechanistic studies on urethane formation suggest that the alcoholysis reaction occurs either via a concerted mechanism or stepwise mechanism. In the concerted mechanism, the addition of alcohol is carried out across the N=C bond of isocyanate and immediately results in the product (Figure 5-2a). In the stepwise path, the additional of the alcohol across the C=O bond of isocyanate yields an enol intermediate, which can tautomerize via a proton transfer to give the urethane product (Figure 5-2b). The free energy profiles calculated by Coban et al [68] showed that the concerted path is more likely to occur than the stepwise route. Therefore the concerted path structures were used for calculations in this study.

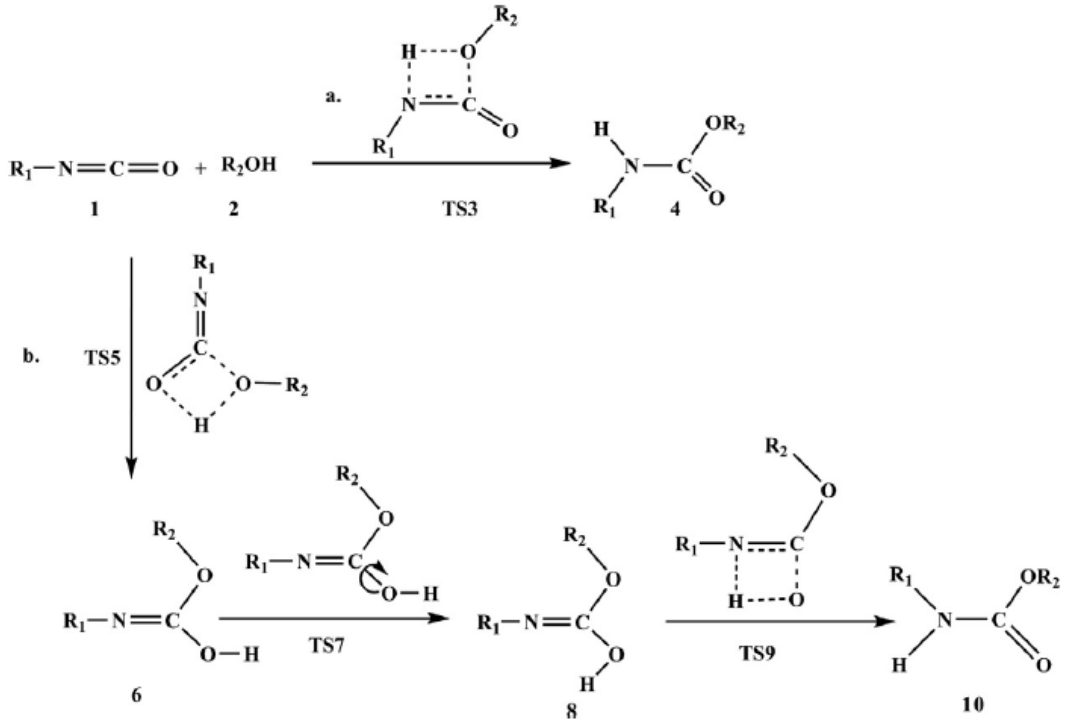

Figure 5-2 Proposed reaction mechanisms for the alcoholysis reaction of isocyanate. (a) Concerted mechanism, (b) Stepwise mechanism.

Urethane reactions have been extensively studied with PM3 semi-empirical method [68, 69], as well as ab initio calculations [70, 71]. The most extensive semi-empirical studies are (B3LYP/6-31 + G(d,p)) of Coban et al [68]. They used density functional

theory (DFT) calculations to calculate rate constant ratios (k_1/k_2) in which k_1 is the rate constant of the first alcohol attack on the diisocyanate molecule and k_2 is the rate constant of the second alcohol attack on the diisocyanate molecule. Raspoet et al [71] compared experimental data and theoretical results obtained by ab initio MO calculations. They found the bulk solvent effect, which is treated by a polarizable continuum model (PCM), does not affect the preference of the alcohol to attach across the N=C bond as pointed out by the gas-phase values.

This work is a computational study on the alcoholysis reaction during polyurethane foaming process. Different aromatic isocyanates (2,4-TDI, 2,6-TDI, 2,4-MDI, 4,4-MDI) were considered to react with 1-Butanol, 2-Butanol, and tert-Butanol; and so, to calculate the reaction enthalpies. Impact of functional group location, molecular size and chain length on reaction enthalpies were evaluated based on the computational results. The impact of conformations will not be discussed in this work because it can be neglected comparing to the impact of molecular sizes and configurations. Computational results were used to improve the database of kinetic and thermodynamic parameters used in simulation studies [19, 26, 28, 60].

5.2 Methodology

The Gaussian 09 package was used to speed up calculations compared to those using Slater-type orbitals, a choice made to improve performance on the limited computing capacities of then-current computer hardware for Hartree-Fock calculations. The computations were performed on the HPC resources at the University of Missouri Bioinformatics Consortium (UMBC). Chemical structures were optimized at the

B3LYP level using a 6-31G(d,p) basis set in the gas phase. Chemical geometries were input and the structures were subjected to vibrational frequency analysis toward their characterization as local minima. Throughout this paper, calculated bond length are given in angstroms, calculated bond angles in degrees, total enthalpies in hartrees, and zero point energies and calculated relative enthalpies, unless otherwise stated, in kilojoules per mol.

The solvent effects were studied using a single-point Integral-Equation-Formalism Polarizable Continuum Model (IEF-PCM) to make calculations in toluene (which is used as a solvent in some of the experimental studies to avoid over heat) and benzene. Hartree-Fock and MP2 were also calculated using 6-31G(d,p) basis set to verify accuracy of the results. SPARTAN, GAMESS and MOPAC calculations will be performed in the future study to verify the results obtained by Gaussian.

The general computation procedures can be summarized as five steps:

1. Draw chemical structures (reagents and products)
2. Optimized chemical geometries
3. Calculate total electronic and thermal enthalpies using Gaussian
4. Calculate relative enthalpies corrected by ZPEs
5. Compare reaction enthalpies of all reactions

Simulations were performed on the reactants, transition states, and products. Figure 5-3 shows the molecular models and how the reaction enthalpy was calculated from the reactants and products.

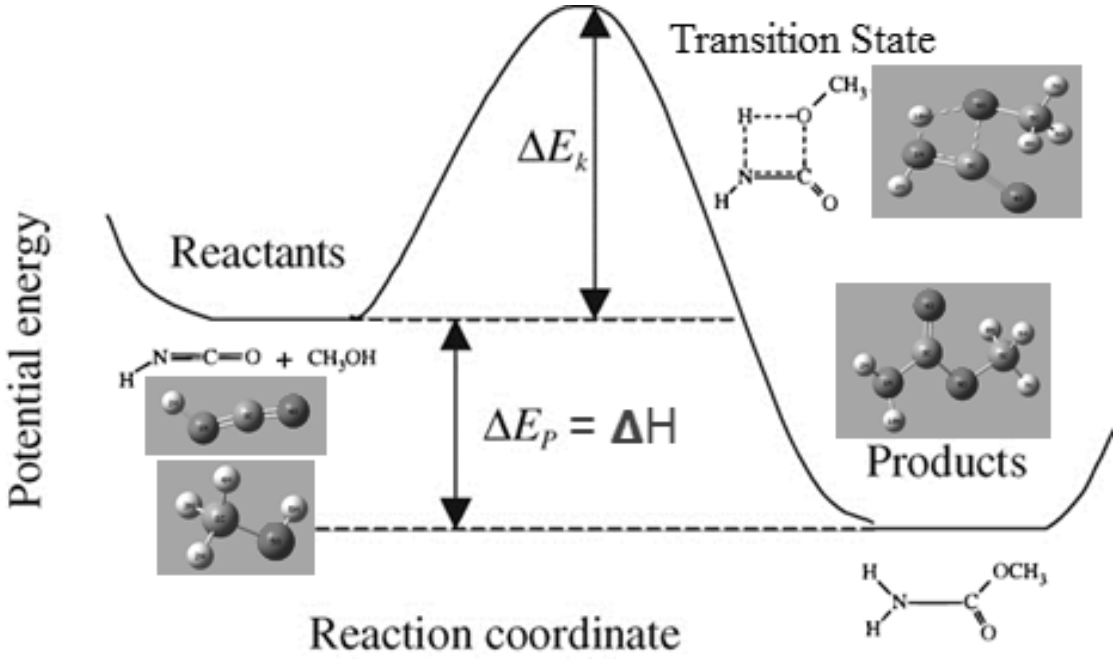

Figure 5-3 Graphical depictions of molecular models and energy profile

The usual way to calculate enthalpies of reaction is to calculate heats of formation, and take the appropriate sums and difference. H_{total} is used for the total enthalpy, ε_{ZPE} is used for the zero point energy and the reaction enthalpy $\Delta_r H^0$ can be calculated by Equation 5-1:

$$\Delta_r H^0 = \sum (H_{total} + \varepsilon_{ZPE})_{products} - \sum (H_{total} + \varepsilon_{ZPE})_{preactants}$$

Equation 5-1

In general, convergence was questionable or not possible on the transition states, and so, it is not possible to report impacts on activation energies from this work. Useful results were obtained to allow enthalpies of reaction to be estimated; these are reported in the discussion. When simulation results predicted more than 5% variation in parameters that could be experimentally measured, experimental data were collected. In the case of heats of reaction, the simulation heats of reaction were used as a basis to curve-fit the Arrhenius parameters. Experimental methods have been previously published [19, 28, 60].

5.3 Results and Discussion

5.3.1 Location and Molecular Size of Isocyanate Groups

Figure 5-4 presents examples of isocyanates used in this study. The impact of isocyanate group location on reaction enthalpy was evaluated by reacting isocyanate functional groups on different locations with the same alcohol groups. MDI was compared with TDI to evaluate the impact of molecular size on reaction enthalpy.

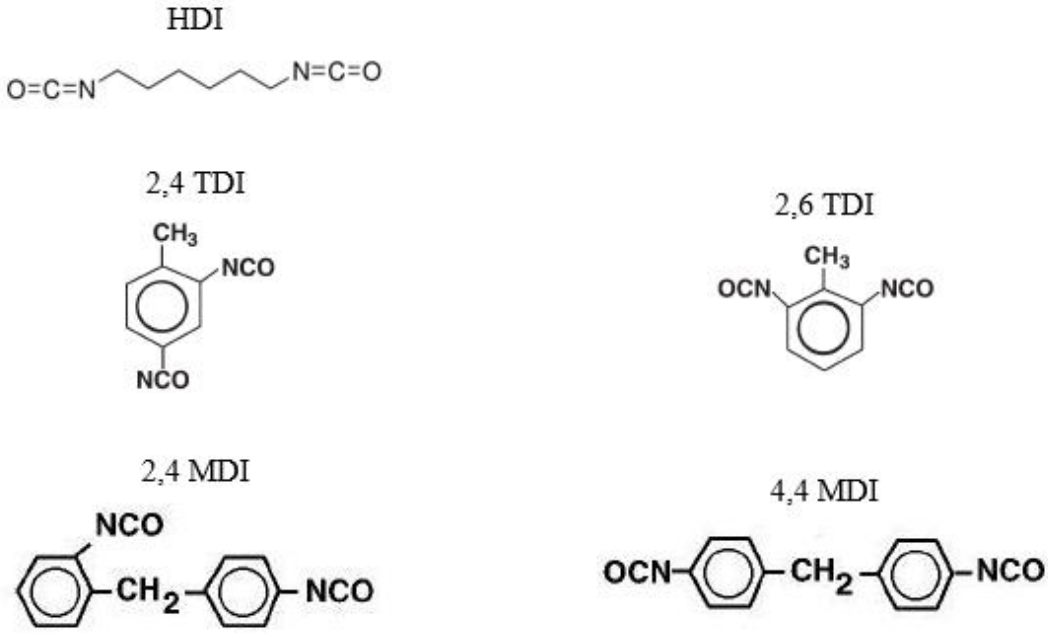

Figure 5-4 Example isocyanate structures

Table 5-2 lists total electronic and thermal enthalpies and zero-point vibrational energies of all the reactants and products based on B3LYP/6-31G(d,p) geometries. Notation 2 means the reacted isocyanate was on carbon 2 and notation 4 means the reacted isocyanate was on carbon 4 based on the convention that the 1 carbon is where the methyl group attaches to the aromatic ring. The corresponding relative enthalpies (heats of reaction) were reported in Table 5-3.

Table 5-2 Calculated Total Corrected (Hartree) and Zero-Point Vibrational (ZPE, kJ/mol) Energies for studies on isocyanate locations and molecular sizes

	Sum of electronic and thermal Enthalpies	ZPE
HDI	-571.839728	519.4
2,4-TDI	-606.395275	353.8
2,6-TDI	-606.394843	353.7
2,4-MDI	-837.364638	568.0
4,4-MDI	-837.364904	568.0
1-Butanol	-233.533899	360.7
2-Butanol	-233.540773	359.1
Water	-76.394588	56.1
CO_2	-188.565756	30.4

HDI	Sum of electronic and thermal Enthalpies	ZPE
HDI + 1-Butanol	-805.373627	880.1
1-Butanol Urethane	-805.411671	892.9
HDI + 2-Butanol	-805.380501	878.5
2-Butanol Urethane	-805.417679	892.2
HDI + Water	-648.234316	575.5
Amine	-459.698169	555.5
Amine + CO_2	-648.263925	585.9

2,4-TDI	Sum of electronic and thermal Enthalpies	ZPE
2,4-TDI + 1-Butanol	-839.929174	714.5
1-Butanol Urethane2	-839.965776	727.9
1-Butanol Urethane4	-839.967315	727.4
2,4-TDI + 2-Butanol	-839.936048	712.9
2-Butanol Urethane2	-839.971769	726.6
2-Butanol Urethane4	-839.973320	726.1
2,4-TDI + Water	-682.789863	409.9
Amine2	-494.260608	389.6
Amine4	-494.260276	388.7
Amine2 + CO_2	-682.826364	420.0
Amine4 + CO_2	-682.826032	419.1

2,6-TDI	Sum of electronic and thermal Enthalpies	ZPE
2,6-TDI + 1-Butanol	-839.928742	714.4
1-Butanol Urethane2	-839.961240	727.6
2,6-TDI + 2-Butanol	-839.935616	712.8
2-Butanol Urethane2	-839.967266	726.3
2,6-TDI + Water	-682.789431	409.8
Amine2	-494.259986	389.8
Amine2 + CO_2	-682.825742	420.2

2,4-MDI	Sum of electronic and thermal Enthalpies	ZPE
2,4-MDI + 1-Butanol	-1070.898537	928.7
1-Butanol Urethane2	-1070.932860	942.0
1-Butanol Urethane4	-1070.935916	941.6
2,4-MDI + 2-Butanol	-1070.905411	927.1
2-Butanol Urethane2	-1070.938823	940.9
2-Butanol Urethane4	-1070.941948	940.2
2,4-MDI + Water	-913.759226	624.1
Amine2	-725.227689	603.8
Amine4	-725.229052	603.1
Amine2 + CO_2	-913.793445	634.2
Amine4 + CO_2	-913.794808	633.5

4,4-MDI	Sum of electronic and thermal Enthalpies	ZPE
4,4-MDI + 1-Butanol	-1070.898803	928.7
1-Butanol Urethane4	-1070.935949	941.7
4,4-MDI + 2-Butanol	-1070.905677	927.1
2-Butanol Urethane4	-1070.941951	940.4
4,4-MDI + Water	-913.759492	624.1
Amine4	-725.229134	603.0
Amine4 + CO_2	-913.794890	633.4

Table 5-3 Calculated Relative Enthalpies (kJ/mol) of isocyanate-alcohol reactions, All Corrected by ZPE. Using the reference states of zero enthalpy for the reagents, the non-zero values as reported are heats of reaction.

	HDI	2,4-TDI	2,6-TDI	2,4-MDI	4,4-MDI
Isocyanate + 1-Butanol	0	0	0	0	0
1-Butanol Urethane2		-82.7	-72.1	-76.8	
1-Butanol Urethane4	-87.1	-87.2		-85.2	-84.5
Isocyanate + 2-Butanol	0	0	0	0	0
2-Butanol Urethane2		-80.1	-69.6	-73.9	
2-Butanol Urethane4	-83.9	-84.7		-82.8	-81.9
Isocyanate + Water	0	0	0	0	0
Amine2 + CO_2		-85.7	-84.9	-79.7	
Amine4 + CO_2	-67.3	-85.8		-84.0	-83.6

In Table 5-3, the comparison between HDI, 2,4-TDI and 2,4-MDI results show that larger isocyanate molecules lead to lower enthalpies of reaction. Isocyanate group on 4 carbons are less sterically hindered than on either 2 or 6 carbons. The heat released from reaction with the less sterically hindered isocyanate is noticeably larger.

5.3.2 Location of Hydroxyl Groups

To evaluate the impact of hydroxyl group location (e.g. primary versus secondary) molecular modeling was performed using isomers of pentanol. Total electronic and thermal enthalpies and zero-point vibrational energies are provided in Table 5-4. The corresponding relative enthalpies were reported in the table.

Table 5-4 Calculated Total Corrected (Hartree), Zero-Point Vibrational (ZPE, kJ/mol) Energies and Relative Enthalpies (kJ/mol) for study on impact of hydroxyl locations

	Sum of electronic and thermal Enthalpies	ZPE
HDI	-571.839728	519.4
2,4-TDI	-606.395275	353.8
4,4-MDI	-837.364904	568.0
1-Pentanol	-272.820618	435.6
2-Pentanol	-272.827374	434.3
3-Pentanol	-272.827249	434.1

Tert-Pentanol	-272.830000	432.3

HDI	Sum of electronic and thermal Enthalpies (Hartree)	ZPE (kJ/mol)	Calculated Relative Enthalpies (kJ/mol)
HDI + 1-Pentanol	-844.660346	955.0	0
1-Pentanol Urethane	-844.698309	968.0	-86.7
HDI + 2-Pentanol	-844.667102	953.7	0
2-Pentanol Urethane	-844.704307	966.5	-84.9
HDI + 3-Pentanol	-844.666977	953.5	0
3-Pentanol Urethane	-844.703379	966.6	-82.5
HDI + Tert-Pentanol	-844.669728	951.7	0
Tert-Pentanol Urethane	-844.702554	964.4	-73.5

2,4-TDI	Sum of electronic and thermal Enthalpies (Hartree)	ZPE (kJ/mol)	Calculated Relative Enthalpies (kJ/mol)
2,4-TDI + 1-Pentanol	-879.215893	789.4	0
1-Pentanol Urethane4	-879.254034	802.3	-87.2
2,4-TDI + 2-Pentanol	-879.222649	788.1	0
2-Pentanol Urethane4	-879.259948	800.9	-85.1
2,4-TDI + 3-Pentanol	-879.222524	787.9	0
3-Pentanol Urethane4	-879.258996	800.9	-82.8
2,4-TDI + Tert-Pentanol	-879.225275	786.1	0
Tert-Pentanol Urethane4	-879.258207	798.4	-74.2

4,4-MDI	Sum of electronic and thermal Enthalpies (Hartree)	ZPE (kJ/mol)	Calculated Relative Enthalpies (kJ/mol)
4,4-MDI + 1-Pentanol	-1110.185522	1003.6	0
1-Pentanol Urethane	-1110.222663	1016.6	-84.5
4,4-MDI + 2-Pentanol	-1110.192278	1002.3	0
2-Pentanol Urethane	-1110.228568	1015.1	-82.5
4,4-MDI + 3-Pentanol	-1110.192153	1002.1	0

3-Pentanol Urethane	-1110.227643	1015.3	-80.0
4,4-MDI + Tert-Pentanol	-1110.194904	1000.3	0
Tert-Pentanol Urethane	-1110.226724	1013.0	-70.8

Both TDI and MDI results show relative magnitudes of heats of reaction in the sequence: 1-Pentanol > 2-Pentanol > 3-Pentanol > Tert-Pentanol. Primary hydroxyl groups have larger energy potential than secondary, and then secondary has larger energy potential than tertiary. This result does not agree with the assumption used in other kinetics modeling [19, 26, 28, 45, 46] in which only one reaction enthalpy was used for all alcohol-isocyanate reactions.

The trends with the alcohols follow the trends of the isocyanates where the lower steric hindrance of reactive moieties leads to larger heats of reaction. This is consistent with unreacted moieties having less steric hindrance with respective higher energy states; this leads to the release of more energy when the molecules are bound to the urethane configuration.

5.3.3 Chain Length of Hydroxyl Groups

To evaluate the use of Floy's assumption that the reactivity of a moiety can be approximated as independent of the size of the molecule to which the moiety is attached, the heats of reaction for a series of n-alcohols were estimated as reported in Table 5-5.

Table 5-5 Calculated Total Corrected (Hartree), Zero-Point Vibrational (ZPE, kJ/mol) Energies and Relative Enthalpies (kJ/mol) for study on impact of hydroxyl group chain length

	Sum of electronic and thermal Enthalpies	ZPE
4,4-MDI	-837.364904	568.0
Methanol	-115.668313	135.0
Ethanol	-154.960831	210.5
1-Propanol	-194.247438	285.6
1-Butanol	-233.533899	360.7
1-Pentanol	-272.820618	435.6

1-Hexanol	-312.107241	510.6

4,4-MDI	Sum of electronic and thermal Enthalpies (Hartree)	ZPE (kJ/mol)	Calculated Relative Enthalpies (kJ/mol)
4,4-MDI + Methanol	-953.033217	703.0	0
Methanol Urethane	-953.070704	717.6	-83.8
4,4-MDI + Ethanol	-992.325735	778.5	0
Ethanol Urethane	-992.362932	791.8	-84.4
4,4-MDI + 1-Propanol	-1031.612342	853.6	0
1-Propanol Urethane	-1031.649436	866.7	-84.3
4,4-MDI + 1-Butanol	-1070.898803	928.7	0
1-Butanol Urethane	-1070.935949	941.7	-84.5
4,4-MDI + 1-Pentanol	-1110.185522	1003.6	0
1-Pentanol Urethane	-1110.222663	1016.6	-84.5
4,4-MDI + 1-Hexanol	-1149.472145	1078.6	0
1-Hexanol Urethane	-1149.509327	1091.4	-84.8

Figure 5-5 graphically summarizes the results of Table 5-5. The results show that heat of reaction is not dependent on the chain length number of the molecule attached to the hydroxyl group.

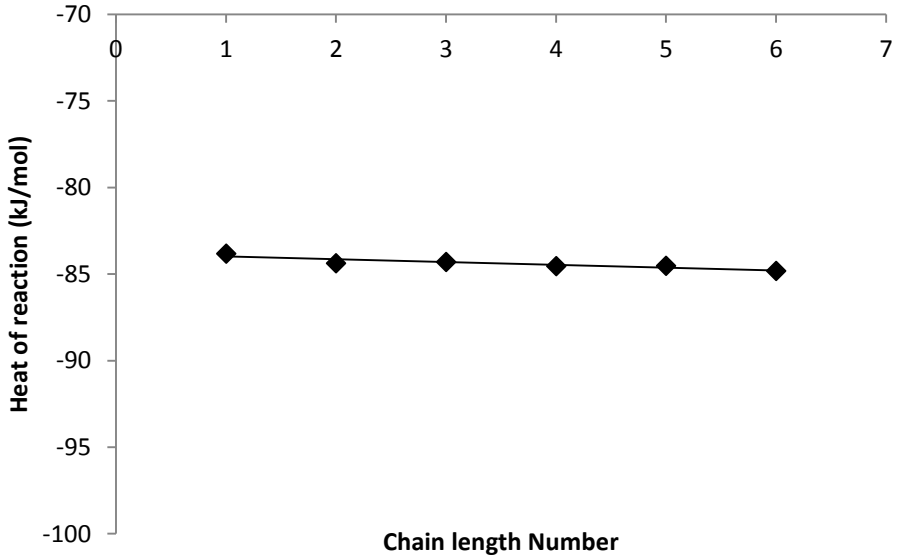

Figure 5-5 Relationship between heat of reaction and the size of the molecule attached to the hydroxyl

5.3.4 Solvent Effects

The solvent effects were studied using a single-point Integral-Equation-Formalism Polarizable Continuum Model (IEF-PCM) to make calculations in toluene (which is used as a solvent in some of the experimental studies to avoid over heat) and benzene. Table 5-6 reports the solvent effects.

Table 5-6 Calculated Total Corrected (Hartree), Zero-Point Vibrational (ZPE, kJ/mol) Energies and Relative Enthalpies (kJ/mol) for study on impact of solvent effects

	Sum of electronic and thermal Enthalpies (Hartree)	ZPE (kJ/mol)	Calculated Relative Enthalpies (kJ/mol)
2,4-TDI	-606.395275	353.8	
1-Butanol	-233.533899	360.7	
2,4-TDI + 1-Butanol	-839.929174	714.5	0
1-Butanol Urethane4	-839.967315	727.4	-87.2
2,4-TDI (T)	-606.398038	353.3	
1-Butanol (T)	-233.536108	360.4	
2,4-TDI + 1-Butanol (T)	-839.934146	713.7	0
1-Butanol Urethane4 (T)	-839.971750	726.3	-86.1
2,4-TDI (B)	-606.397921	353.4	
1-Butanol (B)	-233.536013	360.4	
2,4-TDI + 1-Butanol (B)	-839.933934	713.8	0
1-Butanol Urethane4 (B)	-839.971560	726.4	-86.2

The Results show that the presence of solvent does not have significant impact on reaction enthalpies which matches the conclusion found by Raspoet et al [71]. In his work as for prototypes, PCM calculations were performed in both aqueous and methanol solution, which lead, after all, to similar results. On the whole, the role of the surroundings was found to be less decisive than the specific action of a catalytic cluster. And in fact, the considered reactions had been shown not to be greatly influenced by

the presence of a continuum that does not modify the conclusions emerging from the study carried out for the gas phase species. Based on these, it is assumed that the results with toluene as a solvent are accurate enough to evaluate the reaction enthalpies.

5.3.5 Comparison to Different Models

A primary finding of the molecular simulation results is that the steric hindrance and neighboring molecule effects of reactive moieties on monomers can cause heats of reaction to change up to 17% for urethane-forming reactions. In view of this, the simulation values are compared to literature values and new experimental data in the following paragraphs.

Table 5-7 shows the comparison between computational results and other results from previous literatures for 4,4-MDI which is the most commonly used isocyanate in the industry. Zhao et al [19, 26, 28, 60] results were from previous simulation development. Baser and Khakhar [45, 46] solved differential equations to model the fundamental kinetics in polyurethane foaming reaction. Lovering and Laidler [61] gathered these results experimentally by using a differential microcalorimeter of the Tian-Calvet type. Since Lovering's data was measured in 1961, Zhao and Baser's data seem to be more reliable to be references. The polyols used in their studies have significantly high content of hinder-secondary (tertiary) alcohol, hence their values locate very close to tertiary result of Gaussian values.

Table 5-7 Comparison between molecular modeling results and experimental values reported in literature for reactions of 4,4-MDI with alcohol to form urethane

Reaction Enthalpy (kJ/mol)	Gaussian	Zhao[60]	Baser[45]	Lovering[61]
Primary	-84.5	-72.0	-74.9	-102.9
Secondary	-81.2	-72.0	-74.9	-97.9
Tertiary	-70.8	-72.0	-74.9	NR
Water	-83.6	-66.0	-86.0	NR

The Gaussian values straddle the values of both Zhao et al and Baser providing a level of confidence that the Gaussian values are both reasonable and provide an increased sensitivity to the moiety isomer. The water reaction enthalpy from this study is quite similar to that from Baser and the average gel reaction enthalpy. The deviation between average computational results and literature values is about 5%.

Table 5-8 presents the reaction enthalpy calculation of isocyanate-amine reaction. Only the HDI product result was presented because the calculations of MDI and TDI did not converge.

Table 5-8 Enthalpy calculation of isocyanate-amine reaction

	Sum of electronic and thermal Enthalpies (Hartree)	ZPE (kJ/mol)	Calculated Relative Enthalpies (kJ/mol)
HDI	-571.839728	519.4	
HDI_AMINE	-459.698169	555.5	
HDI + AMINE	-1031.537897	1074.9	0
ISO-Amine_product	-1031.568419	1087.6	-67.4

Values as recommended based on this comprehensive analysis are summarized in Table 5-9. Hindered-Secondary alcohol is assumed to have the same reaction enthalpy as tertiary. PMDI molecules are too large to be computed successfully in Gaussian, and as an approximation are estimated to be 3% less than that of MDI. This assumption is based on the conclusion that heat of reaction decreases as the chain length of isocyanate group increasing when the chain length number is less than 3 [62].

Table 5-9 Recommended values for heat of reaction (kJ/mol)

	PMDI	MDI	TDI	HDI
Primary	-82.0	-84.5	-87.2	-86.7
Secondary	-78.8	-81.2	-84.0	-83.7
Tertiary (HS)	-68.7	-70.8	-74.2	-73.5
Water	-81.1	-83.6	-85.8	-67.3
Amine				-67.4

Simulation results from different modeling were compared to experimental data in Figure 5-6. Symbols are experimental data, dash lines represent the original modeling results using values from Zhao and solid lines represent the revised modeling results using recommended values of PMDI from Table 5-9. "◊" and "□" series represent 1-pentanol and 2-pentanol gel reactions without catalysts, "Δ" and "o" series represent single polyol (G76-635) and mixture polyols gel reactions with catalysts respectively. Temperature profiles of pentanol reactions were cut off at 100 ˚C because the evaporation of toluene impacted results above this temperature. To increase the amount of data collected before reaching 100 ˚C, toluene was used as a solvent at 20% by mass of the mixture.

Due to volatility issues of pentanol, data was also collected using diethylene glycol. Acetophenone was selected as a solvent due to a higher boiling point and better compatibility than toluene. Figure 5-7 compares experimental temperature profiles and modeling results of isocyanate-DEG reaction in presence of acetophenone as a solvent. Symbols are experimental data, dash lines represent the original MATLAB modeling results (-72.0 kJ/mol) and solid lines represent the revised modeling results using Gaussian values (-82.0 kJ/mol). The Table 5-9 recommended heat of reaction for PMDI and primary alcohols (-82.0 kJ/mol) were used in new models (SOLID LINES) to compare with the previously reported values of Zhao et al (-72.0 kJ/mol).

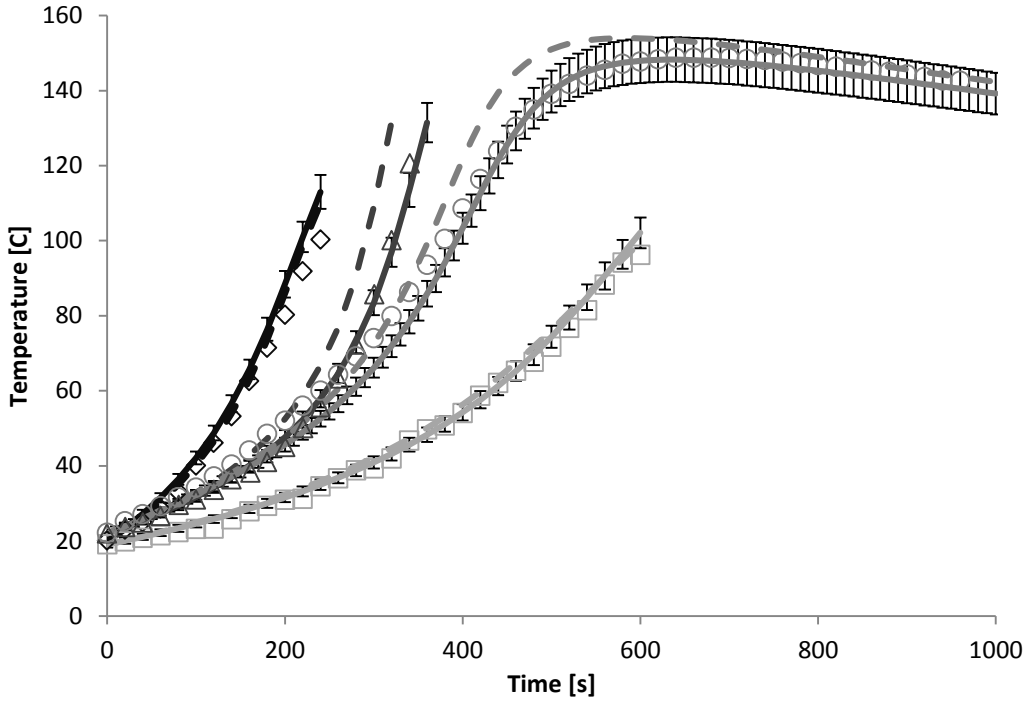

Figure 5-6 Comparison between experimental data and different modeling results of primary, secondary, single polyol and mixture polyols gel reaction

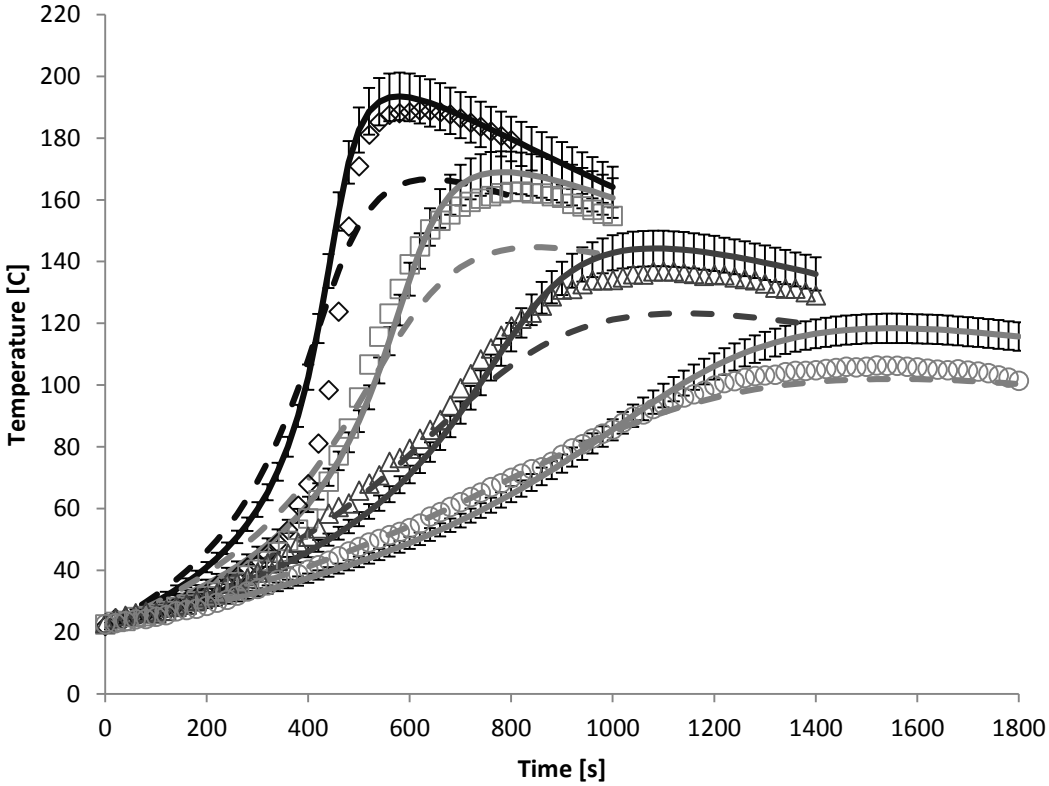

Figure 5-7 Comparison between experimental data and modeling results of isocyanate-DEG reaction in presence of 0%, 10%, 20% and 30% acetophenone (from left to right respectively)

The Table 5-9 value has a clearly better fit in the absence of acetophenone solvent

and at 10% solvent. At higher solvent loadings the lower reaction enthalpy indicated by experimental data may due to the evaporation of solvent due to the combination of longer times and higher fractions of acetophenone.

The new data support that recommended values of Table 5-9 including the distinction between primary, secondary, and tertiary alcohol reagents.

5.3.6 Verification by Other Calculation Methods

The computation of reaction between 2,4-TDI and 1-Butanol was repeated by Hartree-Fock and MP2 method using a 6-31G(d,p) basis set. The molecules were too large to be successfully calculated in higher level basis sets and QM methods. Table 5-10 reports total electronic and thermal enthalpies, zero-point vibrational energies and corresponding relative enthalpies from three different methods.

Table 5-10 Calculated Total Corrected (Hartree), Zero-Point Vibrational (ZPE, kJ/mol) Energies and Relative Enthalpies (kJ/mol) for 2,4-TDI and 1-Butanol reaction

Method		Sum of electronic and thermal Enthalpies (Hartree)	ZPE (kJ/mol)	Calculated Relative Enthalpies (kJ/mol)
B3LYP	2,4-TDI	-606.395275	353.8	
	1-Butanol	-233.533899	360.7	
	2,4-TDI + 1-Butanol	-839.929174	714.5	0
	1-Butanol Urethane4	-839.967315	727.4	-87.2
HF	2,4-TDI	-602.803702	378.8	
	1-Butanol	-232.011583	384.5	
	2,4-TDI + 1-Butanol	-834.815285	763.3	0
	1-Butanol Urethane4	-834.855365	778.1	-90.4
MP2	2,4-TDI	-604.654634	355.1	
	1-Butanol	-232.783505	371.2	
	2,4-TDI + 1-Butanol	-837.438139	726.3	0
	1-Butanol Urethane4	-837.475997	738.7	-87.0

DFT (B3LYP) and MP2 almost have the same results and Hartree-Fock result has a

deviation about 4%. This indicates that the computational results are repeatable and consistent.

5.4 Conclusion

Molecular configurations for a range of reactants and products in polyurethane foaming reaction were optimized at the B3LYP level using a 6-31G(d,p) basis set in the gas phase. Total electronic and thermal enthalpies and zero-point vibrational energies were computed by Gaussian 09 package on a supercomputer from UMBC. The gas phase results were compared to calculations with solvents with the solvent causing only minor decreases (1.2%) in the heats of reaction. The corresponding relative enthalpies were calculated based on ZPE correction and reported in kJ/mol.

Where possible, computational results were compared using different computational methods as a first pass on verifying accuracy of simulations. When variations between different reagent isomers were large, the values were compared to experimental data and values reported in literature. Values of heats of reaction vary by up to 17%, relative values based on hydroxyl isomers (primary vs tertiary). Recommended values for use were made based on experimental observations and these deviations.

Based on the reaction enthalpy results, the following is concluded on heats of reaction: 1) Isocyanate groups on carbon 4 have larger energy potentials than that on carbon 2 and larger isocyanate molecules have lower enthalpy. 2) Primary hydroxyl groups have larger energy potentials than secondary (about 4% larger), and secondary have larger energy potentials than tertiary (about 15%). 3) The heat of reaction is not

dependent on the chain length number of the molecule attached to the hydroxyl group. 4) The presence of solvent decreases the reaction enthalpy slightly with the large molecules self-solvating capability reducing the impact of solvents. 5) Heats of reaction for water-isocyanate reactions were between the two values reported in the literature and provided a basis for recommending values for use.

These studies verify that computational chemistry is a useful tool to estimate changes in reactions due to isomeric variations of reagents or moiety locations on reagent molecules. In a similar manner, simulation of urethane-forming reactions is useful to bridge the gap between fundamental computational chemistry calculations and practical applications.

BIBLIOGRAPHY

1. Chang, M.-C. and S.-A. Chen, *KINETICS AND MECHANISM OF URETHANE REACTIONS: PHENYL ISOCYANATE-ALCOHOL SYSTEMS.* Journal of Polymer Science, Part A: Polymer Chemistry, 1987. **25**(9): p. 2543-2559.
2. Tesser, R., et al., *Modeling of polyurethane foam formation.* Journal of Applied Polymer Science, 2004. **92**(3): p. 1875-1886.
3. Pengjam, W., et al., *Copper-amine complexes as new catalysts for rigid polyurethane foam preparations.* Journal of Applied Polymer Science, 2012. **123**(6): p. 3520-3526.
4. Listemann, M.L., A.C. Savoca, and A.L. Wressell, *Amine catalyst characterization by a foam model reaction.* Journal of Cellular Plastics, 1992. **28**(4): p. 360-398.
5. Strachota, A., B. Strachotová, and M. Špírková, *Comparison of environmentally friendly, selective polyurethane catalysts.* Materials and Manufacturing Processes, 2008. **23**(6): p. 566-570.
6. Farkas, A. and K.G. Flynn, *The catalytic effects of 1,4-diaza [2.2.2] bicycloöctane for isocyanate reactions.* Journal of the American Chemical Society, 1960. **82**(3): p. 642-645.
7. Ni, H., et al., *Effect of catalysts on the reaction of an aliphatic isocyanate and water.* Journal of Polymer Science, Part A: Polymer Chemistry, 2002. **40**(11): p. 1677-1688.
8. Niyogi, S., S. Sarkar, and B. Adhikari, *Catalytic activity of DBTDL in polyurethane formation.* Indian Journal of Chemical Technology, 2002. **9**(4): p. 330-333.
9. Silva, A.L. and J.C. Bordado, *Recent developments in polyurethane catalysis: Catalytic mechanisms review.* Catalysis Reviews - Science and Engineering, 2004. **46**(1): p. 31-51.
10. Van Maris, R., et al., *Polyurethane catalysis by tertiary amines.* Journal of Cellular Plastics, 2005. **41**(4): p. 305-322.
11. Wong, S.-W. and K.C. Frisch, *CATALYSIS IN COMPETING ISOCYANATE REACTIONS. I. EFFECT OF ORGANOTIN-TERTIARY AMINE CATALYSTS ON PHENYL ISOCYANATE AND N-BUTANOL REACTION.* Journal of Polymer Science, Part A: Polymer Chemistry, 1986. **24**(11): p. 2867-2875.
12. Wongkamolsesh, K. and J.E. Kresta. *ORGANOTIN CATALYSIS IN URETHANE SYSTEMS*. 1985. Washington, DC, USA: ACS.
13. Bakirova, I.N. and A.S. Kirillova, *Effect of organometallic catalysts on the synthesis process and properties of molded polyurethane.* Russian Journal of Applied Chemistry, 2013. **86**(9): p. 1399-1403.
14. Hongyu Fan, A.T., Galen J. Suppes, and Fu-Hung Hsieh, *Properties of Biobased Rigid Polyurethane Foams Reinforced with Fillers: Microspheres and Nanoclay.* International Journal of Polymer Science, 2012. **2012**.
15. Singh, H., T.P. Sharma, and A.K. Jain, *Reactivity of the raw materials and their effects on the structure and properties of rigid polyurethane foams.* Journal of Applied Polymer Science, 2007. **106**(2): p. 1014-1023.
16. Thirumal, M., et al., *Mechanical, morphological and thermal properties of rigid polyurethane Foam: Effect of chain extender, polyol and blowing agent.* Cellular Polymers, 2009. **28**(2): p. 145-158.
17. Baker, J.W. and J.B. Holdsworth, *The mechanism of aromatic side-chain reactions with special reference, to the polar effects of substituents. Part XIII. Kinetic examination of the reaction of aryl isoCyanates with methyl alcohol.* Journal of the Chemical Society (Resumed), 1947: p. 713-

726.

18. Yusheng Zhao, M.J.G., Ali Tekeei, Fu-Hung Hsieh, and Galen J. Suppes, *Modeling Reaction Kinetics of Rigid Polyurethane Foaming Process.* Journal of Applied Polymer Science, 2013.
19. Zhao, Y., et al., *Modeling impact of catalyst loading on polyurethane foam polymerization.* Applied Catalysis A: General, 2014. **469**: p. 229-238.
20. R. C. Weast, e., *CRC Handbook of Chemistry and Physics.* CRC Press Inc. Florida, 1990.
21. D. R. Lide, e., *CRC Handbook of Chemistry and Physics. 71st Edition.* CRC Press Inc. Florida, 1990-91.
22. Shawbury, S., Shropshire, *Chemistry and Technology of Polyols for Polyurethanes.* Rapra Technology Limited, 2005.
23. *Priority Product Profile--Spray Polyurethane Foam Systems Containing Unreacted Diisocyanates*. March 2014, California Envirnomental Protection Agency.
24. Jarand, C.W., et al., *Diisocyanate emission from a paint product: A preliminary analysis.* Applied Occupational and Environmental Hygiene, 2002. **17**(7): p. 491-494.
25. Kelly, T.J., *Testing of household products and materials for emission of toluene diisocyanate.* Indoor Air, 1999. **9**(2): p. 117-124.
26. Ghoreishi, R., Y. Zhao, and G.J. Suppes, *Reaction modeling of urethane polyols using fraction primary secondary and hindered-secondary hydroxyl content.* Journal of Applied Polymer Science, 2014. **131**(12).
27. Shen, L., et al., *Density modeling of polyurethane box foam.* Polymer Engineering and Science, 2014. **54**(7): p. 1503-1511.
28. Zhao, Y., et al., *Modeling reaction kinetics of rigid polyurethane foaming process.* Journal of Applied Polymer Science, 2013. **130**(2): p. 1131-1138.
29. Duff, D.W. and G.E. Maciel, *Carbon-13 and nitrogen-15 CP/MAS NMR characterization of MDI-polyisocyanurate resin systems.* Macromolecules, 1990. **23**(12): p. 3069-3079.
30. Singh, P. and J.L. Boivin, *Studies on the stability of the dimer of 2, 4-tolylene diisocyanate.* Canadian Journal of Chemistry, 1962. **40**(5): p. 935-940.
31. Querat, E., et al., *Blocked isocyanate. Reaction and thermal behaviour of the toluene 2, 4 - diisocyanate dimer.* Die Angewandte Makromolekulare Chemie, 1996. **242**(1): p. 1-36.
32. Heintz, A.M., et al., *Effects of reaction temperature on the formation of polyurethane prepolymer structures.* Macromolecules, 2003. **36**(8): p. 2695-2704.
33. Lapprand, A., et al., *Reactivity of isocyanates with urethanes: conditions for allophanate formation.* Polymer degradation and stability, 2005. **90**(2): p. 363-373.
34. Vivaldo-Lima, E., et al., *Modeling of nonlinear polyurethane production in batch reactors using a kinetic-probabilistic approach.* Industrial & engineering chemistry research, 2002. **41**(21): p. 5207-5219.
35. Delebecq, E., et al., *On the Versatility of Urethane/Urea Bonds: Reversibility, Blocked Isocyanate, and Non-isocyanate Polyurethane.* Chemical reviews, 2012. **113**(1): p. 80-118.
36. Dusek, K., M. Spirkova, and I. Havlicek, *Network formation of polyurethanes due to side reactions.* Macromolecules, 1990. **23**(6): p. 1774-1781.
37. Lubguban, A.A., et al., *Isocyanate reduction by epoxide substitution of alcohols for polyurethane bioelastomer synthesis.* International Journal of Polymer Science, 2011. **2011**.
38. Hsieh, F.-H., et al., *Urethane formulation*. 2012, Google Patents.
39. Okumoto, S. and S. Yamabe, *A computational study of base-catalyzed reactions between*

isocyanates and epoxides affording 2-oxazolidones and isocyanurates. Journal of Computational Chemistry, 2001. **22**(3): p. 316-326.

40. Caille, D., J.P. Pascault, and L. Tighzert, *Reaction of a diepoxide with a diisocyanate in bulk.* Polymer Bulletin, 1990. **24**(1): p. 23-30.
41. Morgans Jr, D., K. Sharpless, and S.G. Traynor, *Epoxy alcohol rearrangements: hydroxyl-mediated delivery of Lewis acid promoters.* Journal of the American Chemical Society, 1981. **103**(2): p. 462-464.
42. Flory, P.J., *Principles of polymer chemistry*. 1953: Cornell University Press.
43. Frensdorff, H.K.A., R.K., *Vapor pressure of 2,4-tolylene diisocyanate.* J. Chem. Eng. Data, 1975. **20**(1): p. 13-15.
44. Zalikin, A.A. and Y.A. Streoikheev, *Some physicochemical constants of 4,4'-diaminodiphenylmethane and 4,4'-diphenylmethanediisocyanate.* Zhur. Priklad. Khim., 1966. **39**: p. 2607.
45. Baser, S.A. and D.V. Khakhar, *Modeling of the dynamics of water and R-11 blown polyurethane foam formation.* Polymer Engineering and Science, 1994. **34**(8): p. 642-649.
46. Baser, S.A. and D.V. Khakhar, *Modeling of the dynamics of R-11 blown polyurethane foam formation.* Polymer Engineering and Science, 1994. **34**(8): p. 632-641.
47. Harikrishnan, G. and D.V. Khakhar, *Modeling the dynamics of reactive foaming and film thinning in polyurethane foams.* AIChE Journal, 2010. **56**(2): p. 522-530.
48. Zhang, X.D., et al., *Role of silicone surfactant in flexible polyurethane foam.* Journal of Colloid and Interface Science, 1999. **215**(2): p. 270-279.
49. DOW, *Dow Polyurethanes Flexible Foams.*
50. Hill, R.M., *Silicone surfactants - New developments.* Current Opinion in Colloid and Interface Science, 2002. **7**(5-6): p. 255-261.
51. Yasunaga, K., et al., *Study of cell opening in flexible polyurethane foam.* Journal of Cellular Plastics, 1996. **32**(5): p. 427-447.
52. Kanner, B. and T.G. Decker, *Urethane Foam Formation - Role of the Silicone Surfactant.* Journal of Cellular Plastics, 1969. **5**(1): p. 32-39.
53. Burlatsky, S.F., et al., *Surface tension model for surfactant solutions at the critical micelle concentration.* Journal of Colloid and Interface Science, 2013. **393**(1): p. 151-160.
54. Hill, R.M., *Silicone surfactants.* Taylor & Francis, 1999.
55. Favelukis, M. and R.J. Albalak, *Bubble growth in viscous newtonian and non-newtonian liquids.* Chemical Engineering Journal, 1996. **63**(3): p. 149-155.
56. Nguyen, A.V., *Historical note on the Stefan-Reynolds equations.* Journal of Colloid and Interface Science, 2000. **231**(1): p. 195.
57. Ruckenstein, E. and A. Sharma, *A new mechanism of film thinning: Enhancement of reynolds' velocity by surface waves.* Journal of Colloid And Interface Science, 1987. **119**(1): p. 1-13.
58. Radoev, B.P., A.D. Scheludko, and E.D. Manev, *Critical thickness of thin liquid films: Theory and experiment.* Journal of Colloid And Interface Science, 1983. **95**(1): p. 254-265.
59. Talaia, M.A.R., *Terminal Velocity of a Bubble Rise in a Liquid Column.* World Academy of Science, Engineering and Technology, 2007. **28**: p. 264-268.
60. Zhao, Y. and G.J. Suppes, *Simulation of Catalyzed Urethane Polymerization: An Approach to Expedite Commercialization of Bio-based Materials.* Catalysis Surveys from Asia, 2014.
61. Lovering, E.G. and K.J. Laidler, *Thermochemical Studies of Some Alcohol-Isocyanate Reactions.*

Canadian Journal of Chemistry, 1961. **40**.

62. Flory, P.J., *Principles of Polymer Chemistry.* Cornell University Press, 1953: p. 71.
63. Lu, H., *State diagram of phase transition temperatures and solvent-induced recovery behavior of shape-memory polymer.* Journal of Applied Polymer Science, 2013. **127**(4): p. 2896-2904.
64. Lu, H. and W.M. Huang, *A phenomenological model for the chemo-responsive shape memory effect in amorphous polymers undergoing viscoelastic transition.* Smart Materials and Structures, 2013. **22**(11).
65. Huo, S.P., et al., *Crosslinking kinetics of the formation of lignin-aminated polyol-based polyurethane foam.* Journal of Applied Polymer Science, 2012. **125**(1): p. 152-157.
66. Modesti, M., V. Adriani, and F. Simioni, *Chemical and physical blowing agents in structural polyurethane foams: Simulation and characterization.* Polymer Engineering and Science, 2000. **40**(9): p. 2046-2057.
67. Paciorek-Sadowska, J., et al., *Preparation of rigid polyurethane foams with powder fi ller.* Journal of Polymer Engineering, 2012. **32**(2): p. 71-80.
68. Çoban, M. and F.A.S. Konuklar, *A computational study on the mechanism and the kinetics of urethane formation.* Computational and Theoretical Chemistry, 2011. **963**(1): p. 168-175.
69. Williams, C.I. and M.A. Whitehead, *Semi-empirical study of isocyanate geometries, and β-lactam formation through alkene-isocyanate cyclo-addition reactions.* Journal of Molecular Structure: THEOCHEM, 1999. **491**: p. 93-101.
70. Berry, R.J., A.L. Wilson, and M. Schwartz, *A computational study of bond dissociation enthalpies and hydrogen abstraction energy barriers in model urethanes.* Journal of Molecular Structure: THEOCHEM, 2000. **496**: p. 121-129.
71. Raspoet, G., et al., *The alcoholysis reaction of isocyanates giving urethanes: Evidence for a multimolecular mechanism.* Journal of Organic Chemistry, 1998. **63**(20): p. 6878-6885.

VITA

Yusheng Zhao is a Ph.D. candidate in Department of Chemical Engineering under supervision of Dr. Galen Suppes. He received his B.S. in Materials Science from East China University of Science and Technology and his M.S. in Chemical Engineering from University of Missouri. He has published five papers as the first author during his study in University of Missouri. Yusheng's research has primarily focused on modeling and experimental study of polyurethane foaming reactions. Impact of side reactions, catalysts, and surfactants were evaluated and a MATLAB program was developed to simulate the reaction process and to predict foam properties.